PARAMETRIC OPTIMIZATION OF DI CI ENGINE TO ACHIEVE HCCI COMBUSTION CHARACTERISTICS FOR DIESEL/BIODIESEL BLENDS

A Thesis submitted in the partial fulfillment of the requirements for the award of the degree of

DOCTOR OF PHILOSOPHY

By

PRABHAKARA RAO GANJI
(ROLL NO: 701343)

DEPARTMENT OF MECHANICAL ENGINEERING
NATIONAL INSTITUTE OF TECHNOLOGY
WARANGAL (T.S) INDIA 506 004

JANUARY 2018

PARAMETRIC OPTIMIZATION OF DI CI ENGINE TO ACHIEVE HCCI COMBUSTION CHARACTERISTICS FOR DIESEL/BIODIESEL BLENDS

A Thesis submitted in the partial fulfillment of the requirements for the award of the degree of

DOCTOR OF PHILOSOPHY

By

PRABHAKARA RAO GANJI
(ROLL NO: 701343)

Under the Supervision of

Dr. V. R. K. RAJU

Assistant Professor

and

Prof. S. SRINIVASA RAO

Professor

DEPARTMENT OF MECHANICAL ENGINEERING
NATIONAL INSTITUTE OF TECHNOLOGY
WARANGAL (T.S) INDIA 506 004

JANUARY 2018

Dedicated

to

ALMIGHTY GOD, My Family

My Teachers and friends who encouraged me

NATIONAL INSTITUTE OF TECHNOLOGY
WARANGAL (T.S) INDIA 506 004

DECLARATION

This is to certify that the work presented in the thesis entitled **"Parametric optimization of DI CI engine to achieve HCCI combustion characteristics for diesel/biodiesel blends"**, is a bonafide work done by me under the supervision of Dr.V.R.K Raju and Prof. S. Srinivasa Rao was not submitted elsewhere for the award of any degree.

I declare that this written submission represents my idea in my own words and where other's ideas or words have not been included. I adequately cite and referenced the original sources. I also declare that I have adhered to all principles of academic honesty and integrity and have not misinterpreted or fabricated or falsified any idea/data/fact/source in my submission. I understand that any violation of the above will be a cause for disciplinary action by the Institute and can also evoke penal action from the sources which have thus not been properly cited or from whom proper permission has not taken when needed.

Date **(Prabhakara Rao Ganji)**

Place: Warangal Research Scholar,

Roll No.701343

NATIONAL INSTITUTE OF TECHNOLOGY
WARANGAL (T.S) INDIA 506 004

CERTIFICATE

This is to certify that the thesis entitled **"Parametric optimization of DI CI engine to achieve HCCI combustion characteristics for diesel/biodiesel blends"** that is being submitted by **Mr. Prabhakara Rao Ganji** in partial fulfillment for the award of Doctor of Philosophy (**Ph.D)** in the Department of Mechanical Engineering, National Institute of Technology, Warangal, is a record of bonafide work carried out by him under our guidance and supervision. The results embodied in this thesis have not been submitted to any other Universities or Institutes for the award of any degree or diploma.

Dr.V.R.K.Raju

Assistant Professor
Department of Mechanical Engineering
NIT- Warangal.

Prof. S. Srinivasa Rao

Professor
Department of Mechanical Engineering
NIT- Warangal.

ACKNOWLEDGEMENT

This work would not have been possible without the encouragement, guidance, patience and wisdom of my supervisors, **Dr. V.R.K. Raju, Assistant Professor** and **Dr.S.Srinivasa Rao**, **Professor,** Mechanical Engineering Department, National Institute of Technology, Warangal. Thank you for seeing my potential and giving me an opportunity to be the part of TEQIP-II.

I wish to sincerely thank NITW authorities, **Prof. N.V. Ramana Rao, DIRECTOR**, National Institute of Technology, Warangal. I also thank former **DIRECTORs**, **Prof. G. R. C. Reddy and Prof. R. V. Chalam, Prof. T Srinivasa Rao** and other top officials who gave me an opportunity to carry out research work.

I also sincerely thank **Prof. Bangarubabu Popuri, Head**, Mechanical Engineering Department, National Institute of Technology, Warangal for his continuous support towards carrying out my research work.

Thanks are also due to **Prof. L. Krishnanand** and **Prof. C. S. P. Rao** former Head, Mechanical Engineering Department, National Institute of Technology, Warangal, for their timely suggestions, support and for providing necessary departmental facilities and services during successful completion of research work

I wish to express my sincere and whole hearted thanks and gratitude to my DSC members **Prof. G.Amba Prasad Rao and Prof. K. Madhu Murthy, Professors, Mechanical Engineering Department,** and **Prof. Y. Pydi Setty,** Professor, Chemical Engineering Department for their kind help, encouragement and valuable suggestions for successful completion of research work.

I wish to convey my heartfelt thanks to **Sri. G. R. K. Gupta** Associate professor and **Prof. C. Gururaja Rao** National Institute of Technology who taught me CFD and Heat transfer courses and motivated me in understanding the concepts in completing my research work.

I wish to express my sincere and whole hearted thanks and gratitude to **Dr. Raja Vishwanathan,** Assistant Professor, HSS Department, National Institute of Technology, Warangal.

I wish to thank **Ranjith Kumar Garigipati**, Senior Application Engineer ESTECO Software India PVT. LTD and **Nachiket Kasarekar,** Business Development Manager, ESTECO Software India PVT. LTD. for their help.

I would like to express my sincere thanks to **Mr. Ashish Joshi** CEI, India Pune and **Mr.Phaninder Injeti, Product Manager (EnSight)** from CEI,India Pune for their cooperation and the help extended during this work.

I also like to express my sincere thanks to all my friends and colleagues specially, to **Prakash P, Ramesh Babu Bejjam, Srinivasa Rohit, Karthikeya Sharma, Ranga Babu, Krishna Kishore, Venkateswarlu, Siva Prasad Kattela, Aasrith, Kiran Prasad, Rohitkumar, Viswanath, Arun, Rudranath and Kashyap.**

Lastly, I would like to thank my family members my father, my daughters and my wife for all their love and encouragement. My in-laws P Srinivasa Rao & Family, P Anil Kumar & Family deserve specially mention of appreciation for exhibiting patience during this long and arduous journey.

I want to express my sincere thanks to all those who directly or indirectly helped me at various stages of this work.

Above all, I express my indebtedness to the **"ALMIGHTY GOD"** for all his blessings and kindness.

(Prabhakara Rao Ganji)

CONTENTS

List of Tables

List of Figures

NOMENCLATURE

aTDC	After Top Dead Center
ARAI	Automotive Research Association of India
bTDC	Before Top Dead Center
BSFC	Brake Specific Fuel Consumption
BSEC	Brake Specific Energy Consumption
BS IV	Bharat Stage IV
BTE	Brake Thermal Efficiency
B20	80% diesel and 20% bio diesel
CAD	Crank Angle Degrees
CAT3401	Caterpillar engine model with a single cylinder
CR	Compression Ratio
CO	Carbon monoxide
CO_2	Carbon dioxide
CTC	Characteristic Time Combustion
CFD	Computational Fluid Dynamics
CI	Compression-Ignition
CAT 3401	Single cylinder Caterpillar engine Model
C_p	Specific Heat
DI	Direct injection
DOE	Design of Experiments
EGR	Exhaust Gas Residual
EVO	Exhaust Valve Opening
EVC	Exhaust Valve Closure
FIP	Fuel injection pressure
HCCI	Homogeneous Charge Compression Ignition
HRR	Heat Release Rate
HSDI	High Speed Direct Injection
IC	Internal combustion
IMEP	Indicated Mean Effective Pressure
ISEC	Indicated Specific Energy Consumption (MJ/kWh)
ISFC	Indicated Specific Fuel Consumption (g/kWh)
IVC	Intake Valve Closure
IVO	Intake Valve Opening
LISA	Linearized Instability Sheet Atomization
LES	Large eddy simulation
LHV	Lower Heating Value
LLNL	Lawrence Livermore National Laboratory
NO_x	Oxides of Nitrogen
P	Pressure
PB20	80% diesel and 20% Pongamia bio diesel
PM	Particulate Matter
PCCI	Premixed Charge Compression-Ignition
PISO	Pressure-Implicit with Splitting of Operators
PPM	Parts Per Million

RNG	Re-Normalization Group
RSM	Response Surface Methodology
RCCI	Reactivity-Controlled Compression-Ignition
ROHR	Rate of Heat Release
S	Entropy, S° for Standard State
SI	Spark-ignition
SOI	Start of Injection
SOC	Start of Combustion
T	Temperature
TAB	Taylor analogy breakup
tke	Turbulent Kinetic Energy
td	Turbulent dissipation
ULSD	Ultra Low Sulfur Diesel
VCR	Variable Compression Ratio
V	Volume
W	Molecular Weight
X	Molar Concentration
CO	Carbon Monoxide
CO_2	Carbon Dioxide
CH_2O	Formaldehyde
C_2H_2	Acetylene
C_7H_{16}	Normal Heptane, n Heptane (nc7h16)
$C_{14}H_{30}$	Tetradecane
$C_{17}H_{34}O_2$	Methyl Palmitate (mpalm)
$C_{19}H_{38}O_2$	Methyl Stearate (mstear)
$C_{19}H_{36}O_2$	Methyl Oleate (molea)
$C_{19}H_{34}O_2$	Methyl Linoleate (mlinl)
$C_{19}H_{32}O_2$	Methyl Linolenate (mlinln)
HC	Hydrocarbons, General
H_2O	Water
NO	Nitrogen Oxide
NO_2	Nitrogen Dioxide
OH	Hydroxide Radical
NO_x	Oxides of Nitrogen ($NO + NO_2$)
PM	Particulate Matter
MB ($C_5H_{10}O_2$)	Methyl Butanoate
MD ($C_{11}H_{22}O$)	Methyl Decanoate
MD9D ($C_{11}H_{20}O_2$)	Methyl-9-Decenoate
UHC	Unburned Hydrocarbons
φ	Equivalence Ratio

Abstract

In recent years there has been growing requirement to develop more efficient engines with minimum emissions. This is mainly due to increasing demand for fuel economy and stricter regulations for emissions. Hence it is necessary to develop a technology, which will fulfill both of the above requirements. Diesel and gasoline engines power majority of transportation vehicles today. The operation of gasoline engines is limited by low part load efficiencies, since compression ratio is limited to avoid the phenomenon of knocking. Diesel engines are superior to gasoline engines due to their higher power, efficiency, and fuel economy.

In CI diesel engines the fuel is injected into the cylinder which comprises of hot compressed air. Since the time for the mixture formation is very less, there would definitely be zones of rich and lean mixture inside the cylinder. This makes the overall mixture heterogeneous. HCCI is a mode of combustion in which a homogeneous mixture of air and fuel is prepared and is burnt by developing an auto ignition condition inside the combustion chamber. HCCI works on the principle of both SI and CI engine in the sense that a homogeneous mixture of the air and fuel is prepared as that of SI engine and compression ignited as in CI engine.

Computational Fluid Dynamics (CFD), is an effective and widely used tool to design and optimize of an Internal Combustion (IC) engine. The engine performance and emission characteristics are strongly determined by the complex interacting processes of in-cylinder flow, fuel spray injection and combustion. CONVERGE^{TM} CFD code is one of the popular IC engine simulation software which can able to predict the combustion phenomena with reasonably good accuracy.

Two engines were considered for the present study, namely CAT 3401 and VCR engine. The CAT 3401 is a single cylinder version of a CAT 3406 heavy duty, direct injection diesel engine, whereas VCR engine is a genset application laboratory engine. In the present work, three different configurations such as CAT3401 diesel, VCR diesel and VCR PB20 were validated with the experimental results. The study has been extended to evaluate the effect of four design parameters such as Compression Ratio (CR), Start of injection (SOI), Fuel Injection Pressure (FIP) and Exhaust Gas Recirculation (EGR) on the performance and emission characteristics. Regression equations were developed for the responses such as ISFC, NOx and soot. For all the

configurations, the parameters are optimized for the minimizing the NOx, soot and ISFC by using the Response Surface Methodology (RSM). It was observed that the interaction effects also play a major role in determining the performance and emission characteristics of the engine.

Increasing CR reduces ISFC and soot whereas it increases NOx emissions and vice versa, but this trend reverses when the SOI and FIP are at their high levels. Increasing FIP reduces soot and also slightly reduces ISFC but increases NOx significantly. But this is also not valid when the low EGR and advanced SOI co-exist. Advancing SOI reduces soot and increases NOx but the ISFC may decrease or increase and will depend on the compression work. Increasing EGR alone increases the soot and ISFC whereas the NOx emissions decrease significantly, whereas this phenomenon turn round when the CR and SOI are at high levels.

Mixture homogeneity is quantified based on TFDI (Target Fuel Distribution Index) for the baseline and optimized models and was compared for all the three cases. Improved TFDI with simultaneous reduction of NOx and soot through optimized configuration ensures combustion characteristics as that of HCCI in all the three cases. The use of PB20 (80% diesel and 20% Pongamia biodiesel) as a fuel in an optimized case is also justified, and recommended as a replacement for conventional diesel based on its favorable ISEC (**MJ/kWh**).

Chapter 1

Introduction

Fossil fuels are the major sources of energy in the world in the present scenario. These energy sources are converted into useful energy for various applications by means of internal combustion (IC) engines. IC engines have been used for more than one century and have been identified as one of the prime sources of air pollution. Currently, the majority of the transportation is fulfilled by IC engines, either on the road or at sea. Spark ignition and compression ignition engines are the two classifications of conventional IC engines. The operation of gasoline engines (SI) is limited by lower part load efficiencies due to lower compression ratio. Diesel engines (CI) are superior to gasoline engines due to their higher power, efficiency, and fuel economy. However, diesel engines impose environmental concerns due to higher NOx and soot emissions.

Fossil fuels typically comprise of hydrogen and carbon molecules. Complete combustion can take place only when "stoichiometric" fuel- air ratio is supplied to the combustion process and also sufficient time is available to oxidize completely into CO_2 and H_2O. These ideal conditions are far from the reality due to the shorter combustion duration, varying temperature, rich and lean zones of operation could result in incomplete combustion. The undesirable products (pollutants) formed due to the incomplete combustion are particulate matter (PM) or soot, oxides of nitrogen (NOx), carbon monoxide (CO) and unburned hydrocarbons (UHC). The effects of

these pollutants from IC engines are identified as harmful to the human life and therefore, certain regulations have been put on these combustion products by the competent authorities (ARAI, 2016; Heywood, 2005).

The current emission norms in India are Bharat Stage (BS) IV. The automobile manufacturers are required to reduce the pollutants to very low levels in the near future to cope up with these standards. Emission standards for IC engines have been periodically revised all over the world in order to make sure that the usage of energy sources does not hamper the human life.

Emissions and fuel effciency are the two main concerns for the IC engines in the current scenario. The emission control methods can be broadly classified into internal and external methods. External methods include the treatment of exhaust using catalytic converters, particulate absorbers, etc. and these are effective to an extent, but this adds to the weight and cost of the engine. Internal methods that include combustion chamber shape, nozzle parameters, injection pressure, injection rates, etc. directly influence the formation of pollutants. Injection system is considered to be the most important object (or part or component) of an I.C. engine, that can do a lot in improving the efficiency and emission control.

Designing diesel engines that cope with the future emission regulation requires significant improvement of the diesel engines. Improvement may be necessary for catalytic converter equipment or incylinder combustion phenomena and is extremely advantageous. Reducing the amount of emissions coming out from the engine cuts down the demand on the after treatment converters. Moreover, enhancing an engine performance and emission characteristics by modifying the combustion strategy while, keeping existing components can be more cost-efficient. This can be achieved by tuning the operating or design parameters such as compression ratio, fuel injection strategies, exhaust gas recirculation etc.

To accomplish a simultaneous reduction in soot and NOx emissions, combustion strategies must pursue some vital characteristics. Premixed in-cylinder charge prior to ignition and lower combustion temperatures are two important features of an efficient combustion. The fuel and air inside the cylinder must be thoroughly mixed to avoid too rich and too lean regions which will lead to the formation of NO_x and soot (Brakora, 2012). The temperature during the combustion phenomena must be at moderate levels (1000 – 1600 K) in order to avoid formation of NOx and

the soot formation in significant quantities (Yao et al. 2009). A lot of researchers have been formulated combustion strategies that could simultaneously reduce soot and NOx. The features of the strategies include employing of heavy cooled exhaust gas recirculation (EGR) where, exhaust gas is cooled and draw back into the air intake system, and alternation of start of injections (SOI). The methods have also been accomplished for both advanced and retarded start of injections to achieve the desired level of combustion.

The overall performance of the engine increases without a considerable penalty in engine hardware. Nevertheless, the techniques of minimizing the engine emissions should not hamper fuel economy in big margin as this may raise fuel prices, causing the engines less preferable to costumers.

1.1 Biofuels

Earlier researches have shown that bio diesels can be the best replacement for diesel oil to reduce emissions and could be directly used in existing C.I engines without any substantial changes in engine configuration. Faster degradation is another favorable character of biodiesel. It is nontoxic and less carcinogenic compared to diesel emissions. Bio diesels are oxygenated fuels, and it gives a cleaner combustion even with comparatively rich mixtures. Carbon emissions from the burning of these will not add to the greenhouse effect as the CO_2 produced will be absorbed by the plants thus maintaining the balance of CO_2. It contains no Sulphur, and the amount of poly aldehydes that are toxic, is substantially less compared to diesel (Murugesan et al, 2009).

Pongamia Pinnatta, a swiftly growing leguminous tree that is native of Indian sub-continent, is one of the best resource/tree from which biodiesel can be extracted. Common names include Indian beech, Pongam oiltree, **karanj** (Hindi), honge (ಹೊಂಗೆ in Kannada), pungai (புங்கை in Tamil), kānuga (కానుగ in **Telugu**), karach (করচ গাছ in Bengali), naktamāla (नक्तमाल in Sanskrit). Figure 1.3 shows the Pongamia tree and its seeds from which oil can be extracted. It is fast growing, requires only marginal land. Comparing the production cost to palm oil @ € 600per ton and canola oil with @ € 550 per ton, while Pongamia has only @ €48 per ton (Scott et al, 2008).

Scott et al. (2008), Naik et al. (2010) and Bala & Sandeep (2011) presented the proximate composition and fatty acid profiles for the Pongamia. Sahoo & Das (2009) reported that the Pongamia biodiesel is quite appropriate as an alternative to the mineral diesel. The chemical composition of Pongamia is reported in Pandey et al. (2012). B20 (80% diesel and 20% bio diesel) is a viable alternative for diesel in the present scenario of modern context (Raheman & Phadatare 2004). The policy of Indian government is also towards the target of 20% blending of biofuels (http://www.mnre.gov.in/).

From the feasibility study of various oils to be used as biodiesel, Pongamia pinnata is found to be superior in performance as its blend (PB20) properties as a fuel is close to premium diesel, and also its growing conditions are favorable in India, requires very marginable land compared to Jatropha, Neem etc (Atabani et al., 2013). The usage of the biodiesel may be beneficial in reducing the pollutants from the IC engines. It is appreciable because of its renewable nature and also towards the prosperity of the nation.

Fig.1.1 Pongamia Tree and its seeds

1.2 The state of art with diesel combustion modeling

Engine research experiments are often performed by employing metal engines, which can give worthy data pertaining to the performance and emission characteristics. But, because of their

limited viewing ability, investigators can only speculate about spray behavior, formation of species and the combustion duration. One of the possibilities for visualization of the spray and combustion behavior is to install transparent windows into the combustion area (cylinder). Employing advanced lasers camera diagnostics, investigators can visualize the spray and combustion phenomena taking place inside the cylinder. Optical engines help investigators in making worthy contributions to the perception of diesel engine combustion phenomena. But, these equipment and their accessories may be costly and collection of data from the setup, consumes lot of time. In view of this, simulation models play a vital role in engine design and development. Post-processing of results will provide an insight into the combustion chamber without modifying the existing engine setup. Computational models also often reduce much of the costs and time in connection with the experimental setup. With the increasing computational capability of computers, the processes in an internal combustion engine such as turbulence, spray injection, combustion etc. can be modeled in more detail. CONVERGE, KIVA, STAR-CD, FLUENT, FORTE, VECTIS are some of the computational fluid dynamics (CFD) packages used for IC engine combustion modeling and simulation.

The combustion properties are influenced by method of fuel preparation and its distribution in engine. These are managed by in-cylinder fluid mechanics. During liquid fuel injection, there are two phases in engine which changes in three directions as well as with time from dense to lean makes the phenemona complex. A detailed understanding of combustion process should be developed to improve performance while reducing emissions. Diesel combustion introduces complex and inconvenient modelling challenges. There are so many sub-models needed, which works in atomization, turbulence, spray injection, ignition, wall heat transfer, pollutants, vaporization.

1.2.1 CONVERGE software

CONVERGE is one of the few revolutionary computational fluid dynamics (CFD) program that eliminates the time required for grid generation for the simulation process. Unlike many other CFD programs, CONVERGE automatically generates a perfectly orthogonal, structured grid at runtime, based on simple, user-defined grid control parameters. This runtime grid generation method completely eliminates the need to manually generate a grid (Richards et al. 2014). CONVERGE is loaded with the physical models for spray such as Kelvin-Helmholtz

breakup, Rayleigh-Taylor breakup, LISA sheet breakup, TAB breakup, Injection distributions, Wall film model (particle based) etc. For turbulence such as Standard κ-ε, Standard RNG κ-ε, Rapid Distortion RNG κ-ε, LES and etc. For combustion such as SAGE detailed chemical kinetics model, Shell ignition model, Characteristic Time Combustion (CTC) model, General equilibrium solver, Soot and NOx emissions models etc.

1.3 HCCI fundamentals

HCCI is considered as a technology which works on the principle which takes care of the advantages of both SI engine and CI engine. In HCCI mode, a homogeneous mixture of the air and fuel is generated, and then it is burnt by developing an auto ignition condition inside the combustion chamber. This type of combustion is much more efficient and thus leads to a lot of fuel saving and at the same time produces much less NOx and particulate matter. In HCCI, just like SI Engine a homogeneous charge of air and fuel is developed during the intake stroke, and in compression stroke the homogeneous charge reaches auto ignition conditions and burns without any ignition system just as CI engine. To achieve such combustion HCCI needs a high level of control over combustion timing and rate of combustion. HCCI is quite a futuristic technology and once, the challenges imposed on HCCI model tackled successfully; it will dominate the engine market. Most of the automobile companies are working on it with the help of various universities and most of them have launched their test model in the market working on HCCI mode.

1.3.1 Comparison of CI and HCCI combustion

Diesel engine combustion is heterogeneous in nature, fuel is injected into the compressed air and due to the compression the mixture will attain high temperatures that results in auto ignition of fuel. In CI diesel engines, the fuel is injected into the hot compressed air inside the cylinder. The injected fuel at higher pressure diffuses into the compressed air, breaks up into small droplets, evaporates to form a combustible mixture and gets auto ignited. The starting of combustion is determined by injection timing and the power output is controlled by the amount of fuel injected in a cycle. Since the time for the mixture formation is very less, there would definitely be zones of rich mixture and lean mixture inside the cylinders locally making the overall mixture heterogeneous.

HCCI is a mode of combustion in which a homogeneous mixture of the air and fuel is generated and then it is burnt by developing auto ignition conditioning inside the combustion chamber. HCCI works on the principle of both SI and CI engine in the sense that homogeneous mixture of the air and fuel is generated as in SI engine and the homogeneous charge is compression ignited as in CI engine. The comparison of typical operations of CI, SI and HCCI is shown in the Fig.1.2. HCCI has a promising future for automotive and power generation applications.

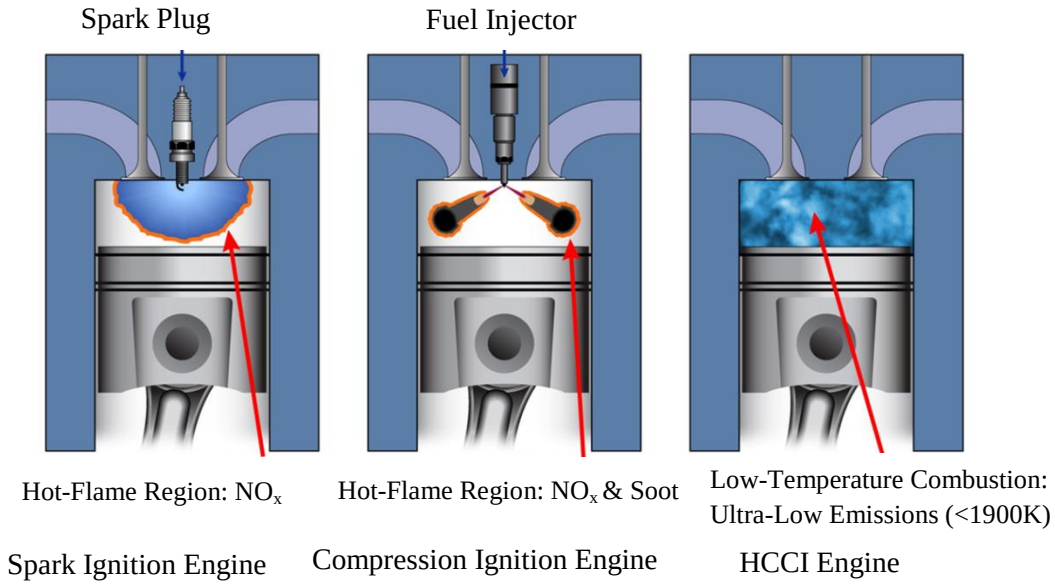

Fig.1.2. Comparison of CI, SI and HCCI combustion

1.3.2 Features of HCCI

- HCCI is not an engine concept, it is a combustion concept. It must be incorporated in an engine concept. It is a low temperature, chemically controlled (flameless) combustion process. It also involves auto ignition of very lean homogeneous mixtures of fuel and air so that the combustion temperatures are low.
- Due to low combustion temperatures NOx formations are negligibly smaller and lower than those of the current SI and CI engines.
- Formation of very little soot takes place as the homogeneous charge is burnt.
- High fuel efficiencies similar to DI diesel engines can be obtained as very lean mixtures are burned.
- HCCI can be considered as a hybrid form between the CI and SI combustion process.

- However, the combustion process is different. So there is neither Diffusion flame (as in a diesel engine) nor a flame front travelling through a premixed charge (as in SI engine).

1.3.3 Challenges associated with HCCI

HCCI technology has several advantages. However, it also encompasses several challenges. Three main challenges are control of combustion timing, limited power output and homogeneous charge preparation. Till date, researchers have been focused on engine models that are used for conventional fossil fuels. Models for renewable fuels are also available now. Only few are comprehensive, well-validated models that include accurate physical property data as well as a detailed description of the fuel chemistry. It is crucial to expand simulation studies by incorporating the well-validated numerical techniques by adopting different fuel options like renewable fuel blends etc.

1.4 Objective of the present study

The objective of the present work is to design and develop a comprehensive engine model by using CONVERGE CFD code. The model will integrate all the physical models that are involved in the diesel/biodiesel combustion modeling. The work concentrates on validation of the models applicable for diesel and biodiesel blends used for the heavy-duty and a Genset engine application. Three simulation models have been used in the present work. The first model is CAT3401 which is a heavy duty engine and diesel is used as fuel. A Genset application type VCR (Variable Compression Ratio) engine is fueled with two fuel, diesel and PB20 (20% Pongamia biodiesel + 80% mineral diesel) are also studied. The two models are named as VCR diesel and VCR PB20 respectively.

Once each of these models is validated, the models are further analyzed for the effect of different parameters such as Compression Ratio, Start of Injection, Fuel Injection Pressure and Exhaust Gas Recirculation.

Design of Experiments (DOE) is used to analyze the effect of the parameters which could drastically reduce the number of experiments needed to be conducted in order to obtain regression relations between the input parameters and the output responses. These regression

equations are useful in determining the optimum parameters. The optimum parameters were simulated using the CONVERGE CFD code and compared to the performance and emission characteristics. The mixture homogeneity of the optimum and baseline cases were also compared for all the 3 cases (CAT 3401, VCR diesel and VCR PB20) chosen.

1.5 Organization of the thesis

The thesis comprises of five chapters. Chapter 1, the present chapter gives an introduction about pollutants and their effects. Also, explaining the need for biofuel, HCCI combustion concept and its similarity features and main challenges associated with it. Along with that, a brief overview of CONVERGE software and objective of the present work is also discussed and the need for this study is also described. Chapter 2 gives a critical literature review on modeling of IC engines, factor influencing the combustion, biodiesel and their impact on combustion and RSM (Response Surface Methodology). Further, this chapter also focuses on literature related to early injection, variable CR, variable injection pressure and EGR. Chapter 3 details about the mathematical modeling used in CONVERGE software for the present study. It elaborates various algorithms used by the software to solve the CFD problem including combustion chemistry. Apart from these, engine specification, initial and boundary conditions are also described in this chapter. Response surface methodology (RSM) is also used to design the numerical experiments. In Chapter 4 the results and findings are discussed in detail and along with the validation of CONVERGE simulations RSM plotted to get optimized. Chapter 5 presents the conclusions of the work and future scope.

Chapter 2

Literature Review

This chapter deals with the review on state of art of numerical and experimental studies on the IC engine with different operating variables which effect the performance and emission characteristics using diesel and biodiesel blends. For better understanding of operating variables, literature is presented separately in each subsection. Further, some important findings from the literatures have been summarized.

2.1 State of the art CI engine

Various researchers have been contributing magnificently towards the development of IC engines from the inception of the idea. From the inception, the CI engine dominates in the IC engine category due to its wide range of applications and fuel efficiency. There are major advantages of CI engine over the SI engine. The thermal efficiency of CI engine is better than a SI engine. CO and HC emissions are also lesser than the gasoline engines. But CI engines cannot overtake the SI engines in all the aspects. The main disadvantages of CI engines are soot or particulate matter, NOx and low power density (Grondin et al., 2004). Apart from the above challenges, for accomplishing cleaner and more efficient engine operating mode, detail information is needed on the processes which take place in an IC engine. Performing experiments on an engine is troublesome due to the complexity involved in varying parameters and with precision of measurements. Simulations have the advantage over an expensive and time consuming experimental set-up. The today's makers of automobiles began

to use various controlling techniques like EGR and advanced fuel injection systems to control the diesel combustion. Unfortunately there is still a pressing need to minimize the exhaust emissions and improve the efficiency of CI engines.

2.2 Influential variables on performance and emission characteristics

Design of efficient engines relies on the several design and operating variables which can influence the performance and emission characteristics of the engine. This section emphasizes on the major influential parameters that affect the performance and emissions of a CI engine. The influence of the variables on each of the emissions characteristics and performance is discussed here. Among the variables, more emphasis is given to compression ratio, exhaust gas recirculation, start of injection, fuel injection pressure, piston bowl geometry and spilt or multiple injection.

2.1.1 Compression Ratio (CR)

Haraldsson et al. (2002) carried experiments on a multicylinder, variable compression ratio (VCR) engine for controlling the combustion phasing. Their experimental results show that intake air preheating can be warded off with increased CR. Brake thermal efficiency was increased with increase in CR, whereas a reduction in NOx emissions was observed. They also observed that increase CO emissions as the CR increases. This phenomenon is attributed to faster expansion, i.e. shorter reaction time. They also opined that cylinder size has an effect on the need for intake air heating and CR, due to cylinder wall heat losses.

Helmantel et al. (2005) used variable compression ratio by changing the intake valve closing timing through camshaft operation. They could operate in both HCCI and conventional modes and found that 60° cone angle was found to be superior compared to conventional 140° cone angle.

Mallamo et al. (2005) tested on a DI diesel engine to evaluate the combined effect of FIP and CR for a given operating range. Interestingly, soot emissions were decreased by reducing both CR (19 to 17.5) and FIP (700 to 550 bar) with the expense of BSFC (6.5%).

Laguitton et al. (2007) have carried out an experimental investigation on a single cylinder DI diesel engine to assess the effect of reducing the compression ratio from 18.4 to 16.0 on the

engine emissions. It was found that, although there was a small penalty in CO and HC emissions. Reducing the compression ratio or retarding the injection timing greatly reduced NOx and soot emissions when both premixed and diffusion–combustion phases were present. This issue was less important when the combustion was solely premixed.

Raheman and Ghadge (2008) tested engine performance for various compression ratios using different blends (Mahua-biodiesel and diesel). It was found that as the compression ratio increased from 18 to 20 the brake thermal efficiency and exhaust gas temperature increases.

Jindal et al. (2010) did an experimental investigation to find out the effect of compression ratio and injection pressure in a direct injection diesel engine fueled with Jatropha methyl ester. They carried out the experiments with FIP's of 150, 200 and 250, Compression Ratio 16, 17 and 18. It was found that with increase in injection pressure and compression ratio results in reduction of the BSFC, CO and soot emissions while HC emissions increased. NOx emissions did not deviate a great deal. They obtained optimum performance at 250 bar FIP and 18 Compression Ratio.

Sayin and Gumus (2011) investigated the impact of compression ratio and fuel injection timing on performance and emissions characteristics. They found the optimum values, with increased CR and fuel injection pressure by keeping the original injection timing fixed. An increase in CR, FIP and SOI leads to decrease in smoke opacity, CO and HC emissions while NOx emissions increase.

Muralidharan and Vasudevan (2011) studied the effect of performance, emission and combustion characteristics of a VCR engine using methyl esters of waste cooking oils. They varied the compression ratio from 18 - 21 with blends varying from B10 - B80. They found that B40 have the superior performance with CR 21. However, the slight increase in NO_x emissions was observed.

Costa and Sodré (2011) investigated the effect of compression ratio on SI engine for compression ratios 10, 11 and 12 using E22 (78% gasoline-22% ethanol) and E100 (Hydrous Ethanol) fuels. The results showed that higher CR improved torque, thermal efficiency, exhaust gas temperature and volumetric efficiency for both fuels for various speeds.

2.1.2 Exhaust Gas Recirculation (EGR)

Ladommatos et al. (1996 a, b, 1997 a, b) have carried out a series of experiments by varying the EGR to understand the various aspects associated with respect to the engine performance and emissions.

Ladommatos et al. (1996a) studied about the dilution, chemical, and thermal effects of exhaust gas recirculation on diesel engine emissions by reducing inlet oxygen with inert gas. The reduction in the inlet charge oxygen resulted in very large reductions in exhaust NO_x level at the expense of the increased soot and UHC emissions. Brake power and fuel efficiency also significantly deteriorated.

Ladommatos et al. (1996b) studied the effect of EGR on diesel engine combustion and characteristics. It focuses on the effects of carbon dioxide, which is a main constituent of EGR. It was established that dissociation of CO_2 had significant influence on emission characteristics. The high specific heat capacity of CO_2 had a legitimate effect on exhaust emissions including NO_x. These observations emphasize the importance of the higher heat capacity of CO_2, in bringing down the NOx.

Ladommatos et al. (1997a) studied the effects of replacing a portion of the inlet charge with water vapor. The entry of water vapor into the engine cylinder resulted in an increment in the soot emissions. This is imputable to the dilution effect of the inlet charge with water vapor. The sum of the various individual effects such as dilution, chemical, and thermal effects on the UHC and soot emissions were not equal to the overall effect of water vapor. This indicated that there might be another effect that increases the soot as well as the UHC emissions. The entry of water vapor in the inlet charge also resulted in a slight increment in the ignition delay, and a slight reduction in the peak cylinder gas pressure and temperature. The decrease in NOx emission was mainly due to the dilution of the inlet charge with water vapor to increase in specific high temperature capacity. The separate effects of water vapor on the unburnt hydrocarbon emissions (UHC) were small, whereas the overall result was relatively strong.

Ladommatos et al. (1997b) studied the effects of CO_2 and water vapor, the two primary constituents of EGR, on diesel engine combustion and emission characteristics. A comparison

was made for different effects of these components on combustion and emission characteristics. The comparison indicated that the dilution effect was the most significant one. Additionally, the dilution effect of CO_2 is more lofty than that for water vapor. On the other hand, the water vapor had a higher thermal effect in comparison to that of carbon dioxide due to the higher specific heat capacity. The chemical effect of carbon dioxide was, generally, higher than that of water vapor. The chemical effect of water vapor resulted in an increase in the soot and CO emissions. The results indicated that the chemical effect of carbon dioxide was to decrease the emissions. Likewise, the opposite chemical effect was observed on the ignition delay.

Buchwald et al. (2004) conducted experiments on a single cylinder diesel engine using diesel and studied parameters influencing homogeneous combustion. The test results show that homogenized combustion of diesel fuel at a lower part load operating point can be realized on an engine if an adequate injection strategy and adequate thermodynamic state and composition of the cylinder charge are selected. As expected lower emission level of NO_x and particulate matter could be sustained. The heat release rate was controlled by reducing compression ratio and increasing EGR rate.

Zheng et al. (2004) carried out a review on diesel engine exhaust gas emissions. They stated that EGR is an effective tool in controlling NO_x emission compared to retarding injection, which reduces combustion efficiency and increases ISFC. Diesel engines operating under stoichiometric conditions are more efficient. Maximum temperature can be controlled by increasing heat capacity of charge by introducing CO_2 and water vapor. CO_2 dilutes oxygen and prevents simultaneous combustion at more points when the mixture is premixed by hindering the availability of oxygen. But, EGR beyond a range could result in erratic combustion, extinguishes the flame etc. and thus at some regime of operation, EGR can give adverse effect.

Maiboom et al. (2008) experimentally investigated various effects of cooled EGR on combustion and emission characteristics of a direct injection diesel engine. They have carried on experiments at low load and part load conditions to measure the effects of EGR on NOx and PM emissions. It was found that at low-load conditions, utilization of high EGR rates at perpetual boost pressure is a manner to effectively reduce NOx and PM emissions, but a small increase of brake-specific fuel consumption (BSFC) and other emissions were observed.

Fathi et al. (2011) studied the influence of EGR on combustion and emissions of n-heptane/natural gas fueled engine operating in HCCI mode. They experimented using various fractions of EGR to investigate the possibility of controlling the combustion phasing and combustion duration. The results showed that EGR reduces mean charge temperature, and retarded the start of combustion and prolonged the combustion duration. They also concluded that increased EGR will improve fuel economy, reduce NOx emissions, and increase HC and CO emissions.

Qi et al. (2011) experimentally investigated the effect of start of injection (SOI) and EGR rate on the combustion and emission characteristics of a direct injection diesel engine with neat soybean biodiesel. The results showed that, with the increase of EGR rate, BSFC and soot emission were slightly increased, and oxides of nitrogen were decreased. Results also showed that retarding main injection timing, BSFC slightly increased, NOx emissions significantly decreased, and soot emissions remained almost same.

Squaiella et al. (2013) explains the strategies for emission control in diesel engine to meet Euro - VI emission standards. They used EGR along with post injection and particulate filters to attain Euro VI emission standard from an engine running under Euro - III. They concluded that an increase in EGR could reduce NOx emission significantly at the expense of increase in particulate matter. So either a high pressure post injection that could reduce PM by 66% or particulate filter that could reduce PM by 99% should be involved to keep the particulate emissions.

Fang et al. (2012) investigated the effect of pilot injection and EGR on combustion and emission characteristics of DI diesel engine operating in HCCI combustion. They concluded that NOx emissions decrease with increase in pilot injection quantity up to a limit and increase slightly beyond that limit. They also concluded that fuel consumption increases with the increase in pilot injection quantity and EGR. Variation of in cylinder pressure decreases with increase in pilot injection quantity up to certain limit from cycle to cycle.

Singh and Agarwal (2012) studied the combustion characteristics of twin cylinder diesel engine in which one cylinder is operated in HCCI mode. They used diesel vaporizer for preparing homogenous fuel air mixture and they used EGR for controlling the heat release rate. They conducted experiments at different mixture strengths and concluded that start of

combustion is highly sensitive to fuel-air ratio, as fuel-air ratio is increased, the combustion duration decreases rapidly.

2.1.3 Start of injection (SOI)

Kim and Lee (2007) studied the effect of narrow spray angle with advanced injection strategy on a diesel engine combustion and emission characteristics as well as engine performance. The start of injection was ranging from 30° bTDC to 50° bTDC. Injecting the fuel at very early helps to create HCCI combustion. Results showed that NOx emissions at 30° bTDC injection timing were remarkably decreased, while unburned hydrocarbon (UHC) and carbon monoxide (CO) emissions increased. Whereas, ISFC has increased as the injection timing was advanced.

Sayin and Canakci (2009) studied the effect of injection timing using various cases (21, 24, 27, 30 and 33° bTDC) on a single cylinder ethanol blended diesel fuel direct injection engine at different loads. NOx and CO_2 emissions have increased and UHC and CO emissions have decreased for retarded SOI. On the other hand, with the advanced SOI, HC and CO emissions reduced and NO_x and CO_2 emissions increased. Results were compared with the original injection timing of 27° bTDC and they found the optimum results at 33° bTDC SOI for 30 N-m load in view of UHC and CO emissions. SOI of 21° bTDC at 15 N-m load resulted in minimum emissions of NO_x and CO_2.

Yoon et al. (2010) investigated the effects of spray angle, single and multiple injections on combustion and exhaust emission characteristics in a common-rail diesel engine using dimethyl ether (DME). In this study, two types of spray angles 70° and 60° were examined and its results were compared with the original conventional spray angle of 156°. It was observed that the in-cylinder pressure is increased with advanced SOI. Advanced injection strategy reduced the soot and NO_x emissions increases. There were two peaks of heat release rate (ROHR) observed with multi-injection strategy. The in-cylinder pressure and ROHR of the first injection with narrow-angle spray were more compared to conventional spray angle. Whereas, ignition delay corresponding to second injection is shorter than the original.

Jayashankara and Ganesan (2010) studied the performance of a diesel engine by varying fuel injection timing and intake pressure at a constant speed engine using a CFD code STAR-CD. They reported that the advanced injection timing can increase in-cylinder pressure,

temperature, heat release rate, cumulative heat release and NOx emissions (6.88%). They also found that retarded SOI results in reverse trend. The results of supercharging showed a significant increase in NOx emissions due to availability of excess air and decrease in soot emissions because of higher rate of soot oxidation.They concluded that optimum SOI and the intake boost pressure are 12^0 bTDC and 1.21 bar respectively.

Mobasheri et al. (2012) analyzed the effect of injection strategies on engine performance and emissions of a heavy duty direct injection diesel engine. Their study focused on optimizing split injection stratagies with and without pilot injection. Three factors namely EGR, injection dwell time and amount of fuel injected were varied for analyzing the performance and emissions. Results showed that using pilot injection along with an optimized main injection has a noteworthy effect on the combustion process since it formed a separate 2nd stage of heat release which reduced the maximum combustion temperature and ultimately reduced the formation of nitric oxides. It was also found that injecting adequate fuel in advanced injection with an appropriate EGR significantly reduces soot without an evident increase in NOx.

Agarwal et al. (2013) found the effect of SOI and FIP on combustion emissions and performance characteristics on a single cylinder diesel engine. The experiments were conducted at a compression ratio of 17.5 for two injection pressures of 500 and 1000 bar with different SOI ranging from 15 to 4.875 °bTDC without EGR. Advanced SOI leads to longer ignition delay that promotes premixed combustion, rapid combustion, higher rate of heat release and increased peak pressure. Superior performance was found at lower FIP (i.e., 500 bar) due to its better combustion characteristics because of the larger droplet size distribution inside the cylinder.

Agarwal et al. (2013) experimentally investigated effect of fuel injection timing and injection pressure on combustion, emissions and performance characteristics of a single cylinder diesel engine. Cylinder pressure and rate of heat release (ROHR) were found to be higher for lower FIPs, however advanced injection timings shows higher ROHR in early combustion stages. For advanced SOI, BMEP and BTE increased, while BSFC and exhaust gas temperature reduced significantly. CO_2 and HC emissions decreased, however NOx emissions increased with increasing FIP. Lower CO_2 and HC emissions, and significantly higher NOx emissions were observed with advanced injection timings.

Agarwal et al. (2013) studied the effect of fuel injection timing and pressure on combustion emissions and performance in a single cylinder diesel engine. The experiments were conducted on a 510 cc single cylinder engine with compression ratio 17.5 with varying injection pressures of 500 and 1000 bar and SOI varying from 15 to 9.375 (°bTDC) without EGR. Advancing SOI leads to longer ignition delay that promotes premixed combustion and increased peak pressure. Also found that advancing injection with higher FIP of 1400 bar leads to knocking indicates the importance of EGR to be used. BSFC was low for advanced injections and so was for CO, HC and soot emission. Similar trend was observed for increasing FIP up to 1000 bar, beyond 1000 bar trend was reversed indicating the jet penetration was high for which the fuel started quenching at wall and entering crevice regions, resulting in tradeoff between NO_x and soot emissions.

Mohan et al. (2013) have reviewed fuel injection strategies to improve performance and emissions in compression ignition engines. They have included topics about changing FIP's SOI, and split injections in various fuels including biodiesel blends etc. They concluded that advancing fuel injection timing can help in reducing fuel consumption CO, HC emission at the expense of increasing soot but beyond a limit it can result in high smoke and poor performance. Advanced SOI combined with higher FIP can result in reduced soot concentration. While retarding SOI helps in decreasing NO_x at the expense of increased HC, CO and soot emissions, whereas deteriorates fuel consumption. Generally the optimized injection timing varies from engine to engine and has to be found for the balance of emission and performance. Ultra-high injection pressures in the range of 2000 bars results in reduction of soot emission mainly due to the better spray atomization and air entrainment

Zeraati et al. (2013) investigated split injection strategies for a diesel engine operating in PPCI mode of combustion. The experiments were designed using Taguchi fractional factorial method. The experiments were conducted at two different loads and factors considered are 1^{st} injection quantity, 1^{st} injection timing and 2^{nd} injection timing. Screening experiments were conducted to select the practical levels for different parameters for DOE. They concluded that Taguchi DOE analysis was feasible and was an effective method for parametric analysis. They found that less NOx emissions were formed using split injection strategy when compared to single injection strategy. They also concluded that NOx formation was mostly dominated by first injection timing.

Caton (2014) studied the importance of specific heat in IC engine combustion for a highly dilute engine (lower equivalence ratio) over the efficiency by experimental as well as simulation. He performed some experiments at higher compression ratio, exhaust gas recirculation, and shorter burn duration at very lean mixture by varying the injection timing at rated speed of 2000 rpm and found that there is an increase in thermal efficiency of engine. For the various condition examined, 21-35% of the total efficiency improvement were estimated due to increase in the ratio of specific heat.

2.1.4 Fuel injection Pressure (FIP)

Knecht (2008) reviewed the literature based on modern technologies and incorporating them in older engines to attain current emission norms. He explained about the importance of FIP being employed to reduce ISFC and soot emission and EGR for dissolving oxygen and increasing the heat capacity of charge, whereas turbo charger is used for engine downsizing and the necessity of alternative fuels to be used in part of depleting fossil fuels.

Fang et al. (2009) investigated effects of injection pressure on the combustion characteristics of a (HSDI) diesel engine. It was found that a reduced ignition delay and higher heat release rate peaks for higher FIP. It was also observed that the charge is more homogenous and most of the heat was released with an ultra low luminosity cool flame. The combustion characterstics at retarded SOI and higher FIP attributed to the simultaneous reduction of NOx and soot.

Jindal et al. (2010) conducted experiments on a single cylinder Genset engine by varying injection pressures (150, 200 and 250 bar) with Jatropha biodiesel. The best performance in terms of BSFC and BTE was obtained at 250 bar injection pressure. They observed that HC, NOx and soot emissions decreased with higher fuel injection pressure but a marginal increase in of CO emissions were reported.

Singh and Agarwal (2011) studied the effect of fuel injection pressure on diesel particulate size and number distribution in a CRDI single cylinder diesel engine. They varied fuel injection pressure from 300 to 750 bar and with various injection timings. The experimental data shows that the particulate size increases with increasing load and at full load particulate emissions were found to be highest. However, particulate size reduced with advanced injection timing and increasing fuel injection pressure. At lower injection pressures the

particulate number first increased and then decreased with retarding injection time because at lower pressures mixing depends on pressure and temperature prevailing in the combustion chamber.

Sayin et al. (2012) studied the effect of injection pressure on the emissions and performance characteristics of a single cylinder engine using different blends of canola oil methyl esters (COME). The experiments were carried out for various fuel injection pressures (180, 200, 220 and 240 bar) at a constant speed at various loading conditions. The results revealed that the fuel blends show distinct combustion and performance characteristics for various engine loads and fuel injection pressure. Increased fuel injection pressure resulted in lowered BSFC, BSEC and increased thermal efficiency for diesel and COME blends. The increased fuel injection pressure also augmented the maximum in-cylinder pressure due to more homogenized combustible mixture.

Sharma (2013) conducted experiments on single cylinder, direct injection diesel engine in HCCI mode. Initial experiments were performed on the conventional CI engine i.e. (23° bTDC injection timing, 3 hole nozzle with 180 bar injection pressure and 16.5:1 compression ratio) to generate baseline data. Later, experiments were performed with diesel as fuel, by advancing the injection timing, changing the compression ratio, injector nozzle and pressure i.e. (27° bTDC injection timing, 14.5:1 compression ratio and 5 hole nozzle with 220 bar and 240 bar injection pressure). Result shows that for 240 bar, NOx emission were significantly reduced as advanced injection timing gives sufficient time for the charge to mix homogeneously and leads to efficient combustion of charge, while low compression ratio reduces in-cylinder temperature to suppress NOx emission. Smoke concentration in the exhaust is decreased due to faster evaporation and relatively superior fuel–air mixing. Brake thermal efficiency is marginally reduced at 240 bar as compared to conventional diesel mode. Lower heat transfer losses helped to minimize the efficiency loss with the reduced compression ratio as compared to conventional mode. The exhaust gas temperatures (EGT) were found to be lowered, which signifies superior heat utilization and thereby reducing NOx emissions as compared to conventional diesel mode.

Agarwal et al. (2015) conducted experiments for various Pongamia biodiesel blends (10%, 20% and 50%) to study the effect of fuel injection pressure ranging from 300 to 1000 bar. Injection pressure influenced the injection rate profile and Sauter mean diameter. Advancing SOI resulted in lower soot emissions.

2.1.5 Piston Bowl geometry

The combustion of air and fuel mixture and emission formation in diesel engine show very close relationship with piston bowl geometry (Li et al., 2014). Experimental studies on the effects of different bowl geometries of diesel engines were represented by Jaichandar & Annamalai (2012). In their study, three bowl geometries, namely HCC (Hemispherical Combustion Chamber), TCC (Toroidal Combustion Chamber) and SCC (Shallow depth Combustion Chamber), were tested with diesel and biodiesel fuels. All the three piston bowl geometries were compared and found that NO_x emission is slightly higher but in CO, UHC and PM emission decreases in HCC and SCC bowl geometry as compared to TCC. The brake thermal efficiency of TCC piston bowl geometry was higher than HCC and SCC piston bowl geometry. Piston bowl geometry affects the combustion and hence, the performance characteristics of a diesel and biodiesel fuel operated engines. Further simulation studies have been used to optimize the piston bowl geometry and spray angle in order to increase the performance and reduce the emissions (Lim & Min 2005). The flow of gas inside the cylinder is controlled by swirl and turbulent kinetic energy. Optimized piston bowl geometry along with swirl ratio is modelled to reduce fuel consumption and emissions (Saito et al. 1986). Piston bowl geometry plays an important role in the motion of air and fuel inside the cylinder. The high swirl ratio developed from piston geometry may produce better air-fuel mixture (Fuchs & Rutland 1998). Park (2012) studied on DME engine and optimized engine combustion chamber for different operating conditions. Five different types of combustion chamber geometry were analyzed and reported that deeper cup piston bowl geometry, is best for reducing NOx, soot, HC and CO emissions. Béard et al. (1998) discussed different types of piston bowl geometries used, such as flat and W-shaped. It was observed that piston bowl can enhance the mixing rate of air and fuel and control the turbulence level. The small change in piston bowl geometry has an effect on swirl ratio and turbulence intensity. The W-shaped bowl produces more swirl and turbulence at TDC position as compare to flat piston bowl geometry. Prasad et al. (2011) studied three dimensional CFD simulations for flow of air-fuel mixture, swirl, in re-entrant combustion chamber. Several geometries were identified which had produced high swirl ratio and high turbulent kinetic energy (TKE) but a few number of piston bowl designs were identified for smaller engines. Payri et al. (2004) made five different types of piston bowl geometries and the results were validated with CFD analyses. It was observed that piston bowl diameter plays a lead role for flow of fuel near TDC. The CFD analysis got the potential to design equipment with higher performance and fewer emissions.

Song et al. (2008) analyzed seven different piston bowl shapes. It was found that the squish and swirl play a very important role in the turbulent generation in diesel engine. The model has been analyzed by coupling swirl, squish, turbulence and piston bowl shape for the better combustion. Raj et al. (2013) conducted numerical analysis on piston bowl geometry using STAR-CD CFD software. Four different configurations of piston bowl such as flat, inclined, center bowl and inclined offset bowl were analyzed. The center bowl geometry has better performance as compared to other bowl shapes due to its high tumble ratio, swirl, turbulent kinetic energy, and turbulent intensity.

2.1.6 Fuel Modification

The auto ignition properties of the fuel can be altered by fuel blends and additives. Kannan and Anand (2011) conducted experiments on DI diesel engine operating with a blend of 30% waste cooking palm oil (WCO) methyl ester, 60% diesel and 10% ethanol and compared the results with conventional diesel. The blend was named as Diestrol. It was found that maximum brake thermal efficiency of 31.3% was obtained. Compared to diesel, blended diesel showed reduction in carbon monoxide (CO), carbon dioxide (CO_2) and smoke emission by 33%, 6.3% and 27.3% respectively. Diestrol decreased nitric oxide (NO) emission by 4.3%, while slight increase in the levels of unburnt hydrocarbon (UHC) was observed. Several researchers, Koc and Abdullah (2013), Singh et al. (2014), Chavan et al. (2015) found that fuel modification is an effective way of controlling the combustion phasing, thereby achieving optimal combustion characteristics.

2.3 Biodiesel

The energy demand for various applications and appliances are growing at faster rate. Fossil fuels are the major contributor in achieving the demand. Use of Biofuel could minimize the world's dependency on fossil fuels and simultaneously reduces the CO_2 production. Since biofuels are produced from plants and biomasses, their renewable nature attracts all over the world. Biodiesel is an effective alternative source for the beneficial to meet the demand for internal combustion engines as it can be used as a substitute for the fossil fuels or it can be blended with the petro diesel. The typical sources of biodiesel are of two types, edible and non-edible. Edible sources of biodiesel may not be feasible option since its sustainability questions the food vs fuel. So the non-edible biodiesel is an attractive option over the former. Examples of such non-edible feed stocks are Jatropha curcas, Madhuca indica (mahua),

Pongamia pinnata (karanja), Hevea brasiliensis (Rubber seed), Azadirachta indica (neem), etc. Atabani et al. (2013) studied about various non-edible oils, with respect to their composition, plants growing conditions and the properties. They brought out the composition of fatty acids in various biofuels and their percentage present in them.

Sahoo and Das (2009) studied and analyzed the combustion of Jatropha, Karanja and Polanga based biodiesel as fuel in a diesel engine and examined the results. He found that bio-diesel blends can be easily incorporated in diesel engine without any major modification of current IC engine. They also analyzed the performance and emission of the engine and observed that brake thermal efficiency increased with reduced emissions except the NO_x. They also observed the effect of this blends over other factor like, temperature, pressure, injection timing etc.

Lapuerta et al. (2008) analyzed the engine emission and BSFC and BTE by varying the torque, load, and varying the speed range between 1500-3000 rpm for diesel, bio-diesel and its blends in diesel engine. They observed sharp reduction in particulate matter (soot) emission for bio-diesel than diesel. This is happening because of absence of aromatic content in the bio-diesel. However, NO_x increases due to availability of more amount of oxygen which is present in the biodiesel.

2.3.1 Why Pongamia

Area requirement of various possible fuel producing seeds to replace 20% diesel requirement are 4.10×10^6 hectare for Azadirachta indica (Neem), 2.33×10^6 hectare for Calophyllum inophyllum (laurel), 4.38×10^6 hectare for Jatropha curcas, and 7.98×10^6 hectare for Ziziphus mauritiana (Jujube), and in which Pongamia pinnata is comparatively favorable which requires marginable land of 1.99×10^6 hectare. Pongamia Pinnatta a fast growing leguminous tree, indigenous to Indian sub-continent, is one of the best from which bio diesel can be extracted. On considering the properties of Pongamia methyl ester as a fuel having cetane number of 55.84 is comparable with premium diesel of cetane number 60. Also it is superior to palm oil, soybean oil, and beef tallow when compared on the basis of flash point, pour point, cloud point etc. and also its composition. (Mohibbe Azam et al., 2005 ;Scott et al., 2008). Comparing the production cost to palm oil with €600 per ton and canola oil with €550 per ton while pongamia has only €48 per ton.

Mohibbe et al. (2005) have studied about prospects and potential of fatty acid methyl esters of some non-traditional seed oils for use as biodiesel in India. Murugesan et al. (2009) have reviewed about various biodiesel blends that are suitable for alternative as diesel and stated that at present India is importing 70% of our fuel requirements. Mixing 5% of biodiesel to this can save our pockets by Rs 4000 crores. Planning commission of India has launched biofuel project to increase the production of oil seeds from Jatropha carcass and Pongamia pinnata and has selected 200 districts in 18 states with this aim. Biodiesel has caught its attention in the global domain. Malaysia has encouraged the production of biodiesel from palm oil. Presently USA uses 50 million gallons and European countries uses 350 million gallons of bio diesel yearly by blending its 20% with diesel while France uses 50% mix of biodiesel. The review of Pongamia biodiesel combustion also reveals the following salient features. Pure Pongamia biodiesel can be directly used in diesel engines without any alterations with slightly inferior performance than that of diesel. Addition of little amounts of biodiesel to mineral diesel is a worthy strategy for increasing alternative fuel consumption and B20 is the best alternative fuel. Brake thermal efficiency of biodiesel (B20) is slightly increased and brake-specific energy consumption is reduced slightly when compared with B100. But in comparison with mineral diesel, the BSFC of B20 could not improve at baseline configuration whereas emission characteristics were reduced and at par with diesel in most of the literature available.

An et al. (2013) studied the physical properties of pure methyl ester for biodiesel and predict some physical properties like surface tension, viscosity, temperature, critical pressure etc. For these physical properties they propose the best prediction model on the basis of standard reference. This prediction model can be used to calculate properties of pure methyl esters namely Methyl palmitate, Methyl stearate, Methyl oleate, Methyl linoleate and Methyl linolenate. Every biodiesel is mainly consisting of these five types of methyl ester, so on the basis of their composition, properties of biodiesel can be calculated.

Scott et al. (2008), Naik et al. (2010) and Bala and Sandeep (2011) presented the proximate composition and fatty acid profiles for the Pongamia. Sahoo and Das (2009) reported that the Pongamia biodiesel is quite appropriate as an alternative to the mineral diesel. The chemical composition of Pongamia is reported in Pandey et al. (2012). B20 (80% diesel and 20% biodiesel) is a viable alternative for diesel in the present scenario of the

modern context (Raheman and Phadatare 2004). The policy goal of Indian government is also towards the target of 20% blending of biofuels (http://www.mnre.gov.in/).

2.4 Homogeneous charge compression ignition (HCCI)

Homogeneous charge compression ignition (HCCI) is a combustion concept which can be incorporated in any engine. The idea is to mix the fuel and air before the start of combustion and it is similar to that of compression ignition as the mixture gets auto ignited.

It can be observed from Yao et al. (2009), Bendu and Murugan (2014) that mixture preparation is the key in achieving combustion characteristics as that of the HCCI. There are two ways to improve the mixture homogeneity. First one is by improving the mixing rate of fuel and air and other is by increasing the ignition delay. The start of combustion can be delayed by decreasing compression ratio which is beneficial in mixing of the charge inside the cylinder but decreasing the CR may hamper the thermal efficiency.

Gan et al. (2011) reviewed the implementation of HCCI combustion in a direct injection diesel engine and its effects on pollutants. They reviewed the implementation of HCCI using early, late and multiple injection strategies. They also reviewed the effect of operating and design parameters such as compression ratio, swirl ratio, injection pressure, internal and external EGR, temperature of intake charge etc. on HCCI emissions particularly soot and oxides of nitrogen.

Bendu and Murugan (2014) reviewed the challenges related to homogeneous charge preparation and HCCI combustion control strategies. According to them, homogeneous charge preparation and combustion phase control are the two main challenges which will consequently affect the thermal efficiency and emissions of the engine. External and internal charge preparations have disadvantages such as low volumetric efficiency and oil dilution respectively.

Achieving HCCI combustion needs a reasonable control over ignition timing and rate of combustion. Several research organizations are working to control these parameters. HCCI technology is only limited to medium load conditions. For meeting heavy loads, HCCI combustion needs to be switched back to conventional CI combustion. Cold start capability is one of the limitations associated with the HCCI because of the lean mixture operation. HCCI operation may also result in high UHC and CO emissions; this is due to the fact that the

homogenous charge may be stored in the crevice region during the compression stroke and escapes the combustion. The lower temperature during the expansion stroke is also one of the reasons for the higher UHC and CO emissions as compared to conventional diesel. These challenges are the main blockages in its commercialization. Therefore, there is a need of research to reap the benefits of this wonderful technology.

2.5. Response Surface Methodology (RSM)

Response surface methodology is a technique to optimize the output parameters of a multi objective function. Response surface methodology has been widely applied in number of applications in the manufacturing fields for the design and development of new products, as well as in enhancing the existing design of the products (Casella et al. 1998).

Pandian et al. (2011) investigated the effect of injection parameters on performance and emissions of DI diesel engine using RSM method. Their work was based on investigation of the effect of injection system parameters injection pressure, injection timing and nozzle protrusion, on performance and emission on a twin cylinder diesel engine using response surface methodology. Injection timing varied from 18 to 30 degree bTDC and FIP from 150 to 250 bar and nozzle protrusion from 1 to 4 mm. They found that advancing the injection timing reduced CO, HC and soot emissions with increase in NOx emissions. They concluded that desirability approach of the RSM was efficient and simplest optimization technique. They also concluded that DOE was highly helpful in designing the experiments and also helped to reduce the number of experiments to be performed.

2.6 Review of literature

The major issues and findings are listed below:

- It is observed that HCCI combustion characteristics can be achieved by ensuring homogeneity in the mixture preparation.
- Mixture homogeneity can be improved by increasing the ignition delay or by improving the mixing rate of fuel and air.
- The parameters that were deemed most influential to improve mixture homogeneity were identified as CR, EGR, SOI and FIP.
- The mixing rate of fuel and air can be improved by higher FIP, whereas ignition delay can be increased by lowering CR, advancing SOI and increasing EGR rate.

- Emission reduction and performance improvement can be achieved simultaneously, by making use of multiple operating parameters and optimizing them considering interaction effects.
- RSM is an effective and efficient method for optimizing engine parameters.

2.7 Gaps observed from the literature

It is observed from the literature that the following areas did not receive much attention:

- Achieving mixture homogeneity of DI CI engines fueled with diesel/ biodiesel blend (PB20) by simultaneously varying CR, SOI, EGR and FIP.
- Achieving efficient performance of DI CI engine by parametric optimization of the above variables.
- Interaction effects of the parameters on the performance and emission characteristics of CI engine.

2.8 Objectives of Present Work

The objectives of the present work is to:

- Analyze the effect of different parameters such as Compression Ratio, Start of Injection, Fuel Injection Pressure and Exhaust Gas Recirculation of a DI CI engine to achieve HCCI combustion characteristics through parametric optimization.
- Analyze CAT3401 engine, on the basis of performance and emission characteristics
- Investigate the effects of different parameters on VCR diesel engine for better performance and emission characteristics.
- Explore the use of VCR engine with PB20 as an alternate fuel without sacrificing the performance and emission characteristics
- Investigate the effect of the parameters by obtaining regression relations between the input parameters and the output responses using RSM.
- To find out the optimum values of parameters suited for different engine configurations.

Chapter 3

Methodology

The present chapter deals with methodology adapted for the modeling and simulation of the CAT3401 and VCR engine using CONVERGE^{TM}. Mathematical modeling, reaction mechanism and physical properties of biodiesel have been covered in this chapter. This chapter also encompasses the geometrical specifications and computational details along with the grid independence test and detail procedure to execute the CONVERGE^{TM} based simulation. The experimental setup of VCR engine has also been discussed at the end of this chapter.

3.1 Engine Modeling and Simulation

The present chapter deals with modeling and simulation of IC engine. An axis symmetric sector model has been prepared in CONVERGE and simulations have been carried out with that model. Mathematical modeling, grid independence test and validation of simulation results have been covered in the current chapter. The detail procedure to execute the CONVERGE software is also described.

3.1.1 CONVERGE™ Solver

The CONVERGE™ (Richards et al. 2014) is a cutting edge CFD code which can eliminate the grid generation issues in the simulation. CONVERGE™ simulates 3-Dimensional (3D) IC engine simulations with elementary chemical reaction mechanisms. CONVERGE™ is a CFD solver package which solves the transient IC engine simulations in a customized manner. The fluid dynamics of the problems are governed by the equations of conservations of mass, momentum and energy. In addition to the conservation equations, transport of passive scalars, species and turbulence are also incorporated to simulate the IC engine combustion phenomena. CONVERGE™ also employs the equations to calculate thermodynamic properties, the equation of state and reaction rates. In order to employ the combustion modeling, the CONVERGE™ requires chemical kinetics which are essential to describe the fuel oxidation process.

CONVERGE™ has its advanced methods for grid generation and boundary behavior. CONVERGE™ also includes pioneering numerical methods and models for turbulence, spray, combustion, heat transfer, and cavitation. It has been observed from the literature ((Matsumoto et al. 2010),(Yang et al. 2013),(Kavuri et al. 2013),(Som and Aggarwal 2010),(Pomraning 2013)) that all of the models have been extensively validated for various examples of IC engines. CONVERGE™ is able of modeling several flow cases, it has been designed with several sub-models, which have the competence to model engines. Other CFD solvers, whose approach for engine modeling is to have an add-on to an existing solver. Whereas CONVERGE™ was designed from its inception to be the leading CFD solver for modeling the IC engines. The ease of grid generation for moving boundaries, adaptive mesh refinement, improved numerical accuracy, and latest sub-models are evidence of this pioneering code.

3.1.1.1 Mathematical Modeling

The in-cylinder flow is simulated by solving the governing equations that describe the conservation of mass, momentum, and energy. Additional equations are also included for the transport of passive scalars, species, and turbulence. It is necessary to solve both the mass and momentum equations together for the suitable computations of the pressure gradient in the momentum equation. Momentum and mass transport can be solved for both compressible and incompressible flows.

3.1.1.2 Mass and Momentum Transport

The compressible equations for mass transport and momentum transport are given by

$$\frac{\partial \rho}{\partial t} + \frac{\partial \rho u_i}{\partial x_i} = S, \tag{3.1}$$

$$\frac{\partial \rho u_i}{\partial t} + \frac{\partial u_i u_j}{\partial x_j} = -\frac{\partial P}{\partial x_i} + \frac{\partial \sigma_{ij}}{\partial x_j} + S_i, \tag{3.2}$$

Where the stress tensor (σ_{ij}) is given by

$$\sigma_{ij} = \mu\left(\frac{\partial u_i}{\partial x_j} + \frac{\partial u_j}{\partial x_i}\right) + \left(\mu' - \frac{2}{3}\mu\right)\left(\frac{\partial u_k}{\partial x_i}\delta_{ij}\right) \tag{3.3}$$

In the above equations, u is velocity, ρ is density, S is the source term, P is pressure, μ is viscosity, μ' is the dilatational viscosity (set to zero), and δ_{ij} is the so-called Kronecker delta. For turbulence model the viscosity is replaced by the turbulent viscosity (μ_t) given by

$$\mu_t = \mu + C_\mu \rho \frac{\kappa^2}{\varepsilon} \tag{3.4}$$

Where, C_μ is a turbulence model constant, κ is the turbulent kinetic energy, and ε is the turbulent dissipation.

3.1.1.3 Energy Transport

The compressible form of the energy equation is given by

$$\frac{\partial \rho e}{\partial t} + \frac{\partial u_j \rho e}{\partial x_j} = -P\frac{\partial u_i}{\partial x_j} + \sigma_{ij}\frac{\partial u_i}{\partial x_j} + \frac{\partial}{\partial x_j}\left(K_t \frac{\partial T}{\partial x_j}\right) + \frac{\partial}{\partial x_j}\left(\rho D \sum_m h_m \frac{\partial Y_m}{\partial x_j}\right) + S \tag{3.5}$$

where ρ is density, Y_m is the mass fraction of species m, D is the mass diffusion coefficient, S is the source term, P is the pressure, e is the specific internal energy, K_t is the turbulent conductivity, h_m is the species enthalpy, σ_{ij} is the stress tensor, and T is temperature. Turbulent conductivity given by

$$K_t = K + C_p \frac{\mu_t}{\mathrm{Pr}_t} \tag{3.6}$$

Where K is the conductivity, Pr_t is the turbulent Prandtl number and μ_t is the turbulent viscosity.

In addition to the usual convection and diffusion terms, the energy equation contains four extra terms. First, a source term is added to account for user specified energy sources, and turbulent dissipation. Second, a pressure work term, $-P\frac{\partial u_j}{\partial x_j}$, is added to account for compression and expansion. Third, a viscous dissipation term, accounts for kinetic energy viscously dissipating into heat. Last, a species diffusion term is added which accounts for energy transport due to species diffusion.

3.1.1.4 Species Transport

The species transport equation solves for the mass fraction of all the species in the domain. The species mass fraction is defined as

$$Y_m = \frac{M_m}{M_{tot}} = \frac{\rho_m}{\rho_{tot}} \tag{3.7}$$

Where, M_m is the mass of species m in the cell, M_{tot} is the total mass in the cell, ρ_m is the density of species k, and ρ_{tot} is the density in the cell. The species equations can be solved alone or together with any of the other transport equations. The compressible form of the species conservation equation is given by,

$$\frac{\partial \rho_m}{\partial t} + \frac{\partial \rho_m u_j}{\partial x_j} = \frac{\partial}{\partial x_j}\left(\rho D_t \frac{\partial Y_m}{\partial x_j}\right) + S_m \tag{3.8}$$

Where

$$\rho_m = Y_m \rho \tag{3.9}$$

and where u is velocity, ρ is density, ρ_m is the species density, Y_m is mass fraction of species m, D_t is the mass diffusion coefficient, and S_m is the source term. The turbulent mass diffusion coefficient is calculated by

$$D_t = \frac{\nu_t}{Sc_t} \tag{3.10}$$

Where, Sc_t is the turbulent Schmidt number. The source term in the species equation accounts for evaporation, chemical reactions (combustion) and other sub-models.

3.1.1.5 Passive Transport

A passive is a transported scalar that does not affect the solution of the other transport equations (e.g., mass, momentum, energy etc.). Some of the sub-models require that passives be added in order to activate the models (e.g., soot models). The passive transport equation will be solved only when passives are defined in the program. The compressible form of the passive scalar transport equation is given by

$$\frac{\partial \rho \phi}{\partial t} + \frac{\partial \rho u_i \phi}{\partial x_i} = \frac{\partial}{\partial x_i}\left(\rho D_t \frac{\partial \phi}{\partial x_i} \right) + S \tag{3.11}$$

Where u is velocity, ρ is density, D is the diffusion coefficient, S is the source term, and is φ a passive scalar. The diffusion coefficient is given by Equation 3.10.

3.1.1.6 Turbulence Modeling

To simulate diesel engine combustion, several processes such as spray dynamics, auto ignition, heat transfer, chemistry and turbulence should be taken into account. Also, the interaction between chemistry and turbulence should be considered. Turbulence greatly affects the reaction zone structure in both non premixed and partially premixed flames. For turbulence modeling in IC engines, the Reynolds Averaged Navier-Stokes (RANS) models are widely used. In these models, two equation models are widely used because of their simplicity and effectiveness. The Renormalization Group (RNG) k-$\mathcal{E}$ is used in this work because it is shown to be particularly suited for IC engine simulations.

When a turbulence model is activated, the boundary conditions for Turbulence Kinetic Energy (TKE) equation and turbulent dissipation (td) Equations should be specified. For TKE equation the three types of boundary conditions available are Dirichlet (d_i), turbulence intensity (*in*), and Neumann (*ne*). For the turbulent intensity condition, the boundary TKE is given as

$$k = \frac{3}{2} u_i^2 I^2 \tag{3.12}$$

Where k is TKE and I is turbulent intensity.

For wall boundary type, only one valid boundary condition Neumann is available for TKE. It is given by

$$\frac{\delta k}{\delta n} = 0.0 \tag{3.13}$$

Where k is TKE and n is wall normal vector.

The three types of inflow and outflow boundary conditions available for turbulent dissipation equation are Dirichlet (*di*), Neumann (*ne*), and turbulence length scale (*le*). The turbulent length scale is special case of Dirichlet boundary condition and the boundary turbulent dissipation is given as

$$\varepsilon = \frac{c_\mu^{3/4} k^{3/2}}{l_e} \tag{3.14}$$

Where c is a model constant (usually 0.09), k is the turbulent kinetic energy, and *le* is the turbulent length scale.

For wall boundary type, the Dirichlet boundary condition can be given as

$$\varepsilon = \frac{c_\mu^{3/4} k^{3/2}}{Ky} \tag{3.15}$$

Where ε is the turbulent dissipation in the center of the near wall cell (not at the wall Surface), y is the distance from the wall to the middle of the cell, c is a turbulence model constant, and K is Karmens constant.

3.1.1.7 Spray Modeling

The computational studies of fuel spray injection and atomization are extremely challenging because of the complex processes. They comprise of transient two phase, turbulent

flows at high injection pressures and with a wide range of temporal and spatial scales. Two approaches used to simulate spray modeling Eulerian–Lagrangian methodology, Eulerian–Eulerian two fluid methodologies. Recent studies also employed the hybrid approach in which Eulerian method is applied in the dense spray region and Lagrangian method in dilutes region. Even though employing these approaches, the accuracy of the simulations very much relies on the sub-models used for various physical phenomena like atomization, droplet collision, deformation and vaporization. Of the above mentioned processes, spray atomization has been proven to be really significant in determining the spray and combustion characteristics of an IC engine. Based on the literature Som and Aggarwal (2010), it was found that Eulerian–Lagrangian approach using the KH-RT atomization models has been widely employed for diesel engine simulations, where KH model is used for the primary breakup and KH-RT is employed for the secondary breakup as shown in Fig. 3.1. The liquid jet break up is caused by the instabilities at the interface of two fluids. The Kelvin-Helmholtz (KH) instability is due to high shear at the interface and Rayleigh Taylor (RT) instability is due to the density differences between two fluids.

If KH-RT breakup model is activated, the breakup length or intact core can be given as

$$L_b = C_{bl}\sqrt{\frac{\rho_l}{\rho_g}}d_0 \tag{3.16}$$

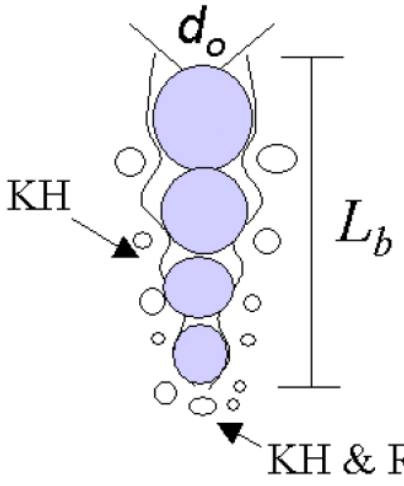

Fig. 3.1 Schematic of KH-RT spray breakup model

This model assumes that only KH instabilities are responsible for drop breakup inside of the characteristic breakup distance, L_b, while both KH and RT mechanisms are activated beyond the breakup length. The code first checks if the RT mechanism can break up the droplet otherwise the KH mechanism is responsible for drop breakup. An alternative to the KH-RT model, modified KH-RT model is used where both the breakup mechanisms are activated without considering the breakup length. In this model, aerodynamic instabilities are responsible for the primary breakup of injected blobs.

For collision and coalescence model, No Time Counter (NTC) collision method is used. This model is faster and more accurate than O'Rourke's model under certain conditions. The NTC method involves randomly determining sub-sampling of the parcels within each cell and this result in much faster collision calculations than O'Rourke's method, which incurs an additional computational cost. O'Rourke's method assumes that multiple collisions can occur between parcels and this process is governed by a Poisson distribution. However, the Poisson distribution is not correct unless collision has no consequences for the parcels. Since collisions change parcels, velocities, size, and number, the method of repeated sampling used by the NTC method generates more accurate answers. For drop/wall interaction rebound/slide model is used. The wall impingement depends on the properties of the drop, wall surface, and gas boundary layer in the near-wall region. If the wall temperature is less than the liquid boiling temperature, a collision of a drop on the solid surface may result in sticking, bouncing, spreading, or splashing. The rebound/ slide mode model is based on Weber number.

3.1.1.8 Combustion Modeling

SAGE is one of the detailed chemistry solvers for CONVERGE^{TM}, which calculates the reaction rates for each elementary reaction based on Arrhenius type correlation, while the CFD code solves the transport equations. The governing equations for mass and energy conservation can be solved for a given computational cell and at each computational time-step; and the species are updated appropriately. With an accurate reaction mechanism, SAGE can be applied for modeling any combustion regime such as ignition, premixed and mixing-controlled in gasoline and diesel combustion scenarios. It is to be noted that the SAGE is commonly used with a multi-

zone solver, which solves the cells with similar thermodynamic conditions in groups and saves run-time.

3.1.1.9 Soot Emission Modeling (Hiroyasu-NSC)

For the prediction of soot in IC engine simulation Hiroyasu's two step soot model (Hiroyasu and Kodota 1976) is widely used. This model considers soot formation from soot precursors and soot oxidation by oxygen.

Empirical Hiroyasu Soot model which is coupled with Nagle and Strickland-Constable model (NSC) is used to model the soot in the computational domain. Soot and particulate matter formation are mainly responsible due to improper combustion in the cylinder.

The production of soot mass M_s (g) can be determined in a single-step equation between the soot mass formation rate M_{sf} (g) and the soot mass oxidation rate M_{so} (g) according to Hiroyasu and Kadota (1976) given in eqn. (3.17)

$$\frac{dM_s}{dT} = M_{sf} - M_{so} \tag{3.17}$$

And the rate of formation is given in eqn. (18 and 19)

$$M_{sf} = SF.M_{form} \tag{3.18}$$

$$SF = A_{sf}P^{0.5}\exp(\frac{-E_{sf}}{R_uT}) \tag{3.19}$$

M_{form} is the mass of soot formation species,

P is the cell pressure,

R_u is the universal gas constant in cal/(Kgmol),

T is the cell temperature in K,

E_{sf} is the activation energy in cal/gmol and

A_{sf} is the Arrhenius pre-exponential factor.

Nagle and Strickland-Constable model (1962) model considers carbon/soot oxidation by two mechanisms reactions. This mechanism involves greater reactive areas 'A' and lesser reactive areas 'B'. The net reaction R_{total} given in eqn. (20)

$$R_{total} = \left(\frac{K_A P_{O_2}}{1+ K_Z P_{O_2}}\right) X + K_B P_{O_2}(1 - X) \ \left(\frac{mol}{cm^2 s}\right) \tag{3.20}$$

Where X is given in eqn. (21)

$$X = \frac{P_{O_2}}{P_{O_2} + \left(\frac{K_T}{K_B}\right)} \tag{3.21}$$

P_{O_2} is the oxygen partial pressure in atmospheres and the K value are rate constants for carbon shown as follows in eqn. (22, 23, 24 and 25)

$$K_A = 20 \exp\left(-\frac{30{,}000}{R_u T}\right) \quad \left(\frac{mol}{cm^2 s} atm\right) \tag{3.22}$$

$$K_B = 4.46\, x\, 10^{-3} \exp\left(-\frac{15{,}200}{R_u T}\right) \quad \left(\frac{mol}{cm^2} s\ atm\right) \tag{3.23}$$

$$K_T = 1.51\, x\, 10^{5} \exp\left(-\frac{97{,}000}{R_u T}\right) \quad \left(\frac{mol}{cm^2} s\ atm\right) \tag{3.24}$$

$$K_Z = 21.3 \exp\left(\frac{4{,}100}{R_u T}\right) \quad \left(\frac{1}{atm}\right) \tag{3.25}$$

The rate of soot oxidation according to Nagle Strickland-Constable oxidation model is given eqn. (3.26)

$$M_{so} = A_{so} . \left(\frac{6 M_s}{\rho_s D_s}\right) R_{total}\ MW_c \tag{3.26}$$

Where ρ_{pre} is the partial density of soot precursor; p is the pressure; T is the temperature; temperature; E_{sf} = 12500 cal/mol is the activation energy; A_{sf} is the Arrhenius pre-exponential factor normally set to 40; and the exponential factor for pressure, n is set to 0.5. The soot oxidation rate can be given by Nagle and Strickland-Constable model as

Where M_s is the soot mass, ρ_s is soot density, D_s is the soot particle diameter, W_c is the molecular weight of carbon. When a simple reaction mechanism is employed, the soot precursor is usually set as the fuel vapor. Acetylene or benzene may be taken as soot precursors as long as they have been included in the reaction mechanism.

3.1.1.10 NOx Emission Model

Extended Zel'dovich mechanism is employed in CONVERGE™ for solving the NO_x formation and it was formulated by Heywood (1988). The set of mechanism reactions are as follows: in eqn. (3.27, 3.28 and 3.29)

$$O + N_2 \Leftrightarrow NO + N \tag{3.27}$$

$$N + O_2 \Leftrightarrow NO + O \tag{3.28}$$

$$N + OH \Leftrightarrow NO + H \tag{3.29}$$

The rate constants of the following above eqn. (3.27 and 3.28) are shown in eqn. (30 to 35)

$$k_{R1f} = 7.6x10^{13} \exp\left(\frac{-38000}{T}\right) \tag{3.30}$$

$$k_{R1b} = 1.6x10^{13} \tag{3.31}$$

$$k_{R2f} = 6.4x10^{9}Texp\left(\frac{-3510}{T}\right) \tag{3.32}$$

$$k_{R2b} = 1.5x10^{9}Texp\left(\frac{-19500}{T}\right) \tag{3.33}$$

$$k_{R3f} = 4.1x10^{13} \tag{3.34}$$

$$k_{R3b} = 2.0x10^{14}exp\left(\frac{-23650}{T}\right) \tag{3.35}$$

where subscript ‘f’ denotes the forward reaction and ‘b’ denotes backward reaction.

In order to obtain quantitative comparisons with experiments an additional factor $\beta = 1.533$ is used. It is also used to convert NO to NOx, according to Environmental Protection Agency standard.

3.1.1.11 Reaction Mechanisms

The oxidation process of the fuel is modeled using a chemical kinetics reaction mechanism that contains species and their reactions with specified thermodynamic data for any given fuel. The fuel chemistry also includes reactions and their rate details that illustrate the oxidation process. Practical fuels are commonly composite mixtures of several species, and it is common to select a surrogate species from a chemical class to replicate the fuel. For example, diesel fuel is largely composed of alkanes, and is often represented by n-heptane for reaction mechanism. These fuel surrogates are chosen for their similar chemical properties and ignition behavior compared to the real fuel. The chemical kinetics essentially contains reactions that form products such as CO, CO_2 and hydrocarbons. Formation of NOx is also one of the crucial combustion characteristics, which is also adopted and modeled using extended Zeldovich Mechanism (Heywood 1988). SAGE chemical kinetic solver (Senecal et al. 2003), with n-heptane mechanism (Chalmers mechanism) is used for combustion modeling. The reason for choosing n-heptane is the H/C ratio of the n-heptane that is very close as that of the diesel. The mechanism consists of 42 species and 168 reactions for n-heptane combustion and NOx formation. Brakora et al. (2012) performed a reduction in the chemical mechanism which suits to the multi fuel component species like biodiesel and its blends; the reaction mechanism contains 69 species and 192 reactions.

3.1.1.12 Solution Order

Figure 3.2 summarizes the order of solution of transport equations for a single time step.

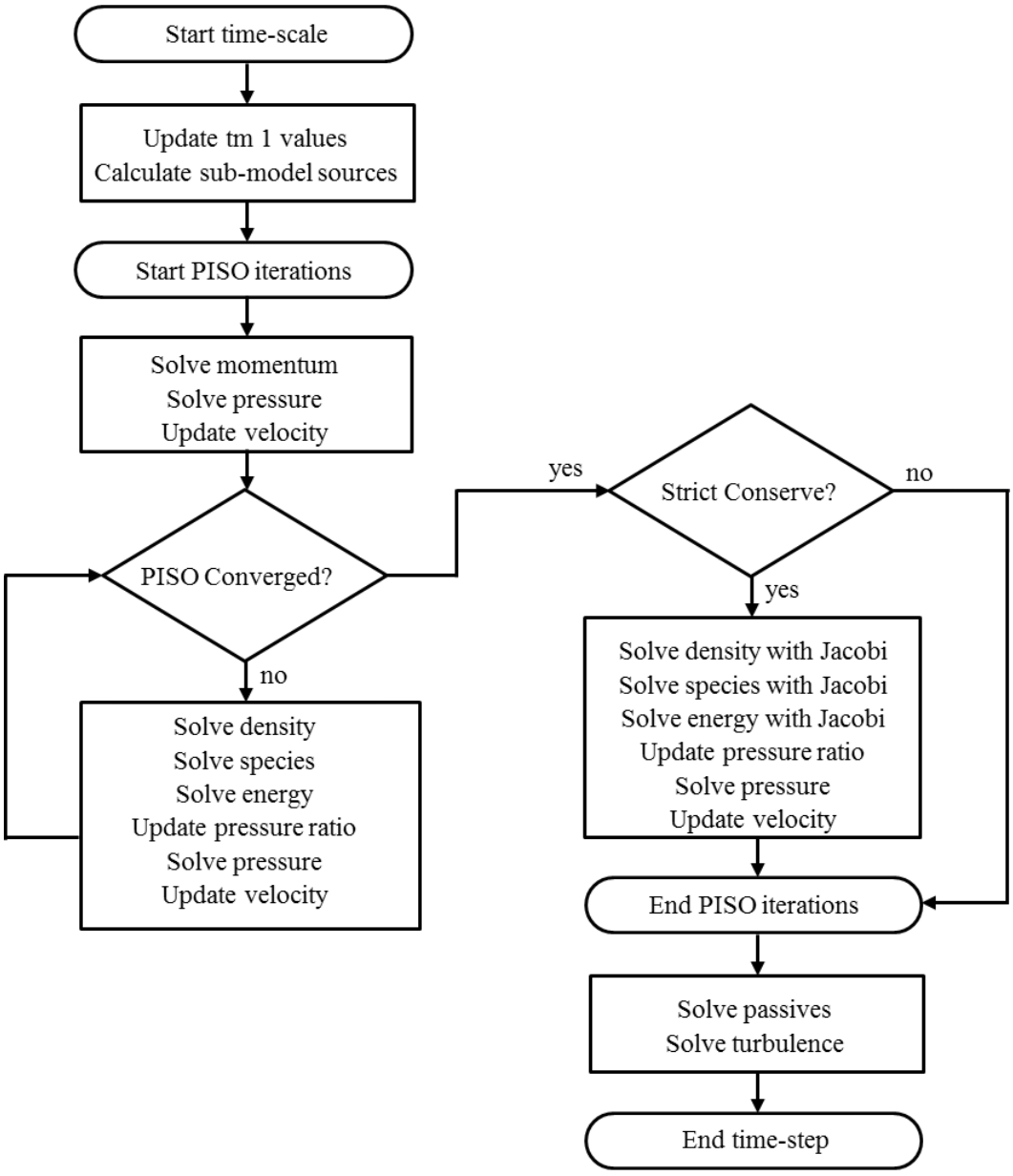

Fig.3.2 Solution order at each time step of the CONVERGE CFD code

3.1.1.13 Engine Geometry and Computational Details

A single cylinder DI diesel engine with the specifications given in Table 3.1 is simulated by using CONVERGE (CFD code). To reduce the computational time, a periodic engine sector case is adapted for the engine simulation. For a periodic engine sector case, CONVERGE automatically multiplies respective physical variables in the output files by a factor. The multiplier is used to provide the total quantity as if the entire engine cylinder (i.e., 360 degrees)

was simulated. The multiplier factor *is* given by mult_out = 360/angle of rotation. The sector model used in the present work has an angle of rotation 60°. This means the current sector model has the multiplier factor of six. CONVERGE^{TM} also uses Adaptive Mesh Refinement (AMR) to automatically refine the grid based on fluctuating and moving conditions, such as temperature and velocity. Computational domain of each sector model has 200,000 cells. The CFD analysis for two different engine geometries, viz, one is CAT3401 heavy duty engine and the other is VCR engine which is a Genset type engine. The computational domain for the two engines are shown in Fig.3.3 (a) & (b).

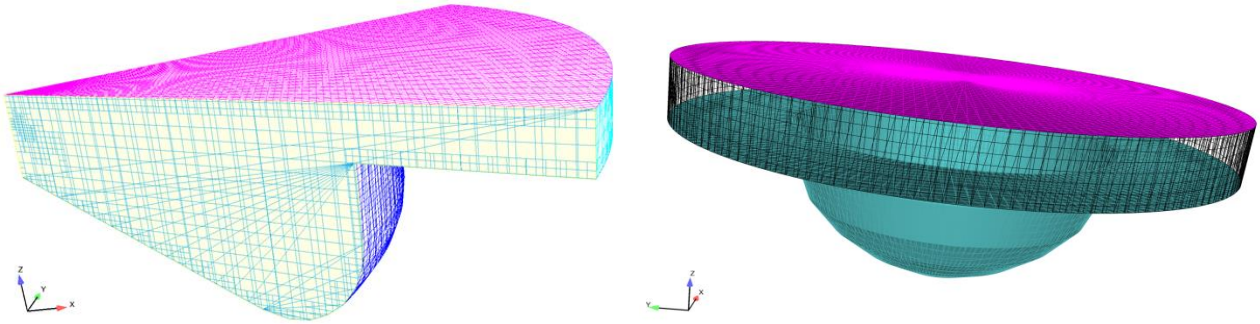

a) CAT 3401 engine model b) VCR engine model

Fig.3.3 Computational domain of CAT 3401 and VCR engine sector models

Table 3.1 Specifications of CAT3401 and VCR engine

	CAT 3401	**VCR engine**
Cylinder bore x stroke (mm)	137.6 x 165.1	87.5 x 110 mm
Connecting Rod length (mm)	261.62	234 mm
Displacement Volume (L)	2.44	0.66
Compression Ratio	15.1	17.5
Number of nozzle orifice x diameter (mm)	6 x 0.259	3 x 0.255
Hole angular position	30°,90°,120°, -30°,-90°,-120°	36.4°,-62.3° and 180°
Orifice orientation relative to the injector	125° included angle	145° included angle
Piston crown	Mexican Hat	Hemispherical
Intake valve closure (CA)	147° bTDC	144.5°bTDC

Swirl ratio (nominal)	1.0	0.7
Engine speed (rpm)	1600 rpm	1500 rpm
Fuel	Diesel	Diesel/PB20
Type of fuel Injection	Common Rail Direct Injection	Direct Injection
Injection Pressure (MPa)	90	28
Fuel Injected (kg/cycle)	0.1622	2.57778e-05
Overall Equivalence ratio	0.46	0.55
Injection duration	21.5 crank angle degrees	21 crank angle degrees
Start of Injection	11 °bTDC (baseline case)	23 °bTDC (baseline case)

3.1.1.14 Boundary and initial conditions

The initial and boundary conditions obtained from Curtis *et al*. (1995) are tabulated in Table 3.2. Total Kinetic Energy is given by $\kappa = 3/2*(UI)^2$, where U is the velocity, I is the initial turbulence intensity (5%). Turbulent dissipation is given by $\varepsilon=C_\mu^{3/4}\kappa^{3/2}le^{-1}$ where, ε is the turbulent dissipation, C_μ is a model constant, κ is the turbulent kinetic energy and le is the length scale.

Table 3. 2 Boundary and initial conditions

	CAT 3401	**VCR engine**
Initial Conditions		
Inlet air temperature (K)	310	303
Inlet air pressure (kPa)	184	111
Temperature Boundary Conditions (Law of Wall)		
Material	Aluminium	Aluminium
Cylinder wall temperature (K)	433	411
Piston wall temperature (K)	553	522
Head temperature (K)	523	495
Velocity boundary conditions		
Cylinder wall	Stationary	Stationary
Piston wall	Translating	Translating
Head	Stationary	Stationary
Turbulent kinetic energy (tke) boundary conditions		

Cylinder wall, Piston wall and Head	Zero normal gradient	Zero normal gradient
Turbulent dissipation (td) boundary conditions		
Cylinder wall, Piston wall and Head	Wall model	Wall model

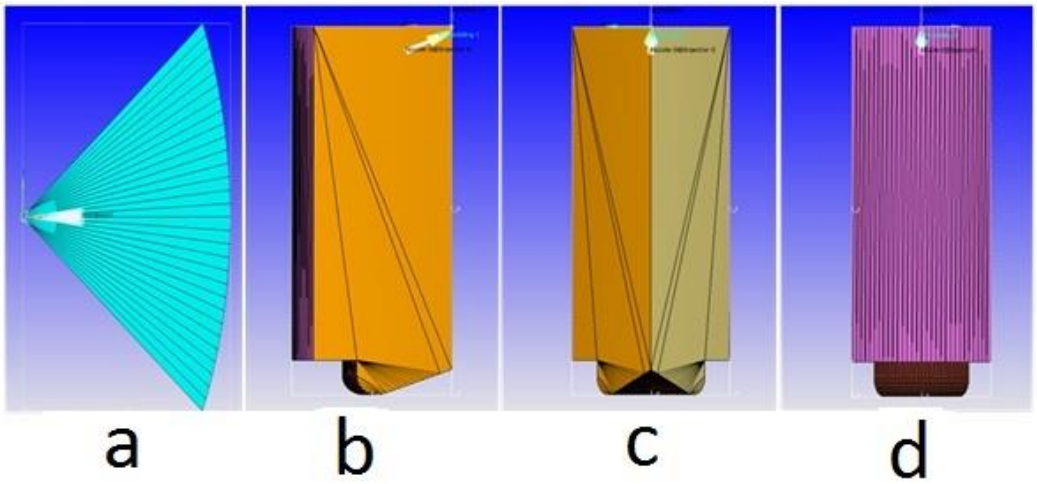

Fig. 3.4 Different views of the computational domain of CAT3401 sector model

3.1.1.15 Simulation Using CONVERGE

The following sequence of operations has been carried out during numerical simulations

1. An axis symmetric model with 60^0 sector angle signifies that 6 hole nozzle has been used for the present analysis. Initially sector model is created in CONVERGE solver and then it is imported in CONVERGE Studio. Geometry has been cleaned and exported as "surface.dat" file. The front and side views of the suface.dat file are shown in the Fig 3.4 : Fig. 3.4 (a) – (d). Figure 3.4 (a) is the top view of the geometrical model in which cylinder head can be seen. Figure (b) and (c), d are the back view, left side view and right side view respectively.
2. Then in case setup a set of initial and boundary conditions has been assigned to the geometry using input files which are written in ASCII format.
3. After assigning all these input and boundary conditions all these files were exported to a specified folder and simulation runs has been conducted using CONVERGE solver.
4. The simulation covers only the closed portion of the engine cycle, from intake valve closure (IVC) at -147 crank angle degree (CAD) after top-dead-centre (aTDC) to the exhaust valve opening (EVO) at +134 CAD aTDC for CAT 3401 engine model.

5. Similarly the VCR engine model is simulated with 360° full sector model from (IVC) -144.5 to (EVO) +144.5 CAD aTDC.
6. Inorder to carryout the simulations different submodels are used. These submodels are given in Table 3.3.

Table 3. 3 Key Sub models used in the CFD analysis

Turbulence model	RNG *k-ε* (Han & Reitz 1995)
Injection drop distribution	$\chi 2$ (chi squared) distribution (Richards et al. 2014)
Drop drag	Dynamic drag model (Liu et al. 1993)
Droplet Collision model	NTC model (Schmidt & Rutland 2000)
Collision outcomes model	Post Collision Outcomes (Post & Abraham 2002)
Drop turbulent dispersion	O'Rourke model (O'Rourke 1981)
Drop/wall interaction	Rebound/slide model (Gonzalez et al. 1992)
Evaporation model	Chiang drop correlations (Chiang et al. 1992)
Spray breakup	KH-RT (Beale & Reitz 1999)
Combustion	SAGE (Senecal et al. 2003)

3.2 Properties of Biodiesel

The use of Transesterified oils is gaining attention because of its renewable and environment friendly characteristic. The accuracy of engine simulations depends on the combustion kinetics and spray modeling. These phenomena are inturn depend upon the fuel composition. Typically there is a wide range of biodiesels available in the market extracted from the Coconut, Jatropha, Karanja (Pongamia), Rapeseed, Soy etc. Algae based biodiesel has been used in the recent times to run the IC engines. Characteristics of a biodiesel vary on the exact amount of methyl esters present in the biodiesel (Hoekman et al., 2012; Pfromm et al., 2011).

In India, Pongamia is widely available feedstock which was converted into a biodiesel by methanol based transesterification. It was also identified that there are five main methyl esters present in the Pongamia biodiesel (Bala and Sandeep 2011). They are as follows: Methyl Palmitate (**C16:0**), Methyl Stearate **(C18:0)**, Methyl Oleate **(C18:1)**, Methyl linoleate (**C18:2**) and Methyl linolenate (**C18:3**). Figure 3.5 shows the structure of the methyl ester components. The first two methyl esters Methyl Palmitate (**C16:0**), Methyl Stearate **(C18:0)** are saturated. The

other three (Methyl Oleate **(C18:1)**, Methyl linoleate (**C18:2**) and Methyl linolenate (**C18:3**)) are having one, two and three double bonds respectively (Brakora, 2012).

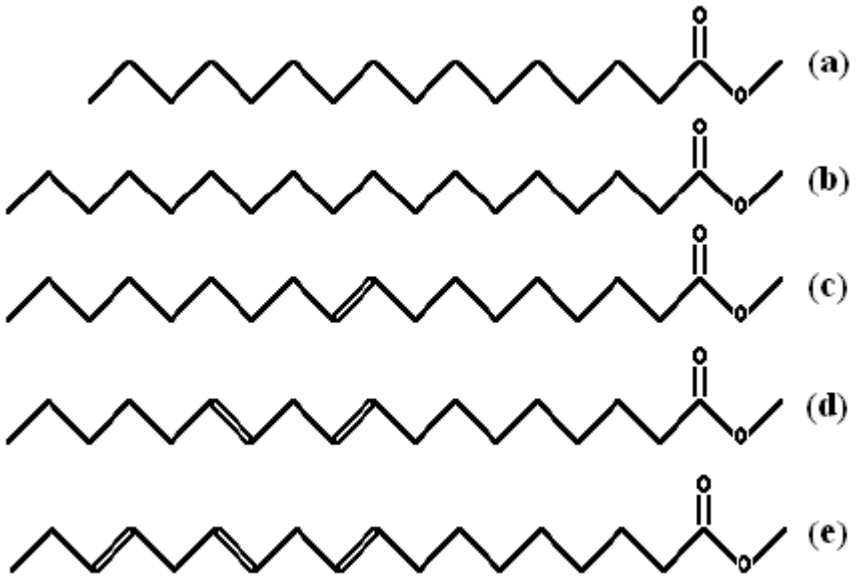

Fig. 3. 5 Structure of the five main Methyl esters: (a) Methyl Palmitate (**C16:0**) (b) Methyl Stearate **(C18:0)** (c) Methyl Oleate **(C18:1)** (d) Methyl linoleate (**C18:2**) and (e) Methyl linolenate (**C18:3**)

3.2.1 Physical Properties of Biodiesel

The properties of pure methyl esters are estimated by the empirical relations available in the various open literatures. The best model is chosen for each property in order to attain the reasonably good accuracy. The methodology to calculate each of the property is given in the present section. Critical properties of each methyl ester are taken from Ambrose method (An et al. 2013).

3.2.1.1 Vapour pressure

Data compilation method (Daubert & Danner. 1989) is one of the efficient way to estimate the vapor pressure over the wide range of temperatures.

$$\ln P_{vpr} = A + \frac{B}{T} + C \times \ln(T) + D \times E^4 \qquad (3.36)$$

Where P_{vpr} is the vapor pressure (Pa), T is the temperature in K, the constants A, B, C, D and E are given in the Table 3.4.

Table 3. 4 Constants used for the calculation of Vapour pressure (Daubert & Danner. 1989)

Methyl ester	A	B	C	D	E
C16:0	$1.705E^{02}$	$-1.818\ E^{04}$	$-2.053\ E^{01}$	$5.807\ E^{-06}$	2
C18:0	$1.812E^{02}$	$-1.905\ E^{04}$	$-2.202\ E^{01}$	$6.319\ E^{-06}$	2
C18:1	$1.875E^{02}$	$-1.915\ E^{04}$	$-2.299\ E^{01}$	$7.277\ E^{-06}$	2
C18:2	$1.765E^{02}$	$-1.910\ E^{04}$	$-2.113\ E^{01}$	$5.628\ E^{-06}$	2
C18:3	$1.748E^{02}$	$-1.910\ E^{04}$	$-2.102\ E^{01}$	$5.579\ E^{-06}$	2

3.2.1.2 Liquid density

Rackett equation is used for the calculation of liquid density (Reid et al. 1987). Different equations are formulated and given in the Table 3.5 based on the type of methyl ester. It is mainly depend on the temperature.

Table 3. 5 Simplified Rackett equation to calculate liquid density for pure methyl esters (Reid et al. 1987)

Methyl Palmitate	$\rho = \left(\frac{0.8508}{0.19364^{\Phi}}\right)$	$\Phi = \left(1 - \frac{T}{782.01}\right)^{2/7} - 0.86402$
Methyl Sterate	$\rho = \left(\frac{0.8498}{0.208501^{\Phi}}\right)$	$\Phi = \left(1 - \frac{T}{774.02}\right)^{2/7} - 0.86231$
Methyl Oleate	$\rho = \left(\frac{0.8595}{0.220175^{\Phi}}\right)$	$\Phi = \left(1 - \frac{T}{764.00}\right)^{2/7} - 0.86011$
Methyl Linoleate	$\rho = \left(\frac{0.8715}{0.202608^{\Phi}}\right)$	$\Phi = \left(1 - \frac{T}{795.08}\right)^{2/7} - 0.86672$

Methyl Linolenate	$\rho = \left(\frac{0.895}{0.264083^{\phi}}\right)$	$\phi = \left(1 - \frac{T}{800.75}\right)^{2/7} - 0.88763$

3.2.1.3 Viscosity

The viscosity is estimated by using two methods such as Orrick and Erbar method and Letsou and Stiel method depend on the value of reduced temperature T_r ,Where $T_r = T/T_c$. Where, T_C is the Critical Temperature.

3.2.1.3.1 Orrick and Erbar method **(Reid et al. 1987)**

This method works well when the T_r is less than 0.75.

$$ln(\eta_L/\rho_L M) = A + (B/T) \quad (3.37)$$

Where η_L is the liquid viscosity (cP); ρ_L is the liquid density at 20^o C (g/cm^3); M is the molecular weight and the constant A and B are as in Table 3.6.

Table 3. 6 Constants used for liquid viscosity in equation (3.37)

	A	B	ρ_L
Methyl Palmitate	-11.31	2279	0.86541
Methyl Sterate	-11.73	2477	0.86395
Methyl Oleate	-10.83	2099	0.87384
Methyl Linoleate	-9.93	1721	0.88570
Methyl Linolenate	-9.03	1343	0.88346

3.2.1.3.2 Letsou and Stiel method **(Reid et al. 1987)**

When the reduced temperature is above 0.7, the assumption that *ln* η is a liner function of the reciprocal of absolute temperature is no longer valid. Hence the following method should be applied.

$$(\eta_{sL}\xi) = (\eta_L\xi)^0 + \omega(\eta_L\xi)^1 \quad (3.38)$$

$$(\eta_L \xi)^0 = 10^{-3}(2.648 - 3.725\, T_r^1 + 1.309\, T_r^2) \quad (3.39)$$

$$(\eta_L \xi)^1 = 10^{-3}(7.425 - 13.39\, T_r^1 + 5.933\, T_r^2) \quad (3.40)$$

$$\xi = 0.176 \left(\frac{T_c}{M^3\, P_C^4}\right)^{\frac{1}{6}} \quad (3.41)$$

where η_{sL} is the liquid viscosity (cP) and P_C (critical pressure). All the critical properties are taken from Ambrose Method (An et al. 2013).

3.2.1.4 Liquid thermal conductivity

Thermal conductivity of the methyl esters were estimated by using the equation (3.42).

$$\lambda_L = A + BT \quad (3.42)$$

Where the A and B are taken from the Data Compilation (Daubert & Danner. 1989) and are given in the Table 3.7.

Table 3. 7 Constants used for thermal conductivity in Eqn (3.42)

	Methyl Palmitate	Methyl sterate	Methyl Oleate	Methyl linoleate	Methyl Linolenate
A	0.1546	0.1411	0.14015	0.1463	0.1471
B	-1.439E-4	-1.331E-4	-1.3316E-4	-1.33E-4	-1.33E-4

3.2.1.5 Surface tension.

Surface tension of the pure methyl esters was calculated by using the formulae given in the Table 3.8 over the range of temperatures.

Table 3. 8 Formulae for Surface Tension (An et al. 2013)

Methyl Palmitate	$\sigma = 50.63601(1 - \frac{T}{782.01})^{\frac{11}{9}}$

Methyl State	$\sigma = 49.4631(1 - \frac{T}{774.02})^{\frac{11}{9}}$
Methyl Oleate	$\sigma = 55.8376(1 - \frac{T}{764.00})^{\frac{11}{9}}$
Methyl Linoleate	$\sigma = 50.7066(1 - \frac{T}{795.08})^{\frac{11}{9}}$
Methyl Linolneate	$\sigma = 51.1895(1 - \frac{T}{800.75})^{\frac{11}{9}}$

3.2.1.6 Specific heat (Cp)

The specific heat of the pure metyl esters were measured as function of n_c. (n_c= no of carbon atoms present in the carboxylic acid moiety – 1) and temperature (Chakravarthy et al. 2007). The correlation is given in the equation (3.43).

$$Cp = \frac{103.16+(16.273*n)+(0.04735*n*T)}{M} \quad (3.43)$$

3.2.1.7 Latent heat of vaporization

Latent heat of vaporization is estimated by using the correlations from the equations (Reid et al. 1987). .

3.2.1.7.1 Pitzer acentric factor correlation

Pitzer et al. showed that ΔHm can be correlated to Tc, Tr, and ω expressed by the following equation. ω is the acentric factor (An et al. 2013).

$$\frac{\Delta H_v}{RT_C} = 7.08(1 - T_r)^{0.354} + 10.95\omega(1 - T_r)^{0.456} \quad (3.44)$$

The above equation holds good for the T_r from 0.6 to 1 as claimed in (Reid et al. 1987). Where ΔH*v* is the latent heat of vaporization (J/mol); and R is the gas constant.

3.2.1.7.1 Fish and Lielmezs method

Fish and Lielmezs suggested another formulation for low temperatures as shown below (Reid et al. 1987).

$$\Delta H_v = \Delta H_{vb} \frac{T_r}{T_{br}} \frac{X+X^q}{X+X^p} \quad (3.45)$$

$$X = \frac{T_{br}}{T_r} \frac{1-T_r}{1-T_{br}} \quad (3.46)$$

Where ΔHvb is the latent heat of vaporization at the normal boiling point (An et al. 2013).

Table 3. 9 Components (Methyl esters) of Pongamia Biodiesel and its composition (Bala & Sandeep 2011)

Name of the Methyl ester	Composition %
Methyl Palmitate	7.18
Methyl Sterate	3.32
Methyl Oleate	66.61
Methyl Linoleate	17.38
Methyl Linolenate	5.51

Composition of the methyl esters is given in the Table 3.9. Based on the composition the mass fractions of individual methyl esters were estimated for PB 20 fuel and its values are given in the Table. 3.10.

Table 3. 10 PB20 fuel composition used for the simulations ((Bala & Sandeep 2011), (Brakora & Reitz 2013))

Mechanism Species	**Property species**	**Chemistry species**	**Composition (mass fraction)**
Mpalm	methyl palmitate	md	0.0162
Mstear	methyl stearate	md	0.0075
Molea	methyl oleate	md9d	0.0511
Mlinl	methyl linoleate	md9d	0.0393
Mlinln	methyl linolenate	md9d	0.0124
nc7bio	methyl oleate	nc7h16	0.0995
nc7h16	tetradecane	nc7h16	0.7737

3.3 Grid independence test

Conventional grid generation is a major drawback for a variety of applications in CFD. Users may spend lots of time in grid generation to model complex geometries. Several models with complex geometries turn out to be unworkable because of the time and costs involved in the manual grid generation. The present CFD solver "CONVERGE" implements a novel approach for automatic generation of grid at run time. It employs a method called modified cut-cell Cartesian grid generation. In this method, the surface of the geometry is immersed inside a Cartesian block. The cells are cut at the intersecting surface; later the intersection information (e.g., surface areas, normal vectors, etc.) is reduced and then stored in each cell. The method enables for complicated surface intersection can be much easier for the simulations. The method also creates the grid internally during the transient simulation. In case of moving surfaces, the process includes: moves the surface to a proper location, cuts the boundary cells, refines any embedded areas, and then removes the refinement from the embedded location. For fixed surfaces, it performs the process only once at the time of the start of the simulation and then again whenever refinement or removing embedding is identified. For moving geometries, it performs this grid generation process at each time-step.

3.3.1 CAT3401 engine

Computational grid is generated by the above said inbuilt methods. Three basic grid sizes were selected to study the in grid dependency test. The base grid sizes were taken as 2.5mm, 2 mm and 1.4 mm shown in the Table 3.11. Pressure vs crank angle corresponding to three basic grid sizes are shown in Fig 3.6.

Table 3. 11 Grid independence test results for CAT3401 engine model

Mesh resolution	Fine	Intermediate	coarse
Basic grid size (mm)	1.4	2.0	2.5
Normalized time required for a simulation	1	0.75	0.47
Peak pressure (bar)	99.29	90.26	85.17
Peak pressure difference against experimental	1 %	-8.0%	- 13.18%

The experimental results of (Curtis et al. 1995) has been taken as reference for the simulation analysis. Major findings from the grid independence test are summarized in Table 3.11. Among the fine, intermediate and coarse grids, the fine mesh performed well with respect to the deviation of peak pressure from the experimental study. There is no improvement in the accuracy is found if the mesh size is reduced further. Therefore the fine mesh is considered to be the best for the simulation accuracy. But the computational time is increased by 33.3% and 112.7% respectively as compared to intermediate and coarse grids. Though the fine mesh takes longer computational time the usage of the same is justified because the simulation of IC engine has modeling of main physical phenomena such as spray, turbulence, combustion and emissions. These physical models require a large number of cells in order to predict different entities related to the models with reasonably good accuracy. The computational time for a fine mesh case averaged for 18 hours. A closer inspection on both the experimental cases shows that the in-cylinder pressure trace is asymmetrical. The in-cylinder pressure of experimental and simulation cases are compared and found that the results are in good agreement with each other. It is also observed that the in-cylinder pressure for simulation case is slightly higher than the experimental case. This may be due to the fact that the tendency of escaping of air- fuel charge through the crevice wear region. This will lead to decrement in in-cylinder pressure during the combustion phenomena.

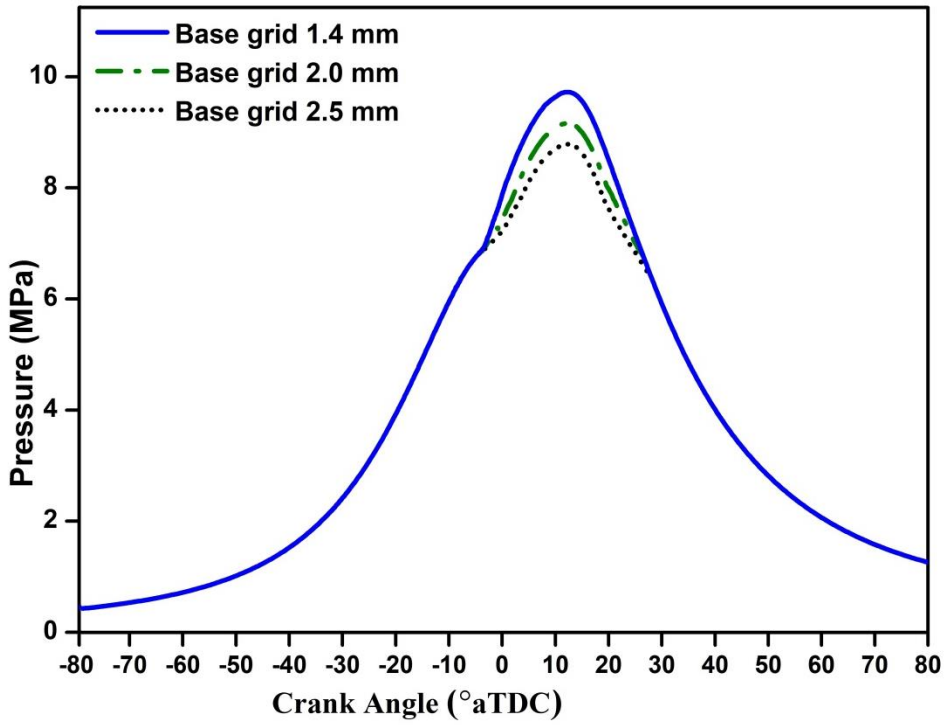

Fig. 3.6 Variation pressure vs crank angle for different basic grid sizes for CAT3401 engine

3.3.2 VCR engine

VCR engine model has also been tested for the grid independency. Three types of base grids were selected 2.6, 1.9 and 1.4 mm, based on the previous experiences. The VCR engine model was simulated based on the selected base grids and compared for pressure vs. crank angle in Fig.3.7. It was found that the pressure traces were differing significantly at the top dead center from 2.6 to1.4 mm. It is also observed that the difference between 1.9 and 1.4 were minimal. Hence base grid size 1.9 mm ×1.9 mm ×1.9 mm preferred over the other in view of computational time and accuracy. The computational time for the 1.9 mm base grid was 12 hours.

Table 3. 12 Grid independence test results for VCR engine model

Table.			
Mesh resolution	Fine	Intermediate	coarse
Basic grid size (mm)	1.4	1.9	2.6
Normalized time required for a simulation	1.72	1	0.52
Peak pressure (bar)	65.5	65.4	60.15
Peak pressure difference against experimental	0.77 %	0.61 %	- 8.07 %

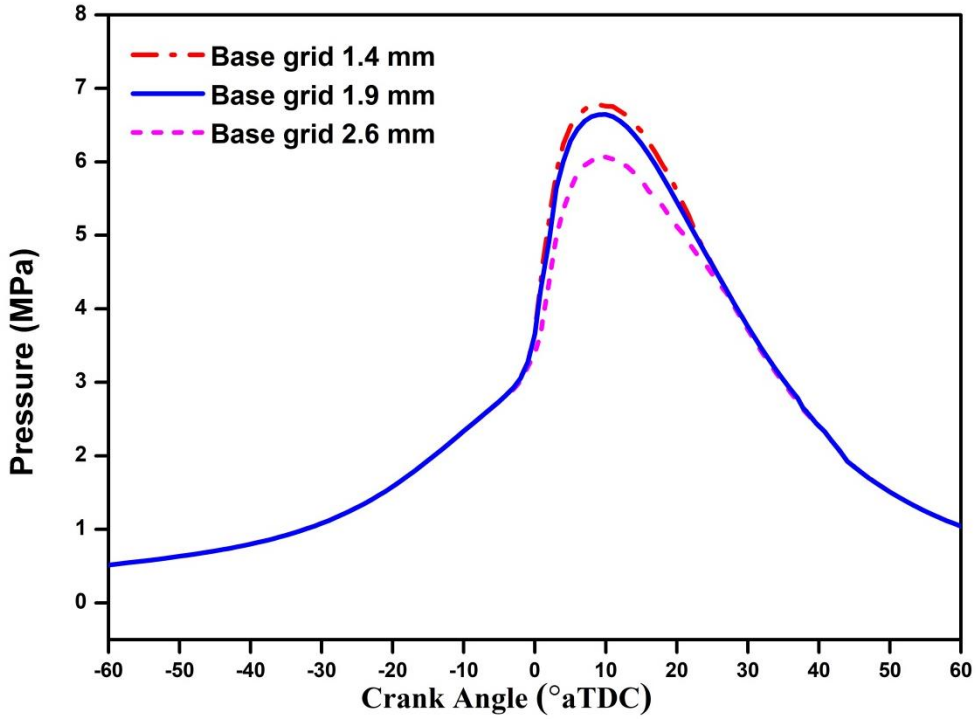

Fig. 3. 7 Variation pressure vs crank angle for different basic grid sizes for VCR engine

3.4 Experimental setup of VCR engine

VCR engine is a single cylinder, naturally aspirated, four-stroke, Compression Ignition type connected to an eddy current dynamometer for loading. This engine is commonly used in farming sector for providing irrigation to the fields.

The experimental setup (Fig.3.8) shows all the essential devices for the measurement of cylinder pressure, injection pressure and crank angle. One pressure sensor is affixed to the engine head by a case to measure the combustion chamber pressure and other sensor is used to measure the fuel line pressure. The test rig also consisting of transmitters for air and fuel flow measurements. Two rotameters were equipped for engine cooling and calorimeter for water flow measurement. Different temperatures such as exhaust gas, cooling water, calorimeter water inlet and outlet were recorded. The specifications of the engine and instrumentation used are given in Table 3.13.

Fig. 3.8 Experimental setup of the VCR engine

Table 3. 13 Specifications of the VCR engine test rig

Product code	240PE
Engine Type	Single cylinder, 4 stroke, Compression Ignition, water cooled.
Stroke	110 mm
Bore	87.5 mm.
Connecting rod length	234 mm
Capacity	661 cc.
Power	3.5 KW
Speed	1500 rpm
CR range	12:1-18:1
Fuel Injection variation	17- 26 degree bTDC
Fuel injection opening pressure	200 bar
Number of nozzle holes	3
Hole angular position	θ = 36.4°, -62.3° and 180°
Nozzle hole Included angle	130°
Dynamometer	eddy current Type, water cooled, with loading unit
Dynamometer arm length	185 mm
Propeller shaft	With universal joints
Air box	M S fabricated with orifice meter and manometer

Orifice diameter	20 mm
Calorimeter	Pipe in pipeType
Piezo sensor	Combustion: Range 0 – 345 bar, with low noise cable Diesel line: Range 0 – 345 bar, with low noise cable

3.4.1 NO_x emission conversion

The units NO_x emission conversion has been converted from ppm to g/kWh using formulae given by Maiboom et. al (2008).

$$NOx\left(\frac{g}{h}\right) = \left(\frac{M_{NO2}.NOx(ppm).Q_{exhaustdry}}{1000*V_m}\right) \quad (3.47)$$

Where M_{NO2}=46.005 g/mol and V_m= 22.41 m^3/mol at standard temperature and pressure

$$Q_{exhaustdry} = FMF.\left[\frac{(1+AFR_{st}).m}{\rho_{burnedgas}} + \left((Y-1).\frac{AFR_{st}}{\rho_{air}}\right)\right] \quad (3.48)$$

Where

$AFR_{st} = 15.176$, $\rho_{burnedgas} = 1.33$ kg/m^3, $\rho_{air} = 1.184$ kg/m^3, m is the mass of dry exhaust gases in one kilogram noncondensed exhaust gas (equal to 0.924 kg).

After getting NO_x emissions in terms of g/h, it is divided by indicated/brake power (i. e kW) to get NO_x in terms of g/kWh.

$$NOx\left(\frac{g}{kWh}\right) = \frac{NOx\left(\frac{g}{h}\right)}{BP\ or\ IP} \quad (3.49)$$

3.4.2 Soot emission conversion

AVL 437Csmoke meter is used to measure the smoke opacity. Smoke meter measures smoke in terms of HSU (i.e. Hatridge Smoke Unit). Soot in HSU is converted into g/h. conversion chart from HSU to g/m^3.

$$Smoke\left(\frac{g}{h}\right) = 10^{-3} * smoke\left(\frac{g}{m^3}\right) * Q_{exhaust} \quad (3.50)$$

$$Q_{exhaust} = FMF.\left[\frac{1+AFR_{st}}{\rho_{burnedgas}} + \left((Y-1).\frac{AFR_{st}}{\rho_{air}}\right)\right] \quad (3.51)$$

$$smoke\left(\frac{g}{kWh}\right) = \frac{smoke\left(\frac{g}{h}\right)}{BP\ or\ IP} \quad (3.52)$$

3.5 Response Surface Methodology

Optimization is known to be, improving the performance of any system in order to get maximum benefit with minimum effort. In general, most of the cases each factor has been analyzed on the basis of output responses. Varying one factor at a time fails to consider any possible interactions between the factors. Hence a systematic approach that could give a better understanding of performance and emissions of the engine by varying several parameters at a time. Design of experiments (DOE) is an effective method in optimizing the engine parameters to evaluate the combined effect of input factors on output responses. Though a few studies were reported using DOE, it was found that much work has not been done in analyzing engine simulations using DOE, and so it offered a scope for this study. Response surface methodology (RSM) is one of the DOE techniques which was originally developed to model experimental responses and then migrated into the modeling of numerical experiments as well. Like fractional factorial designs, RSM is useful in reducing the number of runs to a realizable size to save time (computational/working) and human efforts. It can also predict the model with reasonable accuracy (Pandian et al. 2011; Box and Draper 1987).

Response surface methodology (RSM) (Box and Draper, 1987) is a set of mathematical and statistical techniques for building an empirical model. The objective of RSM is to optimize an output variable (response) which is effected by several input variables (independent variables).

The simple approximating function is a 2nd order polynomial and be represented in eqn. (3.53)

$$y = \beta_0 + \sum_{i=1}^{n} \beta_i x_i + \sum_{i=1}^{n} \beta_{ii} x_i^2 + \sum_{1 \le i \le j}^{n} \beta_{ij} x_i x_j + \varepsilon \quad (3.53)$$

Where, 'n' is the number of variables, β_0 is the constant term, β_i is the coefficient of linear terms, β_{ij} is coefficient of interaction terms and 'ε' denotes the error. Factorial designs allow an experimenter to evaluate not only effects of factors, but also any interaction effects between factors. The linear response surface model shown above is not always accurate since few factors might interact with each other. Factorial designs allow an experimenter to evaluate not only effects of factors, but also any interaction effects between factors. Each level of every factor is

tested with each level of every other factor resulting in all 3n treatment combinations, if it is a three level factorial design. Therefore, the number of experimental runs for three-level factorial designs can become impractical when the number of factors are large. The use of fractional factorials is the most efficient technique to reduce the number of observations and still obtain the desired information.

Summary

This chapter described the methodology adopted for both numerical and experimental procedures. CONVERGE^{TM} is used for engine simulations. The two validated models were tested in a grid independence test. Proper grid size has been chosen for both the models. CAT3401 is a heavy duty engine model with diesel as fuel. VCR is a genset engine model it was tested for both diesel and PB20. RSM is employed for design of experiments for all the three cases.

Chapter 4

Results and Discussion

In the present section, three cases such as CAT3401 diesel, VCR diesel and VCR PB20 are analyzed separately. The CAT3401 is validated against the experimental data available from the literature (Curtis et al., 1995; Mobasheri et al., 2012). The other two cases are validated with the results obtained from experiments conducted on the laboratory VCR engine. Four design parameters, such as CR, SOI, FIP and EGR were chosen to evaluate their effect on the performance and emissions. These simulation results are further optimized for the minimization of the NOx, soot and ISFC by using the Response Surface Methodology.

4.1 Analysis of CAT3401 Engine

Initially the CAT 3401 engine is validated with the experimental results available from Curtis et al. (1995), Mobasheri et al. (2012). The specifications of the engine are given in Table 4.1. The parametric effect on combustion characteristics of CAT3401 is presented and the ranges for each of these parameters were decided based on their combustion characteristics. The CAT3401 engine model has been analyzed based on the responses obtained from different sets of simulations and further optimized using RSM technique. The optimized parameters were used for further simulation and the results are compared with baseline results for ISFC, NOx, soot, HC and CO emissions. The homogeneity of mixture was also compared for both the baseline and optimized cases.

Table 4. 1 Specifications of CAT3401 engine Curtis et al. (1995)

Cylinder bore x stroke (mm)	137.6 x 165.1
Connecting Rod length (mm)	261.62
Displacement Volume (L)	2.44
Compression Ratio	15.1
Number of nozzle orifice x diameter (mm)	6 x 0.259
Piston crown	Mexican Hat
Intake valve closure (CA)	147° bTDC
Swirl ratio (nominal)	1.0
Inlet air temperature (K)	310
Inlet air pressure (kPa)	184
Engine speed (rpm)	1600 rpm
Fuel	Diesel
Injection system	Common Rail
Injection Pressure (MPa)	90
Fuel Injected (g/cycle)	0.1622
Overall Equivalence ratio	0.46
Injection duration	21.5 crank angle degrees
Start of Injection	11 °bTDC (baseline case)

4.1.1 Validation of CAT3401 engine model

Validation of the numerical results has been done using experimental data from Curtis et al. (1995), and Mobasheri et al. (2012). Engine modeling is done with the geometry specifications given in Table 4.1 and the simulation run has been taken by imposing the given initial and boundary conditions. Figure 4.1 shows the variation of pressure with crank angle. From the figure, it can be observed that the experimental results are in good agreement with the simulation results.

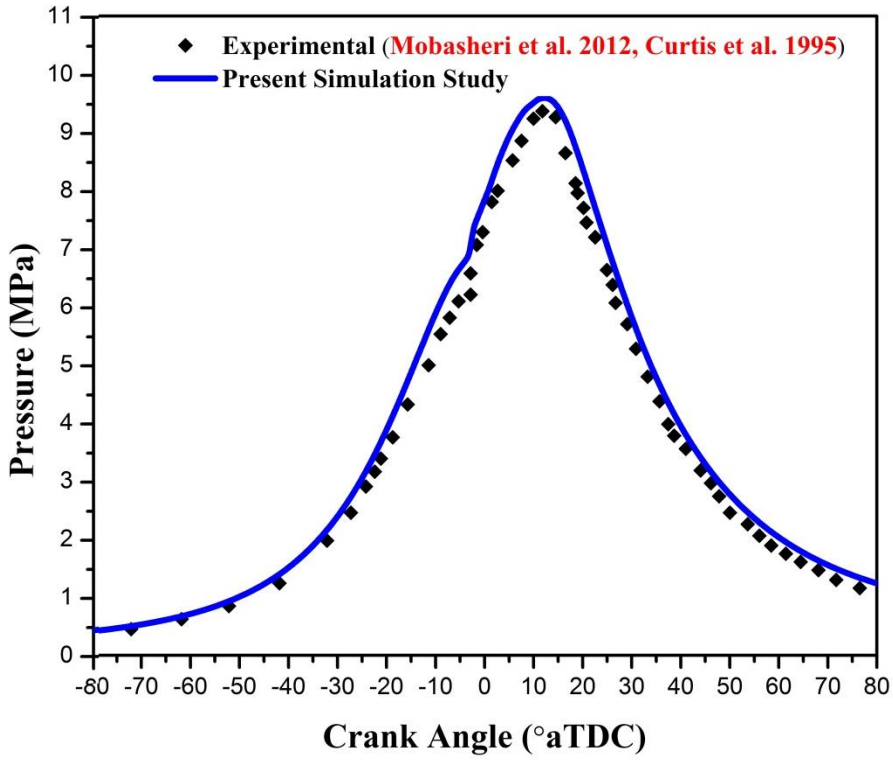

Fig.4. 1 Validation of CAT3401 engine model with the pressure Vs crank angle

4.1.2 Parametric study on CAT3401 engine

It has been observed from the literature that the significant parameters such as compression ratio, start of injection, EGR and fuel injection pressure will have major influence on the combustion characteristics of any engine. But the range of these parameters is not limited in any case. Through the parametric study, the maximum possible range and their pros and cons for each of these effects were explored.

4.1.2.1 Effect of Compression Ratio (CR)

In the present section simulations have been carried out at different compression ratios (12-16) by keeping all other parameters constant as shown in Table.4.1. It can be observed from Fig.4.2 (a) that as the compression ratio is lowered from 16 to 12, the peak pressure decreased from 109.44 to 80.2 bar. Figure 4.2 (d) revels that the peak temperature also decreased from 1910 to 1505 K. This is due to change in states (pressure and temperature) of in-cylinder charge, which directly effects the ignition delay period (Kwon et al., 1990). The ignition delay was found to increase from 6.08 to 7.94 CAD as the CR was decreased from 16 to 12. This also can be observed from the Fig.4.2 (c). that peaks of the heat release rate were increased with decreased CR. Figure 4.2 (b) indicates the work done per cycle, the area under the P-V is decreased as the CR is decreased from 16 to 12. This implies the work output

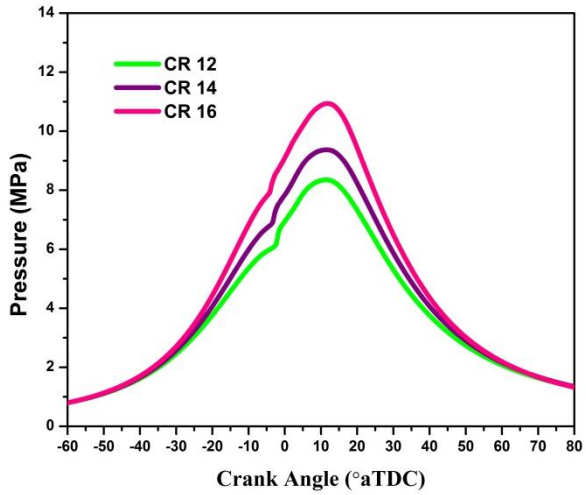

a) Pressure Vs Crank angle for different CR

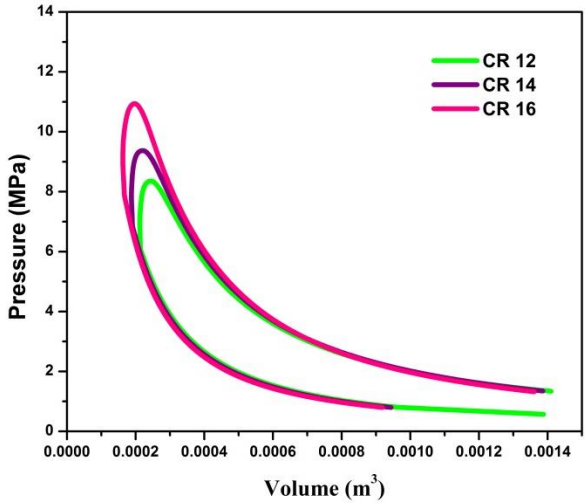

b) Pressure Vs Volume for different CR

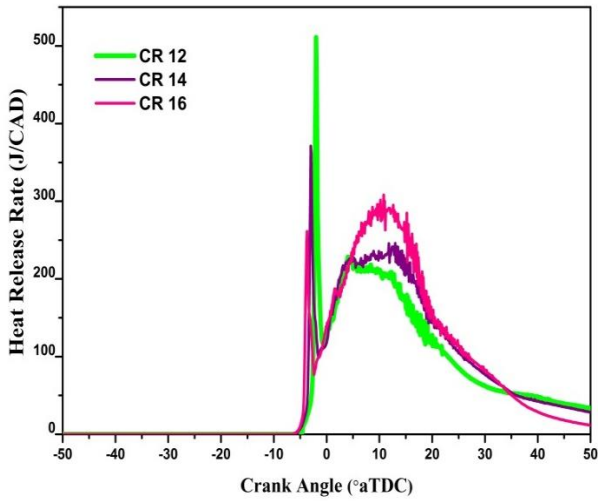

c) Heat release rate Vs Crank angle for different CR

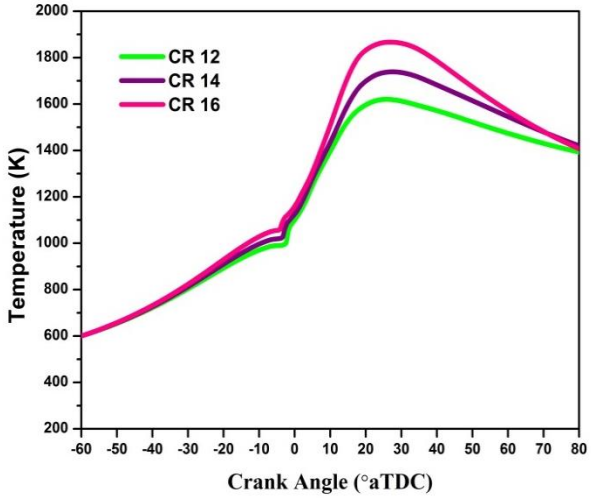

d) Temperature Vs Crank angle for different CR

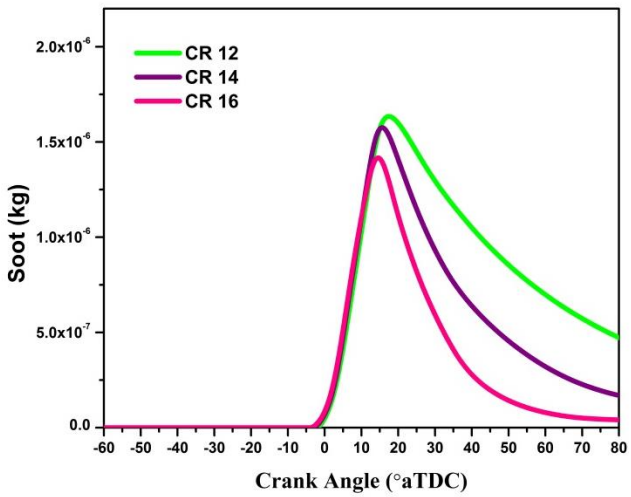

e) Soot Vs Crank angle for different CR

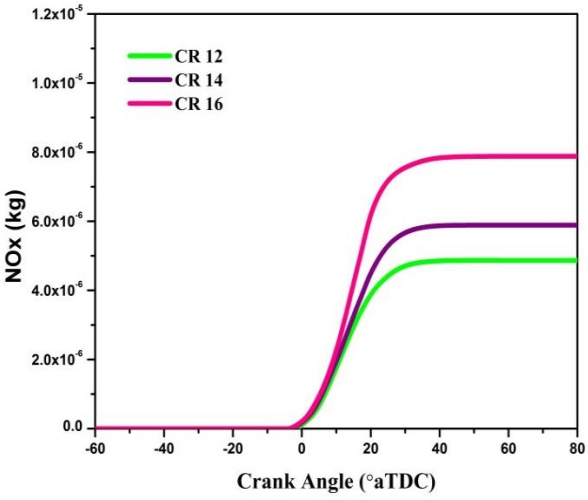

f) NOx Vs Crank angle for different CR

Fig.4.2 Effect of CR on performance and emissions characteristics of CAT3401 DI Diesel Engine

deteriorates when the CR is reduced (Kumar et al., 2013; Mathur et al., 2012). As the CR is lowered from 16 to 12, reduction in NOx emissions were observed (Fig.4.2 (f)), this is due to fact that the decreased in-cylinder temperature favors the reduction of NOx. The soot emissions (Fig 4.2 (e)) increased as the CR is decreased from 16 to 12. This may be because of decrease in the rate of oxidation of soot caused by the lesser in-cylinder temperatures attained from the lower CR (Mallamo et al., 2005; Song et al., 2007; Kumar et al., 2013).

4.1.2.2 Effect of start of injection (SOI)

Simulations have been carried out to study the effect of Start of Injection (SOI) and it is varied from - 11° to - 30° aTDC. It can be observed from Fig.4.3 (a) that as the SOI is advanced from - 11° to - 30° aTDC, the peak of in-cylinder pressure increased from 99.28 to 175 bar. Figure 4.3 (b) indicates that the work done is increased as the SOI advanced from -11 to -20 aTDC and further advancement of SOI to - 30° aTDC leads to decrease in work done. This is due the fact that the peak pressure is attained well before TDC for - 30° aTDC SOI, as a result the compression work increases, which in-turn reduces the indicated work (Song et al., 2007). Figure 4.3 (d) indicates that the average in-cylinder temperature was increased as the SOI is advanced; this is due to higher spikes of the heat release rate observed from the Fig 4.3 (c). As an effect of advanced start of injection, peak value of heat release rate during premixed combustion shoots up due to the larger ignition delay. The ignition delay is increased from 5.5 to 16.1 CAD as the SOI is advanced from -11 to -30°aTDC. The larger ignition delay gives enough time to get the charge premixed before the ignition starts. The peak temperature also increased from 1600 K to 2200 K. This is because of the fact that longer ignition delay leads to fruitful homogeneity as more time is available for mixture formation. The effect of SOI on NO_x and soot emissions is illustrated in Fig. 4.3 (e) and (f) respectively. As the SOI is advanced from - 11° aTDC to - 30° aTDC, NOx emissions increased and soot emissions decreased. Increase in NOx is due to the higher in-cylinder temperatures caused by the early injection. The higher rate of oxidation of soot at higher in-cylinder temperatures may be the reason for this decrease in the soot emissions (Jayashankara & Ganesan, 2010; Agarwal et al., 2013; Sayin et al., 2009).

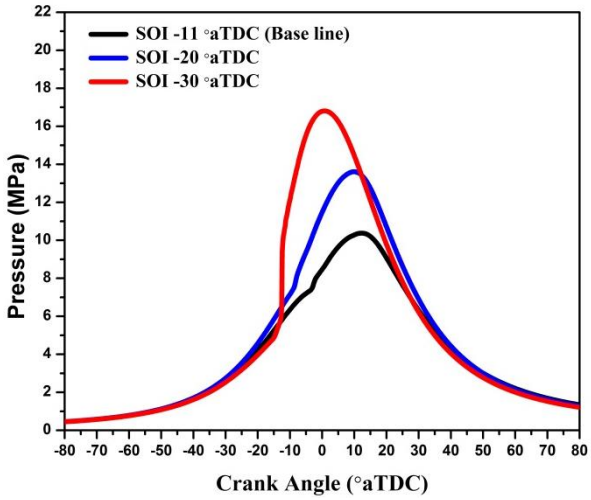

a) Pressure Vs Crank angle for different SOI

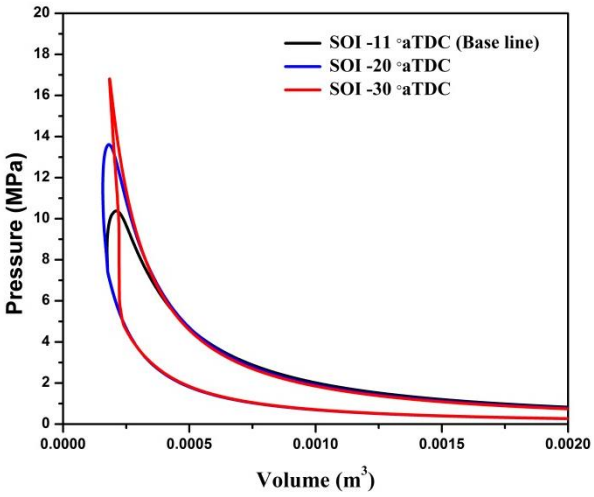

b) Pressure Vs Volume for different SOI

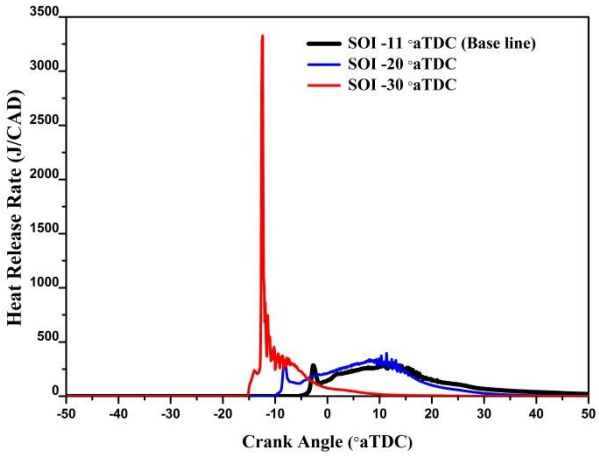

c) Heat release rate Vs Crank angle for different SOI

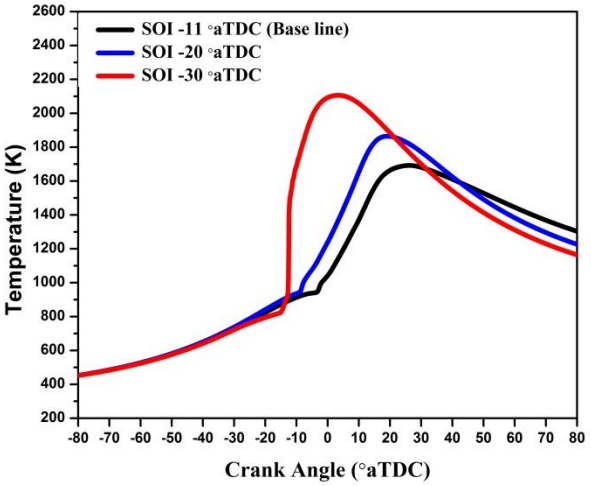

d) Temperature Vs Crank angle for different SOI

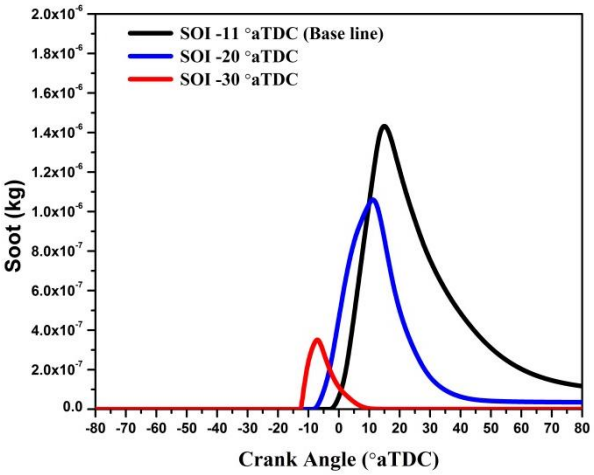

e) Soot Vs Crank angle for different SOI

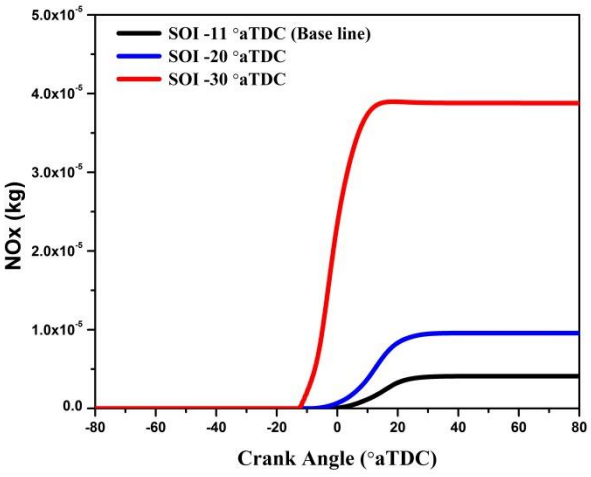

f) NOx Vs Crank angle for different SOI

Fig.4. 3 Effect of SOI on performance and emissions characteristics of CAT3401 DI diesel Engine

4.1.2.3 Effect of fuel injection pressure (FIP)

The current section embraces the results obtained from simulation of fuel injection pressure ranges from 600 to 1400 bar with all other parameters are kept constant as shown in Table 4.1. It can be observed from Fig.4.4 (a) that as the injection pressure is increased from

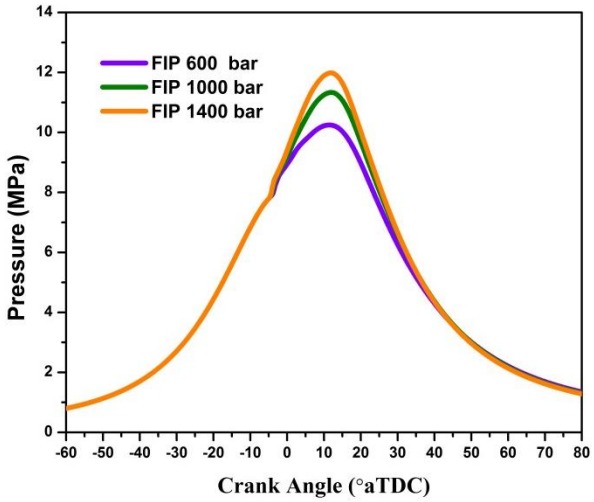

a) Pressure Vs Crank angle for different FIP

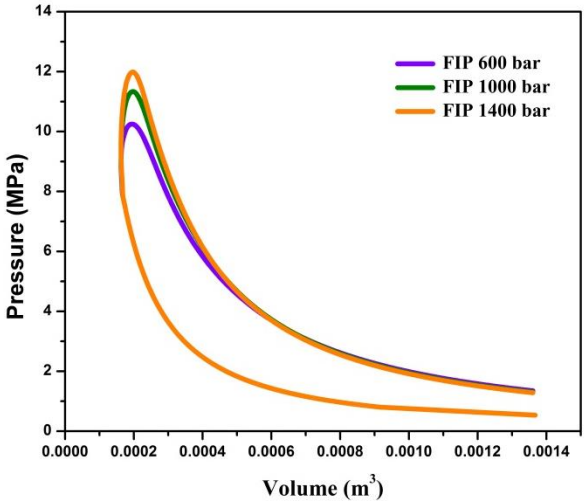

b) Pressure Vs Volume for different FIP

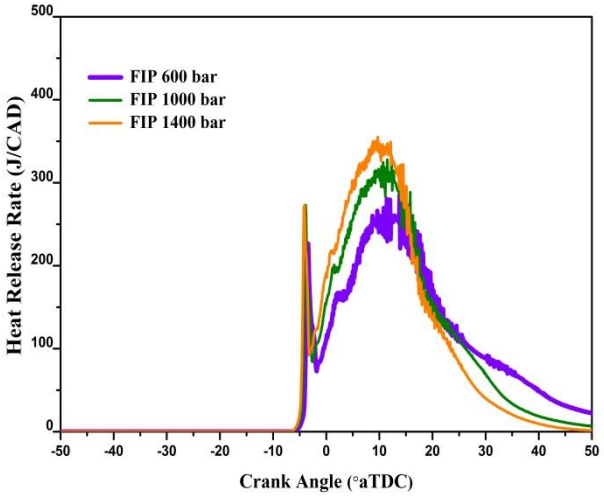

c) Heat release rate Vs Crank angle for different FIP

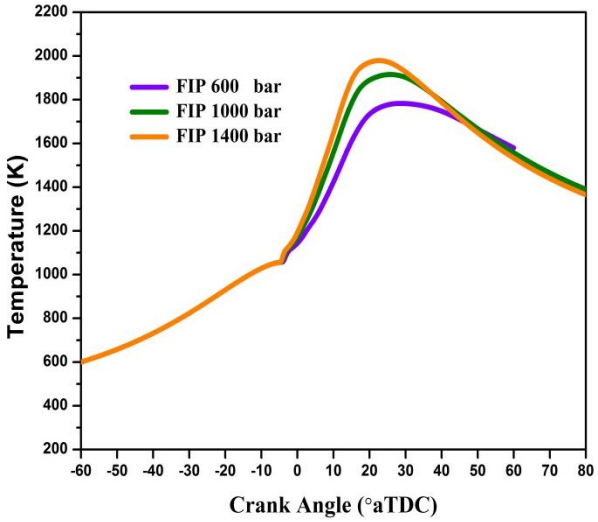

d) Temperature Vs Crank angle for different FIP

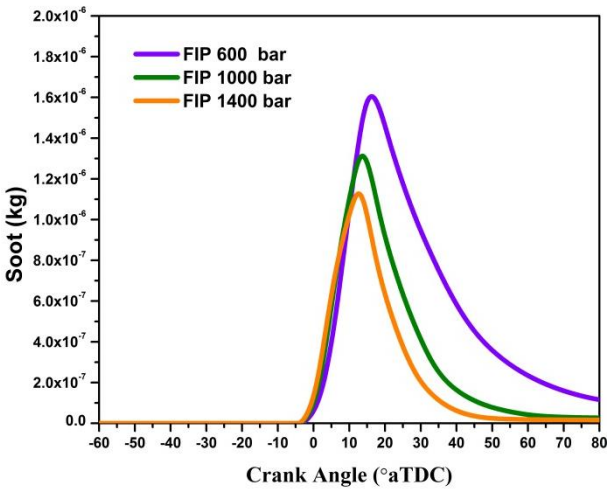

e) Soot Vs Crank angle for different FIP

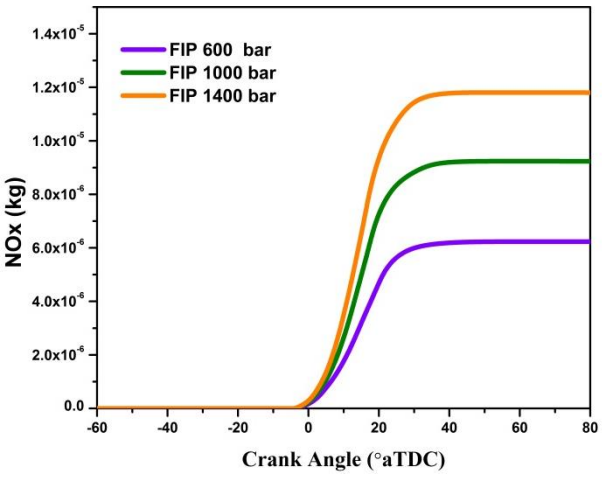

f) NOx Vs Crank angle for different FIP

Fig.4. 4 Effect of FIP on performance and emissions characterstics of CAT3401 DI diesel Engine

600 to 1400 bar, the value of peak pressure increased from 95 to 120 bar and peak temperature also increased from 1650 to 2000 K (Fig 4.4 (d)). Figure 4.4 (b) shows that the indicated power also increased with increase in FIP. Figure 4.4 (c) reveals the heat release patterns for various values of injection pressure. There is a slight decrease in ignition delay observed from 4.8 to 4.6 CAD. This occurs due to better atomization and vaporization and subsequently thorough mixing of fuel inside the cylinder at higher value of FIP (Sayin et al., 2012). This also can be ascertain from the Fig 4.5 that the equivalence ratio distribution at 1400 bar FIP is more homogenous than that of 600 bar. It is observed from Fig.4.4 (f) that there is an increase in NO_x emissions as a result of increased FIP from 600 to 1400 bar. This is due to the high peak temperature in the cylinder caused by the higher FIP. On the other hand, as the FIP is increased from 600 to 1400 bar, soot emissions were decreased because of better combustion at higher FIP due to better penetration and mixture preparation. This is also proved from the increased area observed under the P-V diagram for the higher FIP (Henein, 2006).

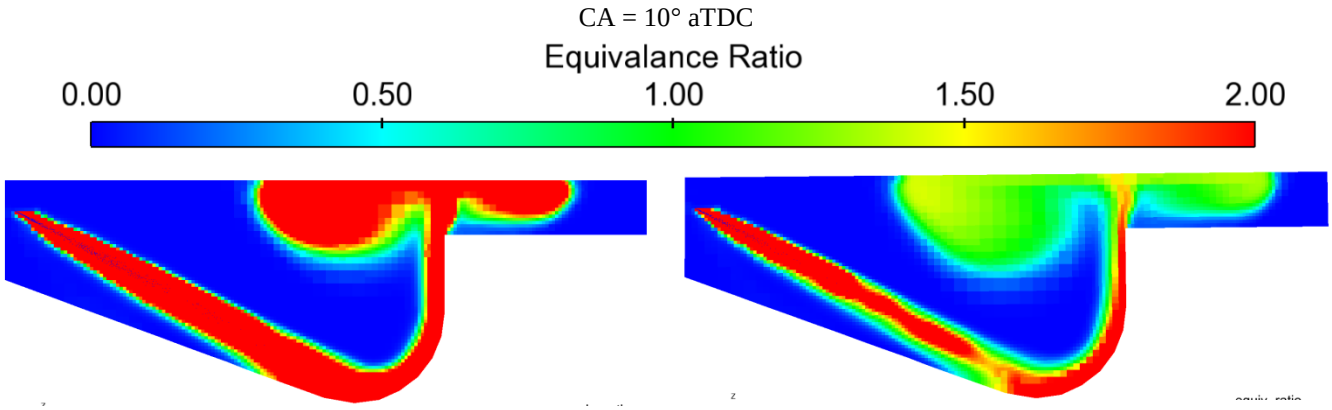

a) Fuel Injection Pressure 600 bar b) Fuel Injection Pressure 1400 bar

Fig.4. 5 Effect of Fuel Injection Pressure on the equivalence ratio Distribution inside the cylinder

4.1.2.4 Effect of Exhaust gas recirculation (EGR)

Percentage of EGR has been varied from 0 to 20%. All other parameters are kept constant as shown in Table 4.1. EGR reduces the concentration of oxygen in the mixture or increases the equivalence ratio from 0.46 to 0.58 when it is varied from 0 to 20%. It is inferred from Fig 4.6 that the peak pressure decreased from 99.28 to 90 bar and peak temperature decreased from 1900 to 1700 K as percentage of EGR was increased from 0 to 20. The specific heat of the mixture increased from 1010 to 1030 J/kg-K due to increased EGR from 0 to 20% which helps in reducing the temperature inside the cylinder. Figure 4.6 (b) indicates that the indicated power is decreased from 41.4 to 39.15 kW with increase in EGR rate from 0 to 20% (Maiboom et al., 2008; Kumar et al., 2013). Figure 4.6 (c) shows that

the ignition delay is increased from 5.3 to 7.1 CAD with an increase in EGR from 0 to 20%. The effect of EGR on soot and NO_x emissions is shown in Fig 4.6 (e) and (f) respectively. NO_x emissions reduced as the EGR is increased from 0 to 20%. There are two major reasons

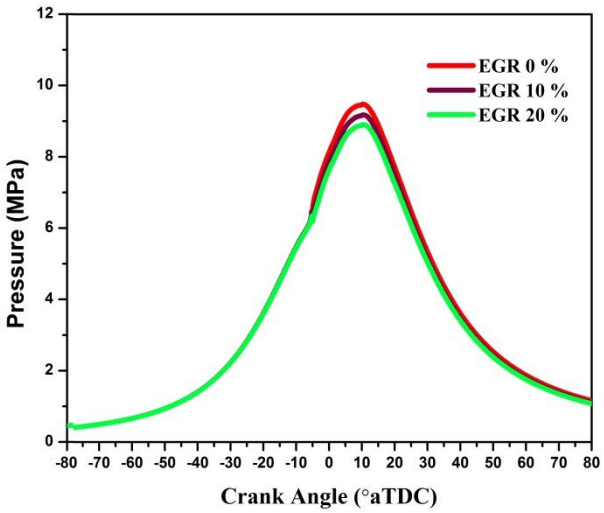

a) Pressure Vs Crank angle for different EGR

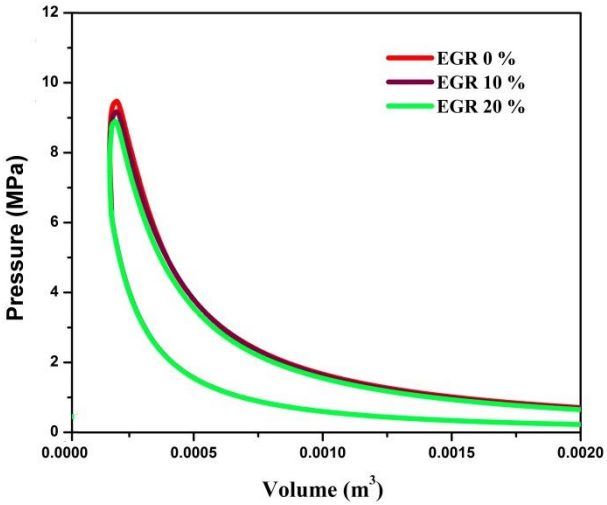

b) Pressure Vs Volume for different EGR

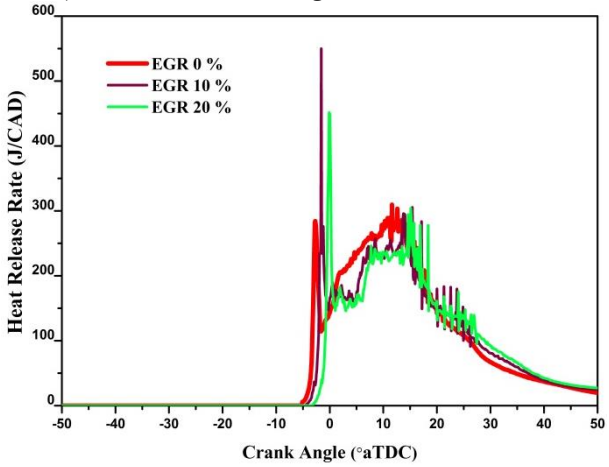

c) Heat release rate Vs Crank angle for different EGR

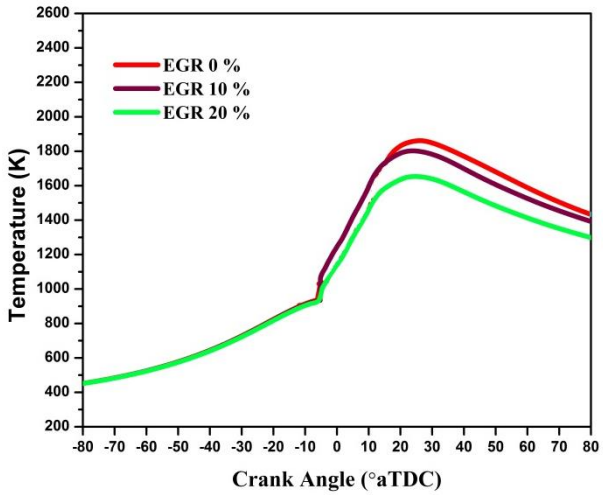

d) Temperature Vs Crank angle for different EGR

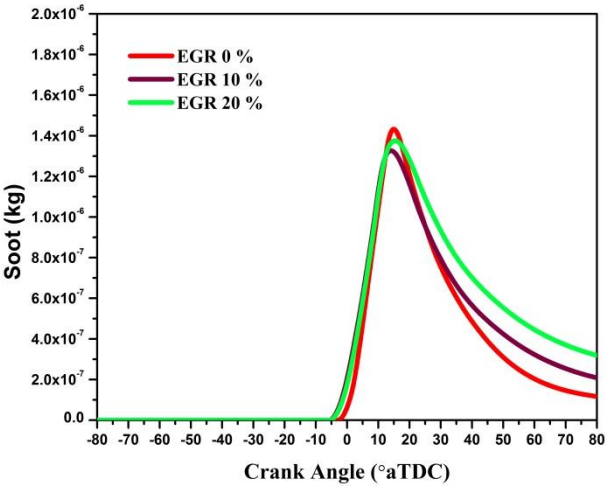

e) Soot Vs Crank angle for different EGR

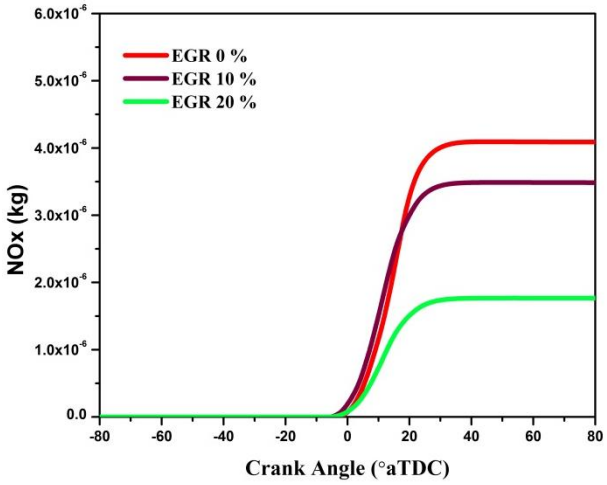

f) NOx Vs Crank angle for different EGR

Fig.4. 6 Effect of EGR on performance and emissions characteristics of CAT3401 DI Diesel Engine

for reduced NO_x emissions with EGR. The first one is decreased oxygen concentration and the other is reduced flame temperatures in the combustion space. EGR reduces the oxygen concentration and creates a lesser chance of reacting nitrogen and oxygen together to form NO_x. On the other hand soot is increased as the EGR increased from 0 to 20% due to relatively incomplete combustion caused by insufficient oxygen. This shows severe drawback with increasing EGR (Squaiella et al., 2013; Sarangi et al., 2010).

4.1.3 Selection of parameter ranges based on ISFC, NOx and soot

It is evident from the above study that the parameters were very much influencing the combustion and emission characteristics of a DI CI engine. The range of each parameter has to be fixed in order to explore the operating range and to analyze them using the DOE technique to obtain optimum parameters based on the three important outcomes (i.e ISFC, NOx and soot) used for any diesel engine optimization problem.

4.1.3.1 Selection of SOI range:

The objective of the present section is to select the operating range of parameters in order to ensure the safe operation. The SOI is varied from 0 to 30 °bTDC to analyze the performance and emission characteristics. The performance characteristic (indicated power) is calculated using the area under the P-V diagram (J) divided by the time taken for one cycle. Similarly soot and NOx are converted into gross specific emissions. These were converted by dividing the absolute mass of the emissions with the area under the P-V diagram.

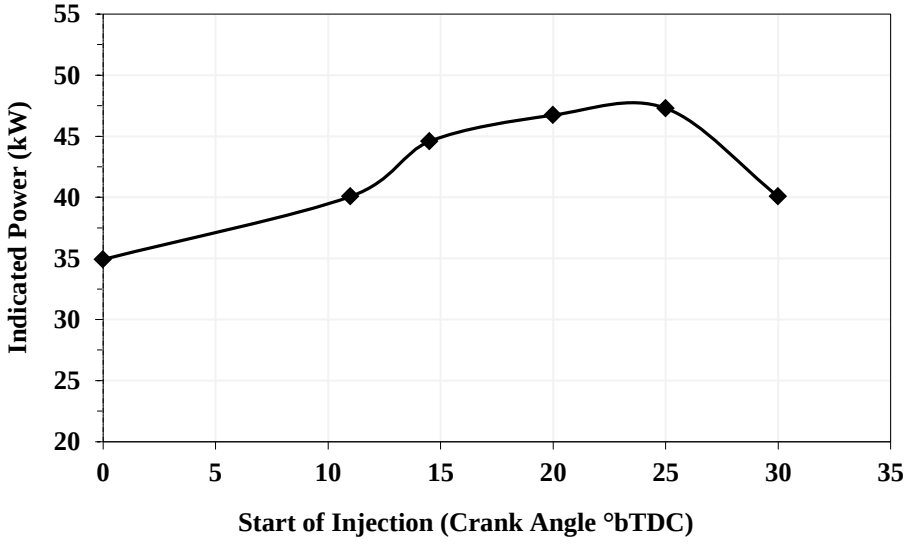

Fig.4. 7 Effect of Start of Injection on Indicated Power

It can be observed from the Fig.4.7 that as the SOI is advanced from 0 to 25° bTDC the indicated power is increased from 35.45 to 47.29 kW. This is due to the fact that advanced start of injection is fruitful in better homogeneity of the mixture as more time is available for mixture formation. Better homogeneity in turn signifies efficient combustion and thus gives a better performance. But if the SOI is further advanced from 25 to 30° bTDC the performance is deteriorated this may be ascribable to the fact that compression work is more in case of 30 bTDC caused by the early start of combustion. These results also suggest that advancing to 30 bTDC and above may not be favorable for controlled-combustion.

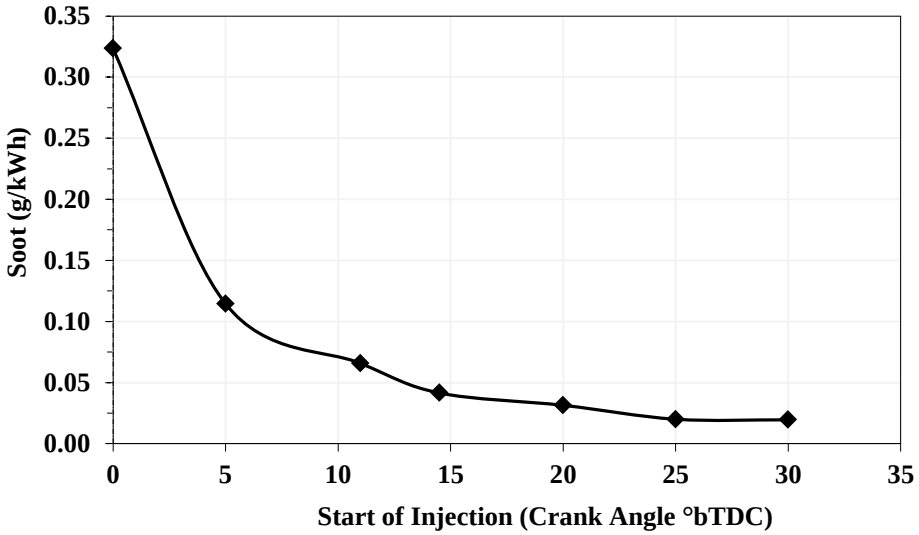

Fig.4. 8 Effect of Start of Injection on soot

It is observed from Fig 4.8 that as the SOI is advanced from 0 to 30° bTDC soot emissions are decreased from 0.325 to 0.0195 g/kWh. But the rate of decrease of soot emissions was not substantial when the SOI is advanced from 25 to 30° bTDC.

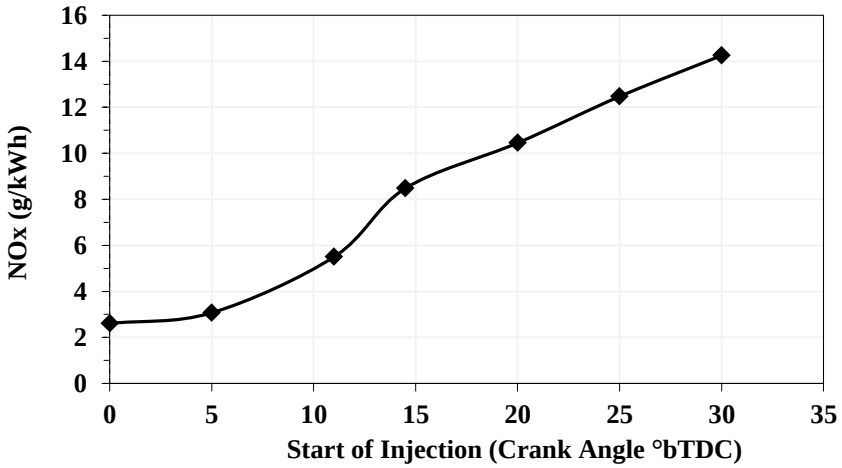

Fig.4. 9 Effect of Start of Injection on NOx

Figure 4.9 shows the effect of start of injection on NOx emissions. It can be observed that as the SOI is advanced from the 0 to 30° bTDC the NOx emissions were increased from 2.6 to 14.25 g/kWh. The higher in-cylinder temperature caused by rapid burning in advanced SOI and more lean regions due to lower value of overall equivalence ratio (φ = 0.46) are responsible for this phenomena.

Thus the range of the SOI is preferred from 0 to 25° bTDC in order to ensure the safe operation for the analysis using design of experiments. This preliminary study helps in selecting the operating range and it may also improve the regression model accuracy.

4.1.3.2 Selection of CR range

The conventional diesel engines can operate at the compression ratios range from 12 to 24 (Heywood, 1988). The compression ratio is mainly dependent on total volume and the clearance volume. There is not much problem to attain lower compression ratio whereas higher limit of CR is limited by its lowest possible clearance volume when the piston at TDC. This lowest possible clearance volume for any particular piston bowl is fixed and thereby restricts the CR on the higher side. The effect of CR is plotted for performance and emission characteristics. The range of CR varied in this present study is limited to 12 to 16.5 because of the above said design constraint of the CAT3401 model.

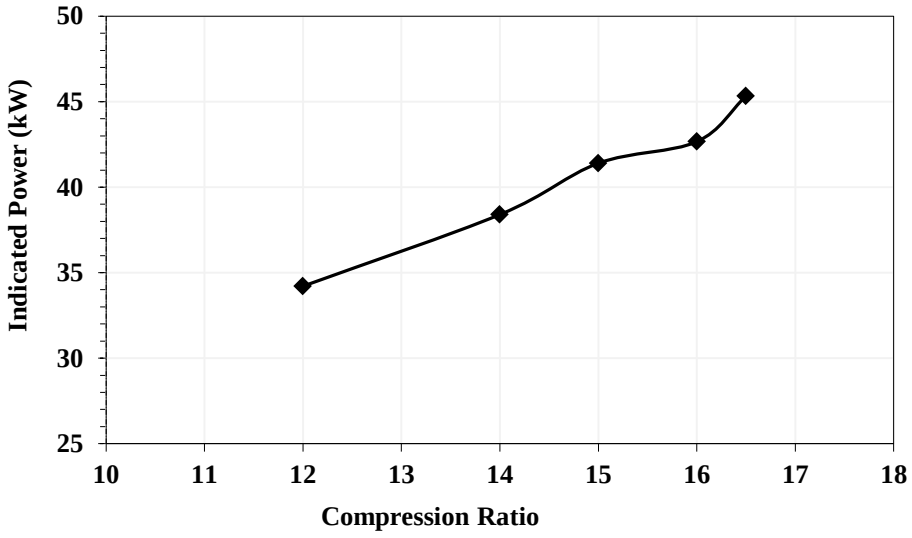

Fig.4. 10 Effect of Compression Ratio on Indicated Power (kW)

As the compression ratio is decreased from 16.5 to 12, the indicated power is also decreased from 45.33 to 34.21 kW (see Fig 4.10). Reduction in the indicated power by 25% is observed when the CR is reduced from 16.5 to 12. This is due to lower values of pressure and temperature caused by the lower compression ratio, thereby deteriorates the combustion

efficiency. Indicated power decreases with lowering the compression ratio as the combustion starts at a relatively lower mean temperature due to which the desired peak pressure could not be obtained.

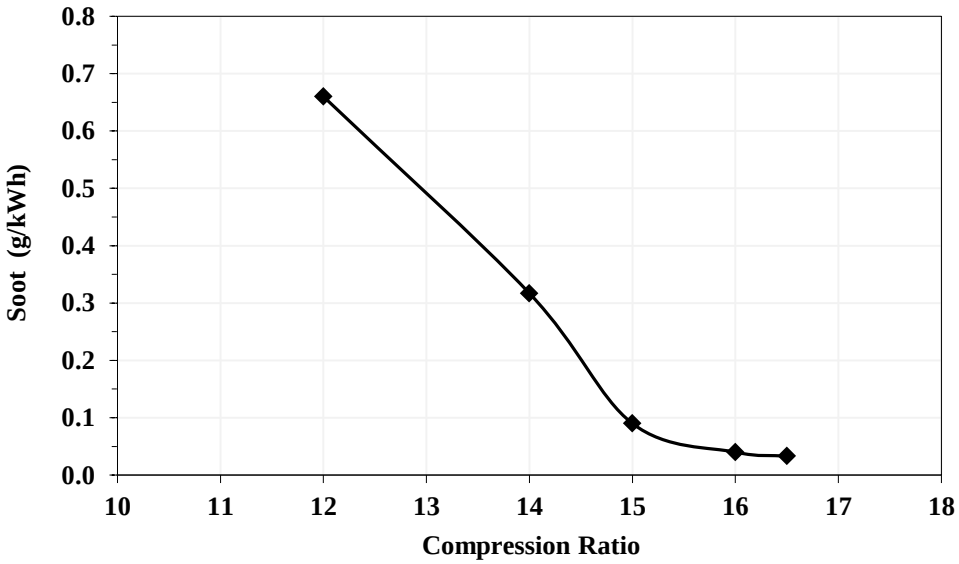

Fig.4. 11 Effect of Compression Ratio on Soot emissions

The soot emissions are increased from 0.035 to 0.66 g/kWh (observed from Fig 4.11) as the CR is reduced from 16.5 to 12. The higher compression ratios would help in better combustion and thereby reducing the soot emissions. It is also observed from the figure that the rate of decrement in soot emissions is almost constant and near to zero level at CR 16.5.

It can be observed from the Fig.4.12 that the NOx emissions have decreased from 9.15 to 5.42 g/kWh of around 40% as the CR is reduced from 16.5 to 12. The higher in-cylinder mean temperature attained by the higher CR could be the reason for the higher NOx formation.

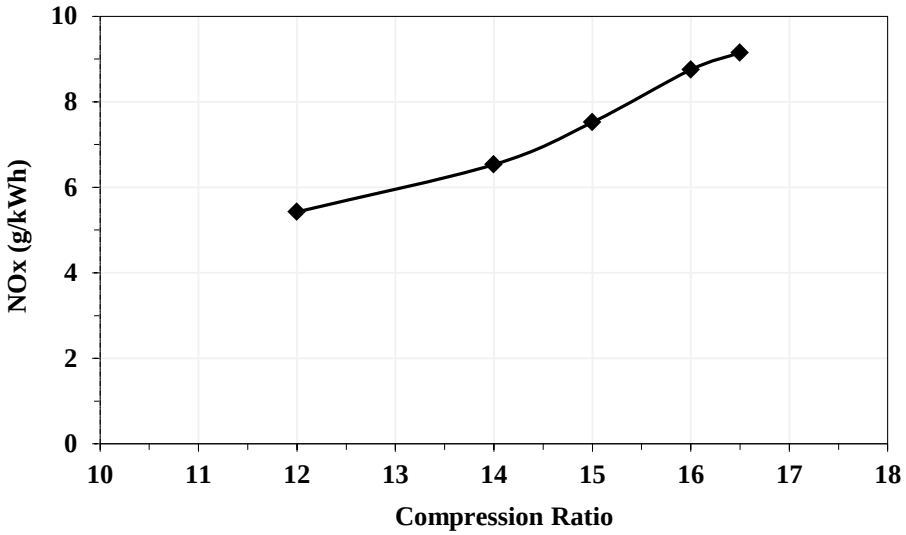

Fig. 4.12 Effect of Compression Ratio on NOx emissions

From the above analysis, it can be concluded that decreasing CR may not be fruitful in obtaining better performance, but it could able to decrease the NOx, on the other side soot emissions are increased. However, the positive aspect of lowering CR is prolonged ignition delay which will be advantageous when it is combined with advanced SOI.

4.1.3.3 Selection of EGR

Exhaust gas recirculation (EGR) is defined as the volume fraction of exhaust gases that were presented in the total intake air. EGR is an efficient way to reduce NOx emissions in diesel engines. However the range has been limited to conventional diesel engine due to the trade-off between the NOx and soot. The decrement in oxygen levels with boosting the EGR rate attains its limit at the stoichiometric condition, and cannot lower further under rich conditions. Furthermore, increment in EGR may result in abnormal combustion or combustion may not possible.

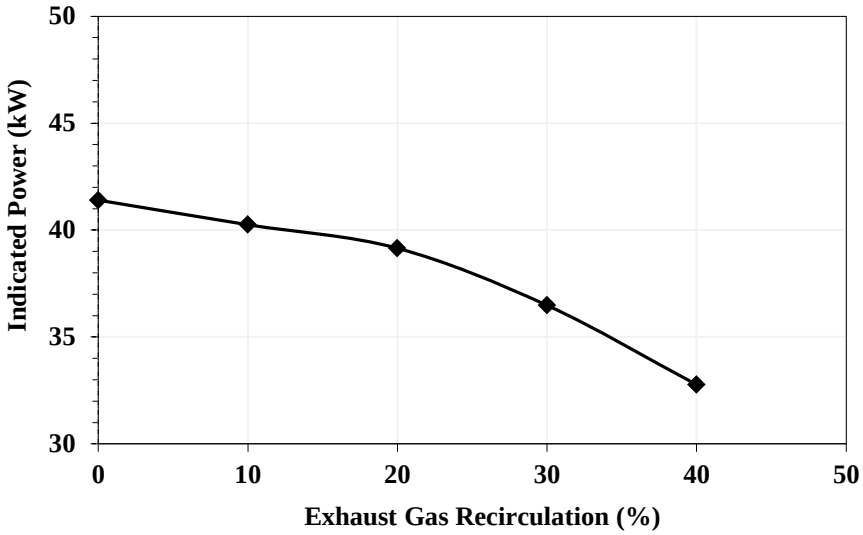

Fig.4. 13 Effect of EGR on Indicated Power (kW)

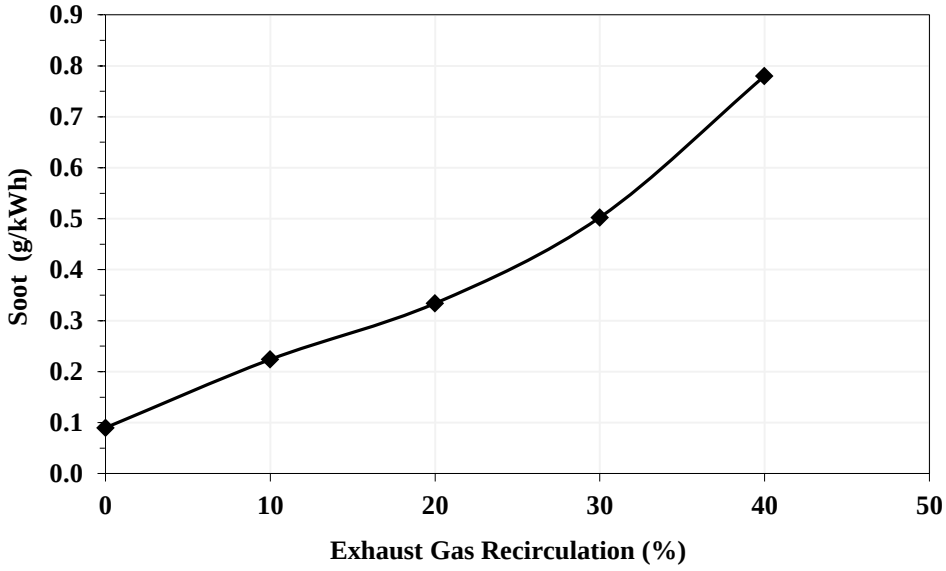

Fig.4. 14 Effect of EGR on Soot emissions

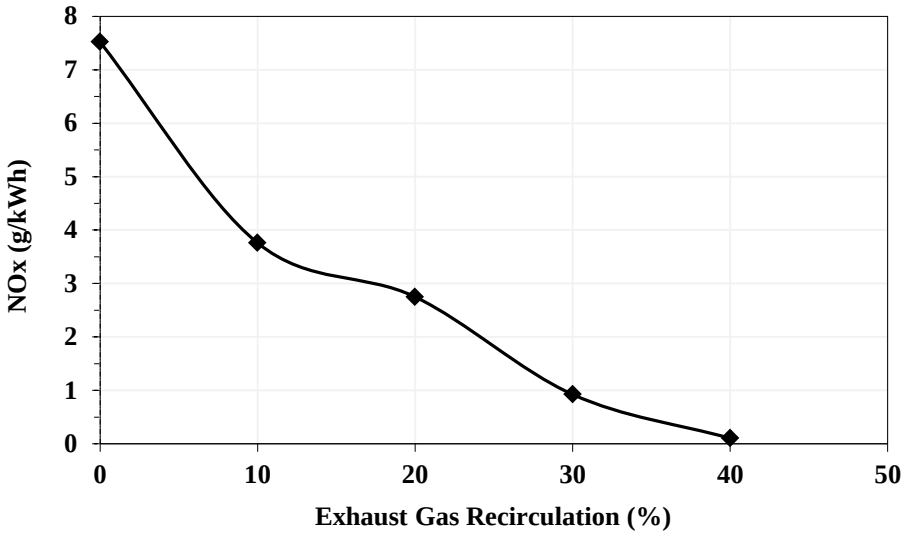

Fig.4. 15 Effect of EGR on NOx emissions

Figure 4.13 shows the influence of EGR on indicated power. As the EGR rate is increased from 0 to 40% the indicated power is reduced from 41.4 to 31.8 kW. This is due to the fact that EGR reduces the oxygen concentration and thus weaken the combustion phenomena and thereby deteriorate the performance of the engine.

Figure 4.14 shows the effect of EGR on soot emissions. As the rate of EGR is increased from 0 to 40% the soot emissions were increased from 0.09 to 0.78 g/kWh which is more than seven times of the baseline case.

It can be observed from Fig.4.15 that as the EGR is increased from 0 to 40% the NOx emissions were decreased drastically and reaches a minimum (0.1 g/kWh) at 40%. The NOx emissions correspond to no EGR has the highest levels, i.e. 7.52 g/kWh.

4.1.3.4 Selection of FIP

Fuel injection pressure plays an important role in performance and emissions characteristics. The fuel injection system is used in a direct injection diesel engine to achieve a high degree of atomization and better penetration into the combustion chamber. Higher injection pressure promotes better evaporation and atomization of fuel in a very short time. The first generation CRDI fuel injector can operate up to 1350 bar average fuel injection pressure. So in the current study the range of FIP is fixed from 220 to 1400 bar.

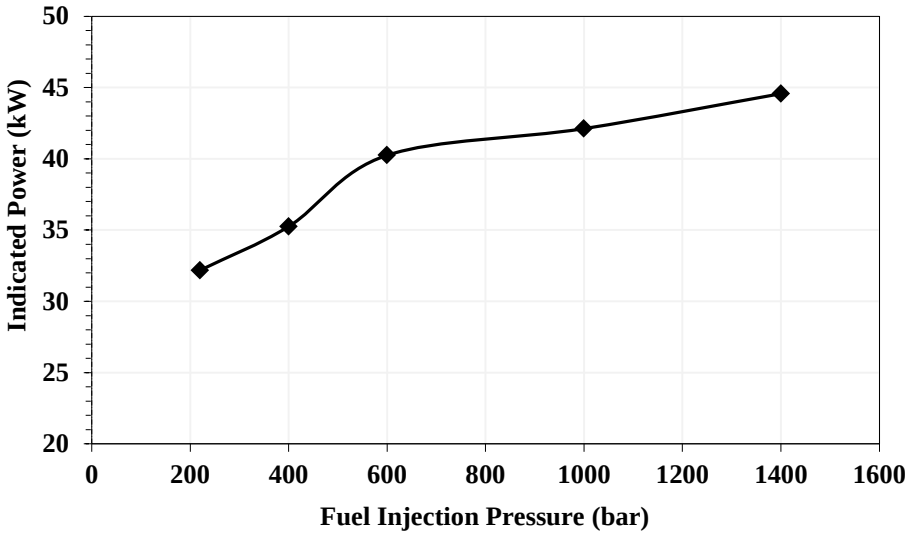

Fig.4. 16 Effect of fuel injection Pressure on Indicated Power

It can be noticed from the Fig.4.16 as the fuel injection pressure is increased from 220 to 1400 bar the indicated power is improved from 32.2 to 44.57 kW. It is observed from Fig.4.17 that the soot emissions are reduced from 1.19 to 0.02 g/kWh whereas the NOx emissions (Fig.4.18) are increased from 4.8 to 12.9 g/kWh. Better homogenous mixture at higher fuel injection pressure aid in better combustion, thereby improves performance and also reduces soot emissions. But the higher in-cylinder temperatures from the improved combustion are accountable for the NOx emissions.

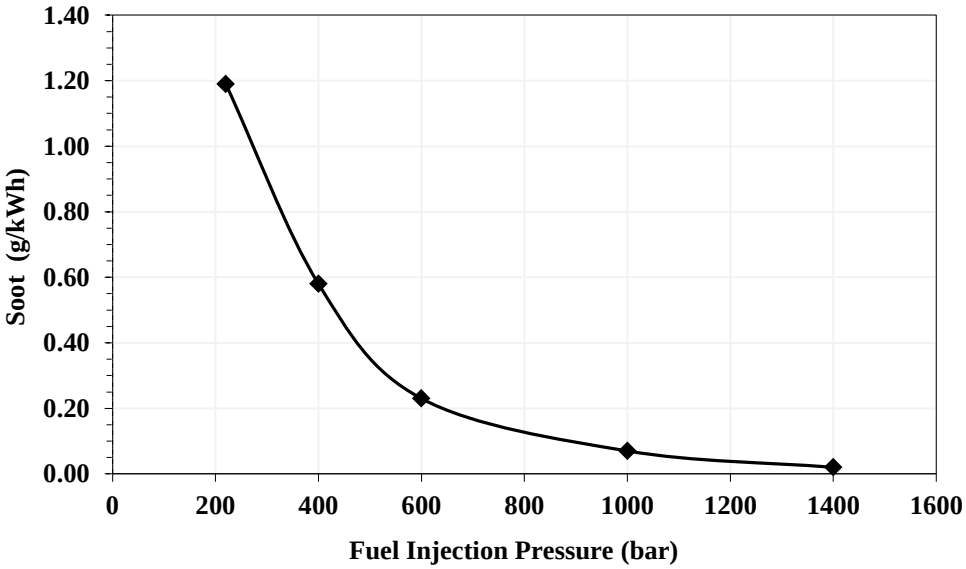

Fig.4. 17 Effect of fuel injection Pressure on soot emissions

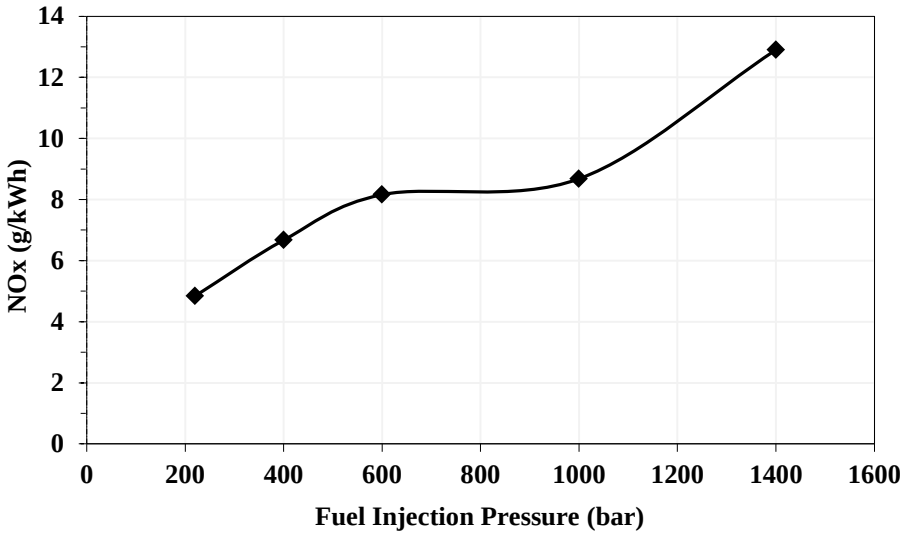

Fig.4. 18 Effect of fuel injection pressure on NOx emissions

Summary

It was identified from the parametric study that the increase in CR, beneficial in reducing the soot and ISFC while detrimental in NOx emissions. Advanced SOI greatly reduces the soot while increases NOx. It is also observed that the advancing of SOI may result in lesser power output due to higher compression work. EGR has the highest potential in reducing the NO_x while the soot increases. Higher FIP is beneficial in reducing the soot and also helps in improving the performance, but it may end up with an increase in NO_x emissions. Thus, the ranges of the selected parameters are selected as follows. CR is fixed from 12 to 16.5, SOI is fixed from 0 to -25 aTDC, EGR is fixed from 0 to 40% and FIP is fixed from 500 to 1400.

4.1.4 Determination of optimal engine parameters using RSM for CAT3401

In the current section the CAT3401 engine is analyzed based the parameters and the ranges (given in Table 4.2) obtained from the independent parametric study. With these input parameters, the analysis has been extended by considering all possible interaction effects in order to obtain an optimized set of design parameters using RSM.

The effect of parameters (CR, SOI, FIP and EGR) and their interactions on the performance and emission characteristics (ISFC, soot and NO_x) of single cylinder direct injection diesel engine (Caterpillar 3401 engine) are analyzed by using the RSM. Box-Behnken design with four parameters consist total of 27 experiments are given in Table 4.3. All these set of

experiments are simulated in the CONVERGE^{TM} CFD code and results have been summarized Table 4.4 as the responses (ISFC, soot and NO_x).

Table 4. 2 Variables and their range

S. No	Parameter	Range	
1.	Compression Ratio (CR)	12 :1	16.5 :1
2.	Fuel Injection Pressure (FIP) bar	500	1400
3.	Start of Injection (SOI) °aTDC	-25	0
4.	Exhaust Gas Recirculation (EGR) %	0	40

Table 4. 3 Design of experiments matrix obtained from the Box–Behnken model

Run order	**CR**	**SOI (ºbTDC)**	**FIP (bar)**	**EGR (%)**
1	16.5	0	950	20
2	14.25	0	1400	20
3	14.25	12.5	1400	40
4	12	12.5	950	40
5	14.25	12.5	500	40
6	14.25	25	950	0
7	12	12.5	500	20
8	16.5	12.5	500	20
9	14.25	25	500	20
10	14.25	0	950	40
11	14.25	0	500	20
12	14.25	25	1400	20
13	16.5	25	950	20
14	16.5	12.5	1400	20
15	14.25	12.5	1400	0
16	14.25	25	950	40
17	14.25	12.5	500	0
18	16.5	12.5	950	40
19	14.25	12.5	950	20
20	14.25	0	950	0
21	12	12.5	950	0
22	12	0	950	20
23	12	25	950	20
24	12	12.5	1400	20
25	14.25	12.5	950	20
26	14.25	12.5	950	20
27	16.5	12.5	950	0

Table 4. 4 Responses of the design matrix used for the CAT3401

	Parameters				Responses		
Run order	**CR**	**SOI (ºbTDC)**	**FIP (bar)**	**EGR (%)**	**ISFC (g/kWh)**	**NO_x (g/kWh)**	**Soot (g/kWh)**
1	16.5	0	950	20	195.7912	2.012374	0.504125
2	14.25	0	1400	20	204.1479	0.013315	0.371462
3	14.25	12.5	1400	40	199.6608	2.085002	0.156426
4	12	12.5	950	40	233.4171	0.227406	1.120781
5	14.25	12.5	500	40	210.4481	0.20	1.12956
6	14.25	25	950	0	198.0838	20.77231	0.032457
7	12	12.5	500	20	232.2662	1.268221	1.044281
8	16.5	12.5	500	20	179.1555	1.935547	0.211449
9	14.25	25	500	20	196.5651	9.357608	0.109455
10	14.25	0	950	40	229.6621	2.842954	1.113332
11	14.25	0	500	20	242.5732	2.066686	1.406643
12	14.25	25	1400	20	197.4102	20.54104	0.051001
13	16.5	25	950	20	174.2421	17.6826	0.106
14	16.5	12.5	1400	20	175.1233	9.085718	0.023815
15	14.25	12.5	1400	0	181.9648	12.03502	0.05
16	14.25	25	950	40	197.2312	7.365714	0.10281
17	14.25	12.5	500	0	197.9509	4.540002	0.16628
18	16.5	12.5	950	40	172.874	1.760736	0.108329
19	14.25	12.5	950	20	185.0433	3.259484	0.091013
20	14.25	0	950	0	214.0143	0.476421	0.370557
21	12	12.5	950	0	198.2974	6.528298	0.312823
22	12	0	950	20	236.2437	0.520808	1.246408
23	12	25	950	20	206.3194	13.66923	0.185236
24	12	12.5	1400	20	199.4541	4.248108	0.251119
25	14.25	12.5	950	20	185.0453	3.259484	0.091013
26	14.25	12.5	950	20	186.0455	3.259484	0.091013
27	16.5	12.5	950	0	178.2531	10.4999	0.014675

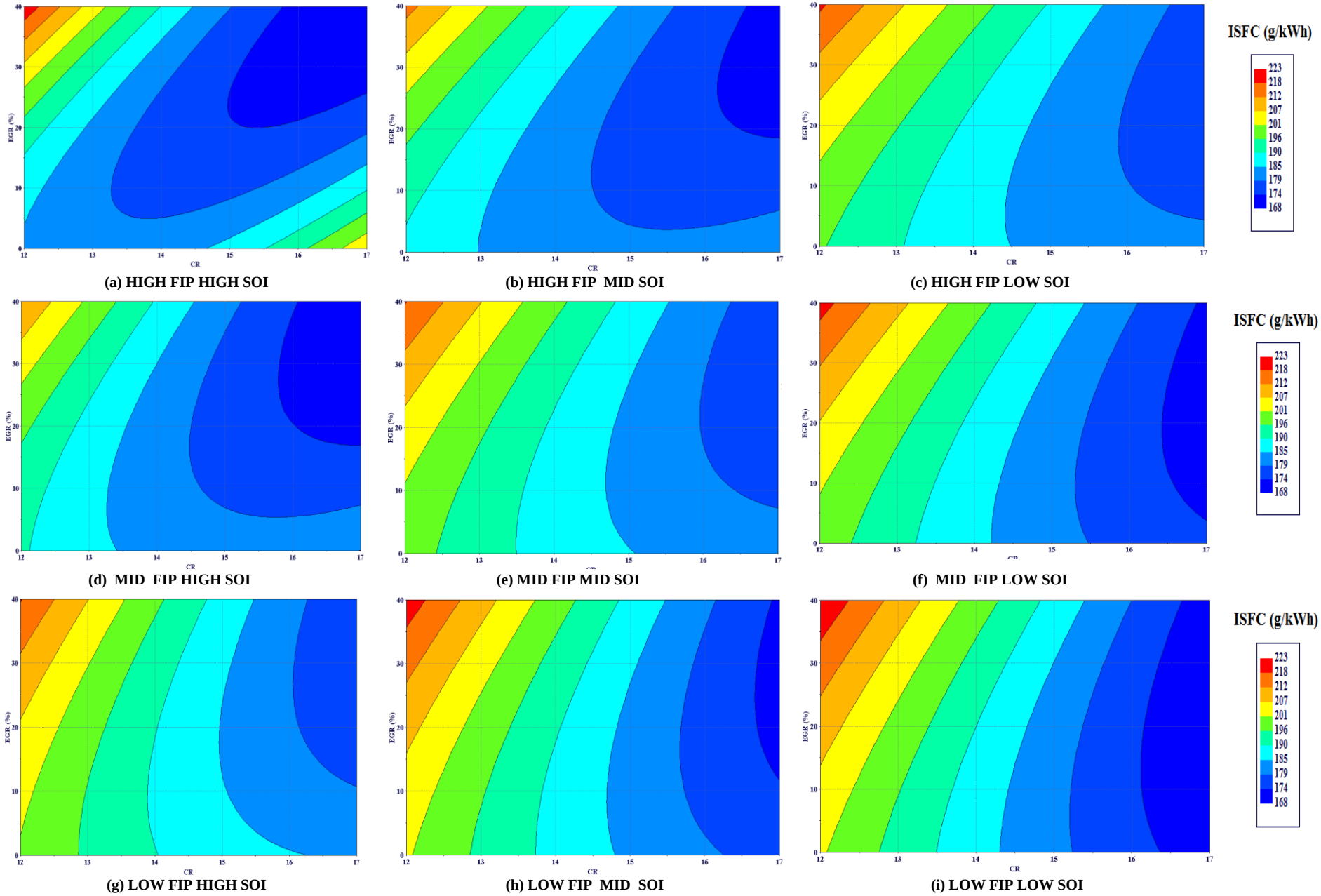

Fig.4. 19 Contour plots of ISFC for EGR and CR at different levels of SOI and FIP (CAT3401)

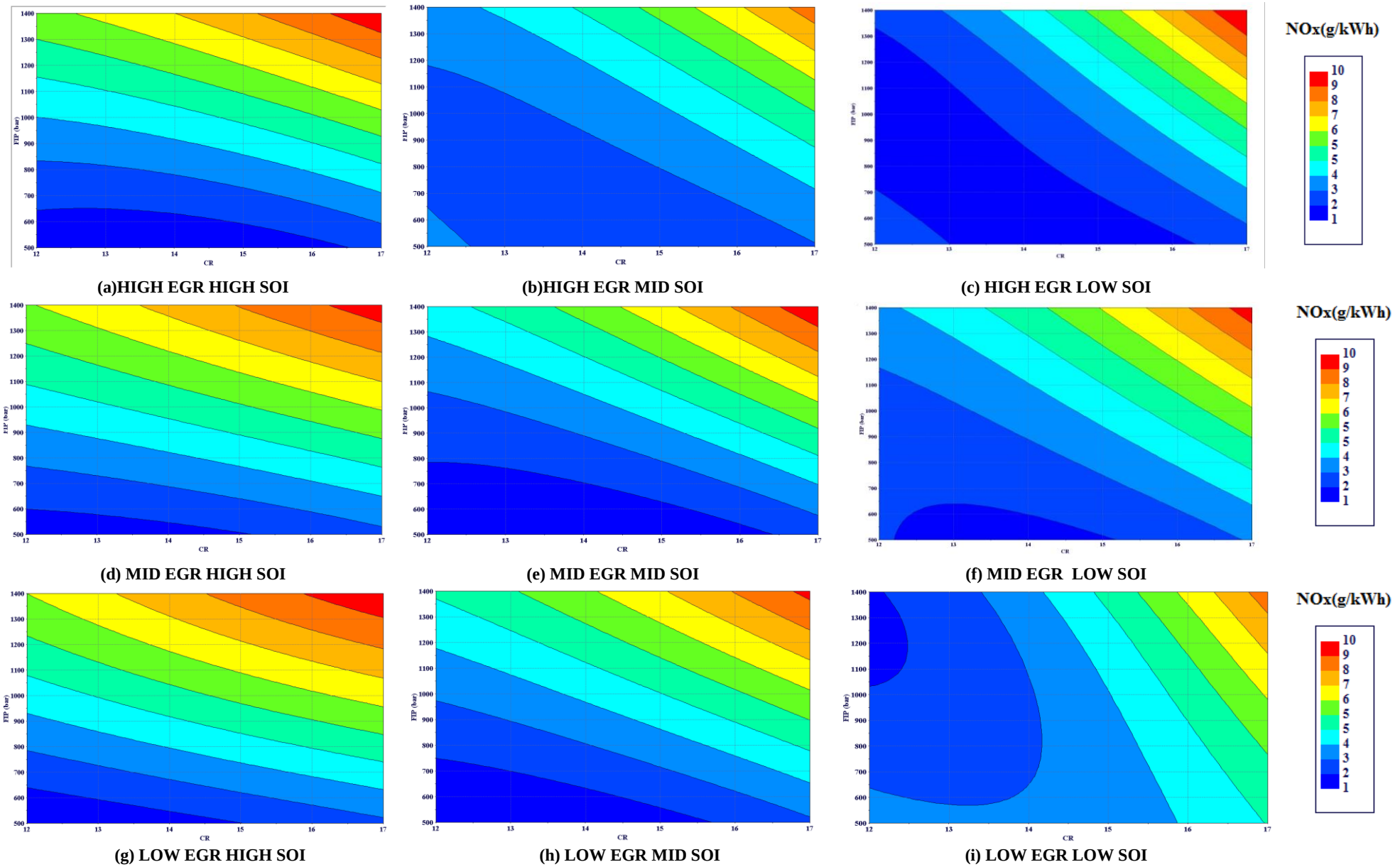

Fig.4. 20 Contour plots of NOx for FIP and CR at different levels of SOI and EGR (CAT3401)

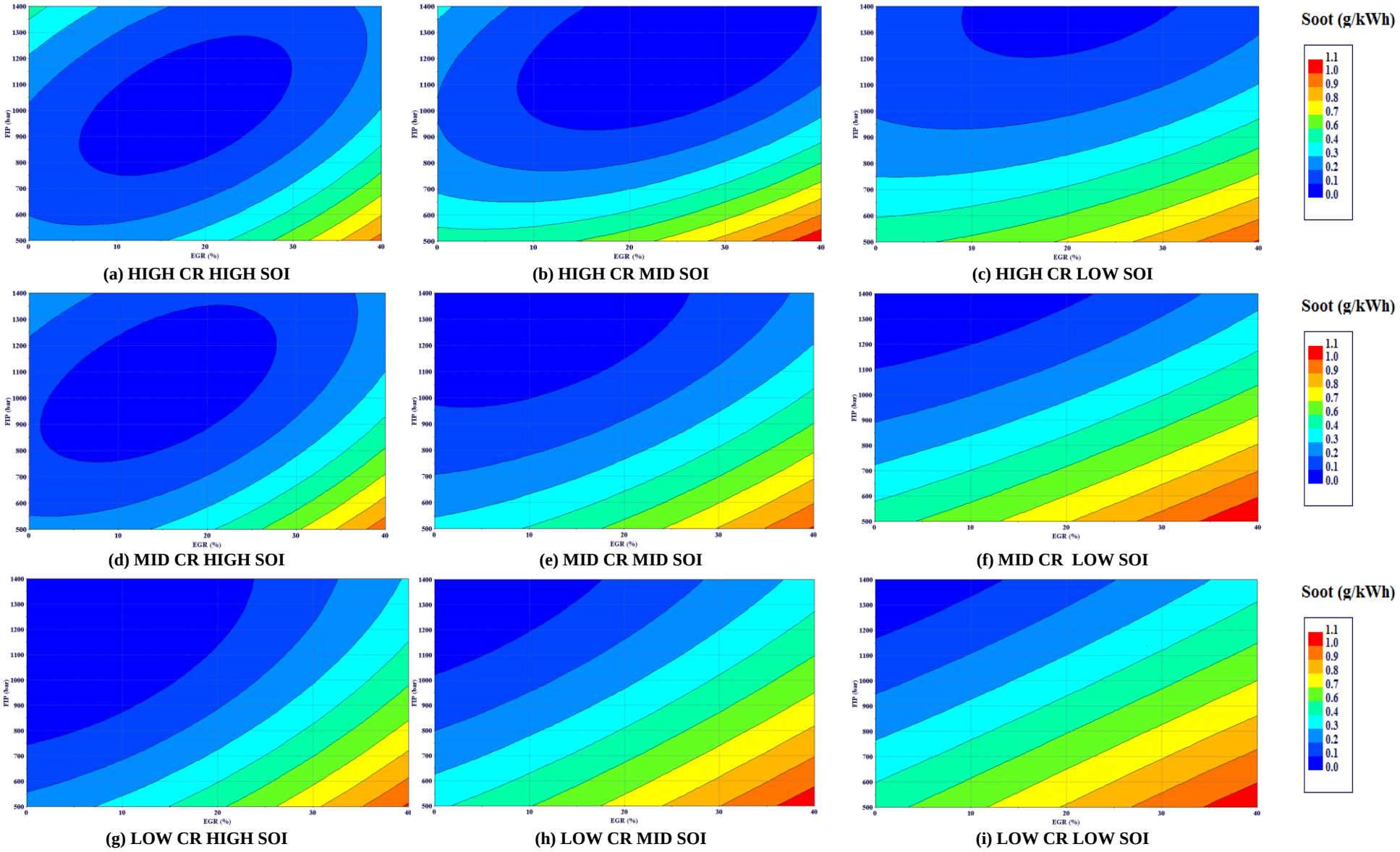

Fig.4.21 Contour plots of soot for FIP and EGR at different levels of SOI and CR (CAT3401)

4.1.4.1 Interaction effects of CAT3401

Interaction arises when the effect due to one parameter fluctuates with the level of the others. The interaction effects may not be identified by conventional one-factor-at-a-time experimentation. One can reveal previously unobserved interactions when you analyze a multi-level design. It is quite often that the results can show a productive insight in the system.

It is observed from the Fig 4.19 that the interaction of EGR and CR for ISFC is shown at nine different combinations of levels of the other two parameters viz FIP and SOI. As the EGR is increased from 0 to 40% the ISFC is increased in most of the instances. Interestingly from the Fig.4.19 (a), at high FIP and high SOI the trend is reversed at higher compression ratios. At higher compression ratios the ISFC decreasing with an increase in EGR. This is due to the fact that at higher CRs are responsible for higher temperatures and pressures inside the cylinder, thereby advances the start of combustion in case of high levels of FIP and SOI. This advanced start of combustion will end up with lesser indicated power due to the more compression work and thus results in higher ISFC.

Figure 4.19 (b) shows the interaction of CR and EGR at high FIP and mid SOI. The extent of the feasible region is more in this instance compared to others. Similarly the Fig 4.19 (c-h) shows the interaction of CR- EGR at different FIP and SOI combinations. For any instance the CR-EGR interaction has a favorable effect at the different levels of FIP and SOI. (High FIP and High SOI), (High FIP Mid SOI) , (Mid FIP High SOI) Fig.4.19 (a), (b) and (d) are quite favorable in reducing ISFC. Further a detailed view can reveal that the operating range was good enough in the case of High FIP and High SOI.

It is observed from Fig 4.20 that the interaction of FIP and CR for NOx is shown at various levels of EGR and SOI. It is observed from the figure that increasing the compression ratio resulted in the increase of NOx emissions. This could be due to the fact that as the compression ratio is increased, it increases in cylinder temperature and pressures which in turn increase flame temperatures. An increase in the fuel injection pressure increases in-cylinder pressure and NOx emissions and decrease soot emissions. This could be due to the fact that the increase in fuel injection pressure leads to better atomization of the fuel, which results in the smallest droplet size, faster evaporation of fuel sprays. This improves reaction between fuel and air. This resulted in comparatively higher temperature regions inside the combustion chamber and contributed to higher formation of NOx. It is also observed from the

figure that advanced start of injection increases NOx emissions. This is due to the fact that in cylinder temperature and pressures were low at the time of fuel injection, which increased the ignition delay and also penetration of fuel spray, enhanced reaction between fuel and air improved which resulted in very rapid burning rates once combustion started with high rates of pressure and temperature rise. Increasing the compression ratio resulted in the increase of in cylinder pressure, NOx emissions. This could be due to the fact that as the compression ratio is increased, it increases in cylinder temperature and pressures which in turn increase flame temperatures. It can also be interpreted that combination of high compression ratios and advanced start of the injection results in high in cylinder temperatures and thereby produces higher NOx emissions.

Fig 4.21 shows the contour plots of the interaction of FIP and EGR on the response soot. It can be concluded from the Fig that the interaction of EGR and FIP is less dominant in the regions of low SOI and low CR. It is also observed that the interaction is sensitive in the region of high EGR and lower FIP. The interaction operating regions are also beneficial where the other parameters (SOI and CR) are at mid to high levels. At a higher compression ratio the interaction is less dominant and also fruitful in minimizing the soot. The Fig also shows the interaction at different levels of the other two parameters (CR and SOI). Out of nine combinations the mid SOI and high CR gives the most profitable area of operation.

If the SOI and CR is brought to their highest levels, the soot reduces. SOI has a limit beyond which, soot again increases this is the point where beyond which spray could reach the comparatively cool cylinder wall which results in increase the soot. At all CR's increasing FIP's reduces soot, and also increase in CR results in lower soot levels. As FIP was increased it leads to more atomization and proper burning results in less soot. It may also increase the surface area of spray which helps in good mixing of air and fuel. Increasing CR raises the temperature of the air inside that will favor the vaporization of fuel, which brings good combustion characteristics and less soot. Increase in EGR increases soot this may be due to dilution of the charge which results in increased unburned parts of charge hence the soot increases. SOI and FIP are the two most important parameters that could reduce soot to a large extend, increasing FIP and advancing SOI brings down the soot, but up to a limit beyond which spray particles entering crevice region resulting in increase of soot emissions.

4.1.4.2 ANOVA analysis of CAT3401

The ANOVA analysis of the three responses is given in Table 4.5-4.7. The regression models are analyzed based on Analysis of Variance (ANOVA) which gives the 'p' value for different response parameters such as ISFC, NOx and soot emissions. The 'p' values for output responses are given in the Table. The effect of parameters is statistically significant if their 'p' values are less than 0.05 Montgomery (2008), Ryan et al. (2004). The reference limit

Table 4. 5 Analysis of variance (ANOVA) for the response (ISFC) of CAT3401

Analysis of Variance CAT 3401 **(ISFC)**						
Source	DF	Adj SS	Adj MS	F-Value	P-Value	Percentage contribution
Model	14	10365.2	740.37	82.84	0.000	98.98
Linear	4	7688.6	1922.16	215.08	0.000	73.42
CR	1	4429.8	4429.78	495.67	0.000	42.30
FIP	1	853.4	853.42	95.49	0.000	8.15
SOI	1	1940.1	1940.07	217.08	0.000	18.53
EGR	1	465.4	465.37	52.07	0.000	4.44
Square	4	1581.6	395.39	44.24	0.000	15.10
CR*CR	1	43.6	43.61	4.88	0.047	0.42
FIP*FIP	1	281.9	281.86	31.54	0.000	2.69
SOI*SOI	1	1490.1	1490.13	166.74	0.000	14.23
EGR*EGR	1	236.7	236.70	26.49	0.000	2.26
2-Way Interaction	6	1095.0	182.50	20.42	0.000	10.46
CR*FIP	1	207.1	207.07	23.17	0.000	1.98
CR*SOI	1	17.5	17.54	1.96	0.187	0.17
CR*EGR	1	410.0	410.04	45.88	0.000	3.92
FIP*SOI	1	385.5	385.54	43.14	0.000	3.68
FIP*EGR	1	6.8	6.76	0.76	0.402	0.06
SOI*EGR	1	68.1	68.07	7.62	0.017	0.65
Error	12	107.2	8.94			1.02
Lack-of-Fit	10	106.6	10.66	31.90	0.061	
Pure Error	2	0.7	0.33			
Total	26	10472.4				
Model Summary S R-sq R-sq(adj) R-sq(pred) 2.98948 98.98% 97.78% 94.12%						

for 'p' value was chosen as 0.05 based on 95% confidence interval. It is observed from the Table 4.5 that CR is most influential parameter for the response ISFC followed by SOI, FIP and EGR. The square term of the SOI also has a strong impact on ISFC. For NOx, SOI is the most influential, followed by EGR, FIP and CR. SOI also has a strong impact on soot followed by CR, FIP and EGR. The interaction FIP×SOI has a strong influence on soot followed by FIP×EGR, CR×EGR, SOI×EGR, CR×SOI and CR×FIP. The square effect of SOI, FIP and CR has also great influence on soot emissions.

Table 4. 6 Analysis of variance (ANOVA) for full quadratic model for the response (NOx) of CAT3401

Analysis of Variance CAT 3401 **NOx**						
Source	DF	Adj SS	Adj MS	F-Value	P-Value	Percentage contribution
Model	14	1005.53	71.823	144.12	0.000	99.41
Linear	4	782.10	195.525	392.34	0.000	77.32
CR	1	22.73	22.728	45.61	0.000	2.25
FIP	1	69.30	69.303	139.06	0.000	6.85
SOI	1	552.92	552.922	1109.49	0.000	54.66
EGR	1	137.15	137.148	275.20	0.000	13.56
Square	4	102.68	25.669	51.51	0.000	10.15
CR*CR	1	2.89	2.890	5.80	0.033	0.29
FIP*FIP	1	1.10	1.097	2.20	0.164	0.11
SOI*SOI	1	95.04	95.039	190.70	0.000	9.40
EGR*EGR	1	2.60	2.600	5.22	0.041	0.26
2-Way Interaction	6	120.75	20.125	40.38	0.000	11.94
CR*FIP	1	4.35	4.348	8.72	0.012	0.43
CR*SOI	1	1.59	1.590	3.19	0.099	0.16
CR*EGR	1	1.49	1.486	2.98	0.110	0.15
FIP*SOI	1	43.80	43.803	87.90	0.000	4.33
FIP*EGR	1	7.32	7.322	14.69	0.002	0.72
SOI*EGR	1	62.20	62.198	124.81	0.000	6.15
Error	12	5.98	0.498			0.59
Lack-of-Fit	10	5.98	0.598			
Pure Error	2	0.00	0.000			
Total	26	1011.51				
Model Summary S R-sq R-sq(adj) R-sq(pred) 0.705945 99.41% 98.72% 96.59%						

Table 4. 7 Analysis of variance (ANOVA) for full quadratic model for the response (soot) of CAT3401

Analysis of Variance CAT 3401 **Soot**						
Source	DF	Adj SS	Adj MS	F-Value	P-Value	Percentage contribution
Model	14	5.17806	0.36986	72.60	0.000	98.83
Linear	4	3.96160	0.99040	194.42	0.000	75.61
CR	1	0.84921	0.84921	166.70	0.000	16.21
FIP	1	0.83416	0.83416	163.75	0.000	15.92
SOI	1	1.63214	1.63214	320.39	0.000	31.15
EGR	1	0.64610	0.64610	126.83	0.000	12.33
Square	4	0.35224	0.08806	17.29	0.000	6.72
CR*CR	1	0.15610	0.15610	30.64	0.000	2.98
FIP*FIP	1	0.12223	0.12223	23.99	0.000	2.33
SOI*SOI	1	0.28186	0.28186	55.33	0.000	5.38
EGR*EGR	1	0.07017	0.07017	13.77	0.003	1.34
2-Way Interaction	6	0.86422	0.14404	28.27	0.000	16.50
CR*FIP	1	0.09167	0.09167	17.99	0.001	1.75
CR*SOI	1	0.10991	0.10991	21.58	0.001	2.10
CR*EGR	1	0.12756	0.12756	25.04	0.000	2.43
FIP*SOI	1	0.23850	0.23850	46.82	0.000	4.55
FIP*EGR	1	0.18355	0.18355	36.03	0.000	3.50
SOI*EGR	1	0.11304	0.11304	22.19	0.001	2.16
Error	12	0.06113	0.00509			1.17

Lack-of-Fit	10	0.06113	0.00611			
Pure Error	2	0.00000	0.00000			
Total	26	5.23919				

Model Summary

S	R-sq	R-sq(adj)	R-sq(pred)
0.0713737	98.83%	97.47%	93.28%

4.1.4.3 Error analysis of the regression model for CAT3401

The model summary of the each of the responses is also given in Table 4.5, 4.6 and 4.7 for ISFC NOx and soot. The regression statistics reveal the goodness of fit (R^2), adjusted R^2, and predicted R^2. These values were shown in the Tables (4.5) – (4.7). It is observed from the tables that the difference between predicted and adjusted R^2 values is less than 0.2 for all the three responses. That implies that the model was able to fit the data with reasonably good accuracy. The normal probability plots of the three responses for ISFC, NOx and soot are also depicted in the Fig.4.22 - 4.24 respectively. The figures indicate that all the models able to predict well with good consistency. This can be observed from the figures as the residuals have been falling almost in a straight line. This is an indication that errors for the ISFC, soot and NOx are normally distributed. This implies that the regression equations are accurate enough.

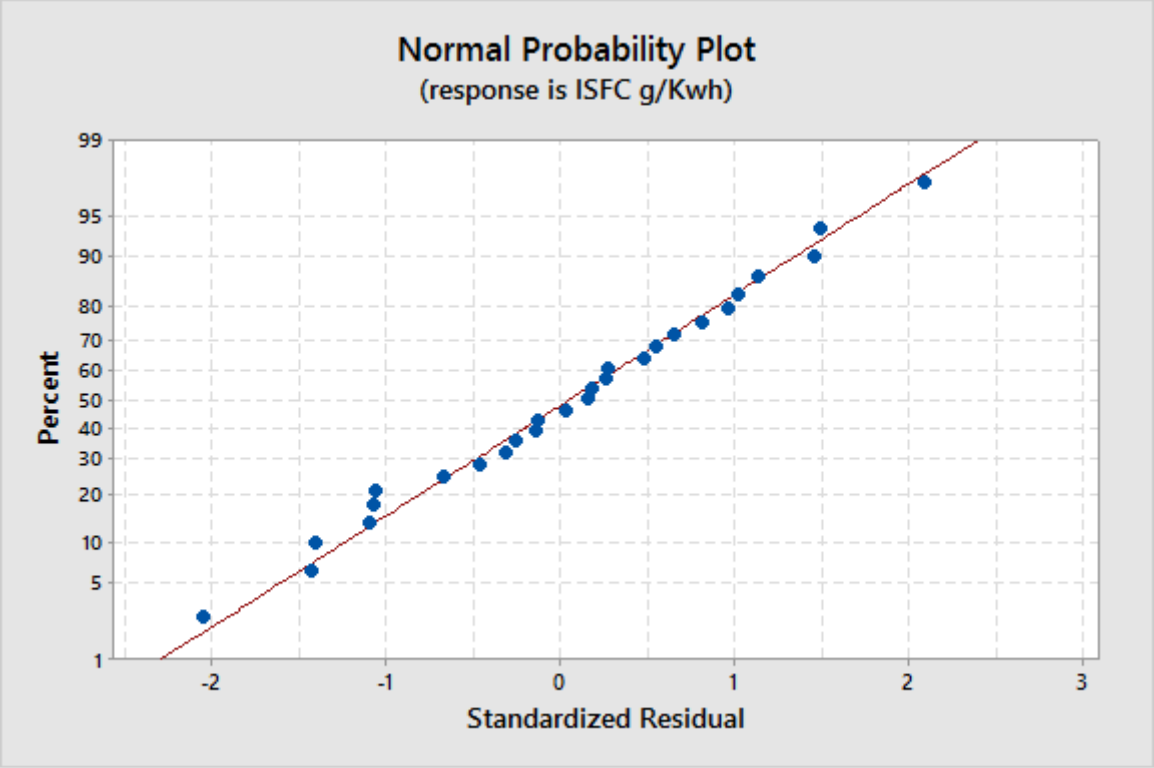

Fig.4. 22 Normal probability plot of the response ISFC for CAT 3401

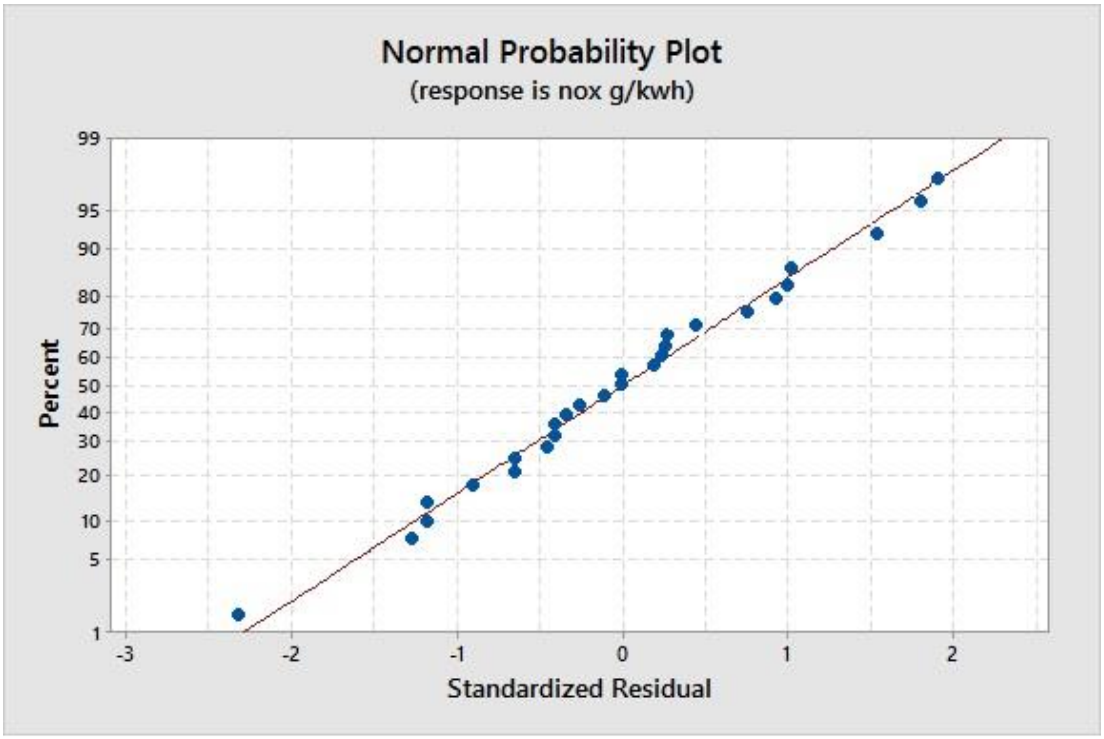

Fig.4. 23 Normal probability plot of the response NOx for CAT 3401

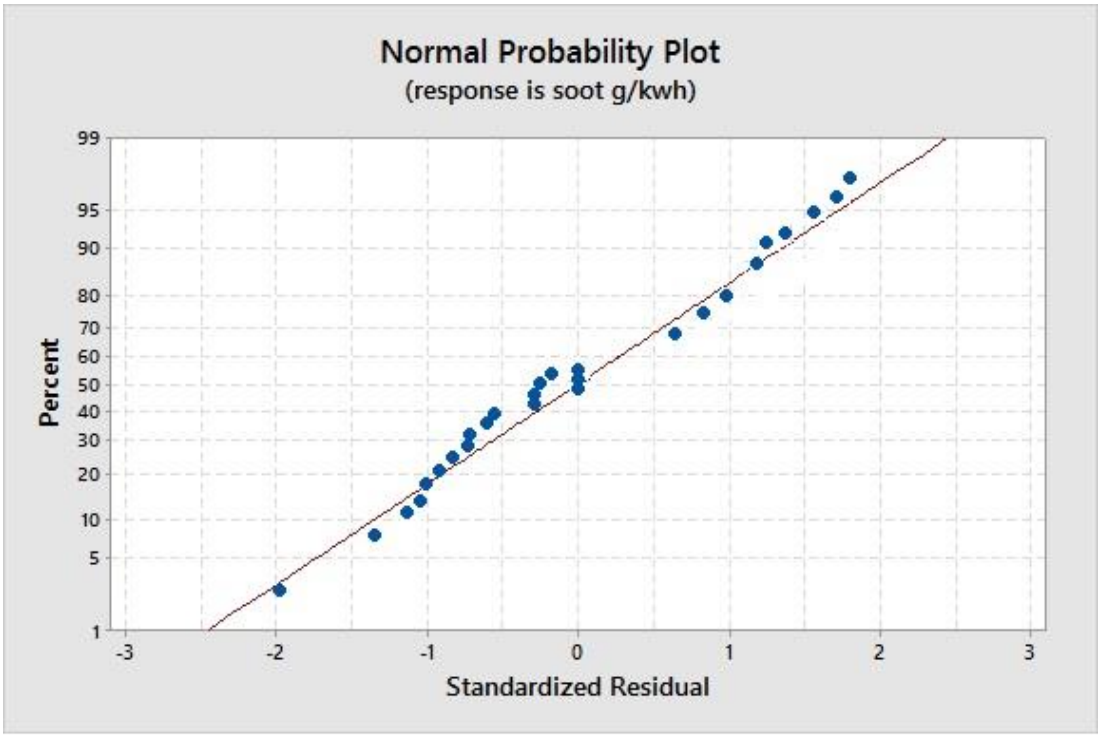

Fig.4. 24 Normal probability plot of the response soot for CAT 3401

4.1.4.4 Optimization of CAT3401 using desirability approach

The detailed effects of the four influencing parameters on the performance and emissions were analyzed for the given operating ranges. It is observed that an absolute tradeoff between NOx and soot, and NOx and ISFC exists. So it is important to optimize the influential parameters in order to minimize the emissions and ISFC.

Table 4. 8 Criteria of optimization used for desirability method for CAT3401

Parameter /Response	Limits		Criterion	Desirability
	Lower	Upper		
Compression Ratio	12	16.5	In range	1
Fuel Injection Pressure (bar)	500	1400	In range	1
Start of Injection (°aTDC)	0	-25	In range	1
Exhaust Gas Recirculation (%)	0	40	In range	1
ISFC (g/kWh)	172.87	242.57	Minimize	0.99
NOx (g/kWh)	0.2	20.77	Minimize	0.85
Soot (g/kWh)	0.01	1.4	Minimize	0.97
Combined				0.94

Based on the DOE analysis, regression equations (4.1) - (4.3) were developed for the responses ISFC, NOx and soot respectively. The equations were useful in deriving the relations between the process parameters and their responses. These are also useful in achieving the optimal parameters. The optimum combination of the parameters was to be found based on the composite desirability approach. Equal weights have been assigned for all the output responses in order to simultaneously minimize the ISFC, NOx and soot.

$$\begin{aligned} ISFC\left(\frac{g}{kWh}\right) = {} & 638.29 - 36.79 \times CR - 0.1910 \times FIP + 8.9406 \times SOI + 2.5218 \\ & \times EGR + 0.8035 \times CR^2 + 0.00028 \times FIP^2 + 0.1243 \times SOI^2 \\ & + 0.010301 \times EGR^2 + 0.006859 \times CR \times FIP - 0.23445 \times CR \\ & \times SOI - 0.16944 \times CR \times EGR - 0.001745 \times FIP \times SOI \\ & - 0.000133 \times FIP \times EGR + 0.115 \times SOI \times EGR \end{aligned} \quad (4.1)$$

$$NOx\left(\frac{g}{kWh}\right) = 28.03 - 3.346 \times CR - 0.01723 \times FIP + 0.6908 \times SOI + 0.2983 \times EGR + 0.10423 \times CR^2 + 0.0002 \times FIP^2 + 0.02968 \times SOI^2 + 0.002474 \times EGR^2 + 0.001030 \times CR \times FIP - 0.02242 \times CR \times SOI - 0.01355 \times CR \times EGR - 0.00633 \times FIP \times SOI - 0.00150 \times FIP \times EGR + 0.097 \times SOI \times EGR \quad (4.2)$$

$$Soot\left(\frac{g}{kWh}\right) = 9.9482 - 0.83719 \times CR - 0.08979 \times FIP + 0.2007 \times SOI + 0.08963 \times EGR + 0.0187 \times CR^2 + 0.0001 \times FIP^2 + 0.001382 \times SOI^2 + 0.0002 \times EGR^2 + 0.00028 \times CR \times FIP - 0.007479 \times CR \times SOI - 0.00498 \times CR \times EGR - 0.00042 \times FIP \times SOI - 0.000014 \times FIP \times EGR + 0.0882 \times SOI \times EGR \quad (4.3)$$

The optimum combination of operating parameters was found to be CR 14.55, SOI 16.29° bTDC, FIP 855 bar, and EGR 26.15 % with a composite desirability of 0.94.

4.1.4.5 Comparison of baseline and optimized configuration

The simulation results of optimized case are compared with the results of baseline case. It is observed from the Table 4.9 that the optimized case has got the best performance in terms of ISFC and produced the least amount of emissions (NOx and soot) as compared to the baseline engine configuration. The corresponding NOx and soot emissions are reduced by 40.3% and 52.38%, respectively, and a marginal reduction in the ISFC is accomplished. Fig 4.25 compares the baseline and optimized cases of CAT3401 for the pressure vs crank angle degree. It was noticed that the pressure rise after TDC is more in case of optimized case as compared to baseline. Temperature, NOx, soot, HC and CO were also compared for both baseline and optimized cases as shown in Fig 4.26 to 4.30 respectively. HC and CO emissions were also reduced in the optimized case. The reason for the reduced HC and CO emissions is the better mixing of charge and post combustion charge temperatures were considerably good enough to get them oxidize.

Table 4. 9 Comparison of Baseline and Optimized cases

	ISFC (g/kWh)	NOx (g/kWh)	Soot (g/kWh)
Baseline Case	**190.27**	**7.46**	**0.042**
Optimized case	**185.48**	**4.45**	**0.020**
	2.51% ↓	**40.3% ↓**	**52.38 %↓**

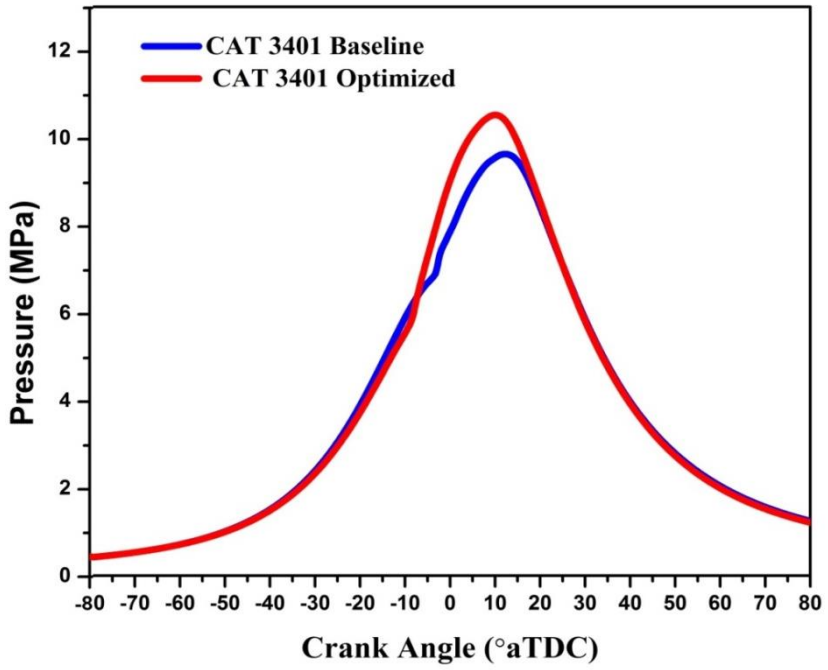

Fig.4. 25Comparision of optimized and baseline cases for Pressure Vs Crank Angle

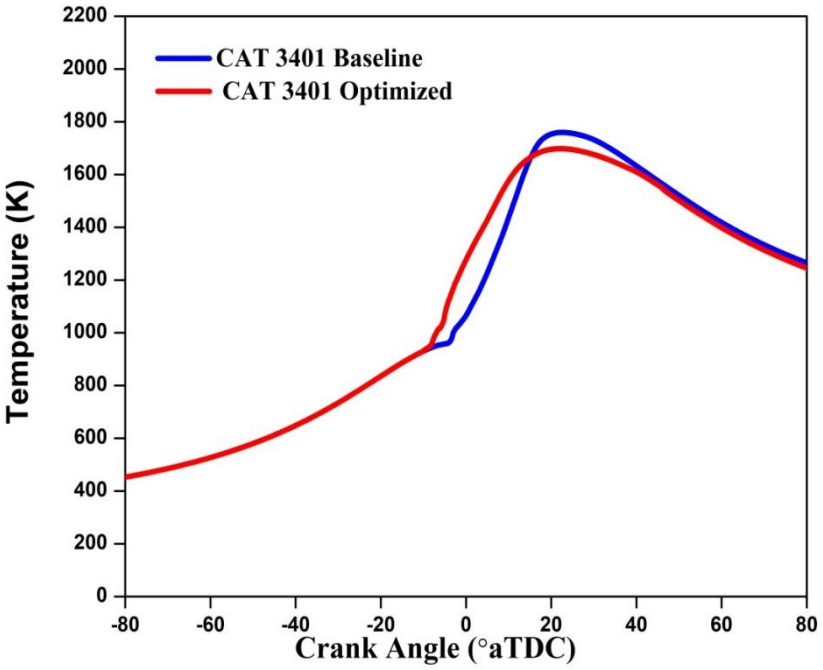

Fig.4. 26 Comparison of optimized and reference cases for Temperature Vs Crankangle

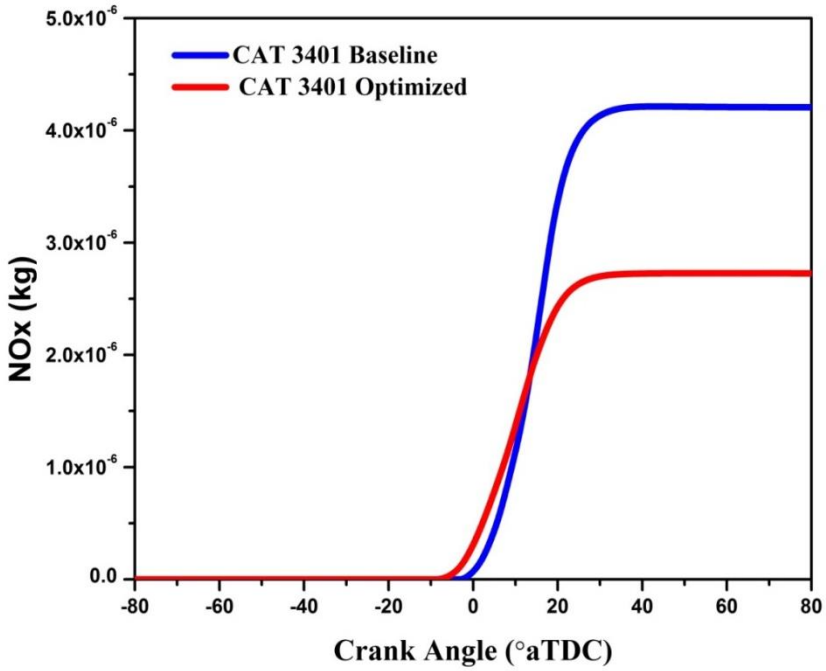

Fig.4. 27 Comparison of optimized and reference cases for NOx Vs Crankangle

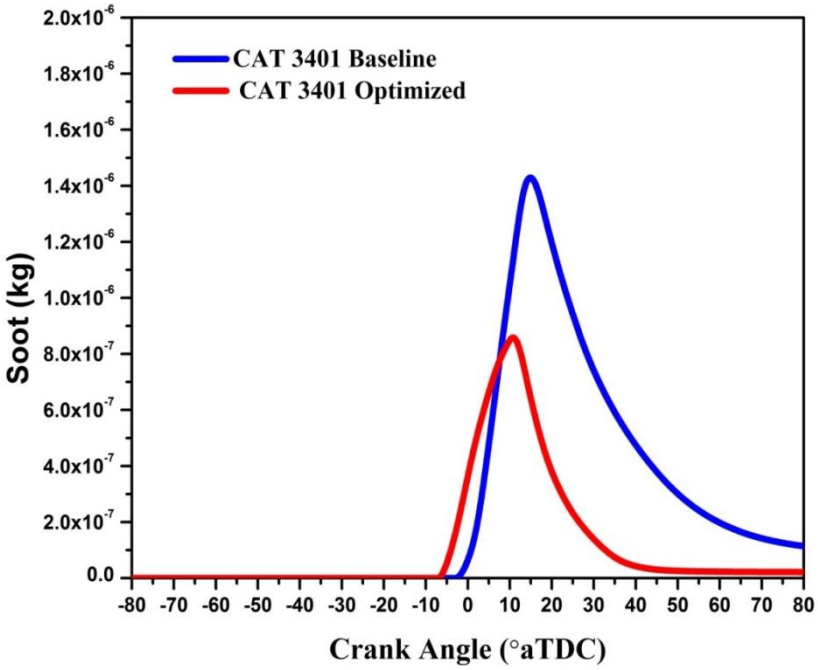

Fig.4. 28 Comparison of optimized and reference cases for NOx Vs Crank Angle

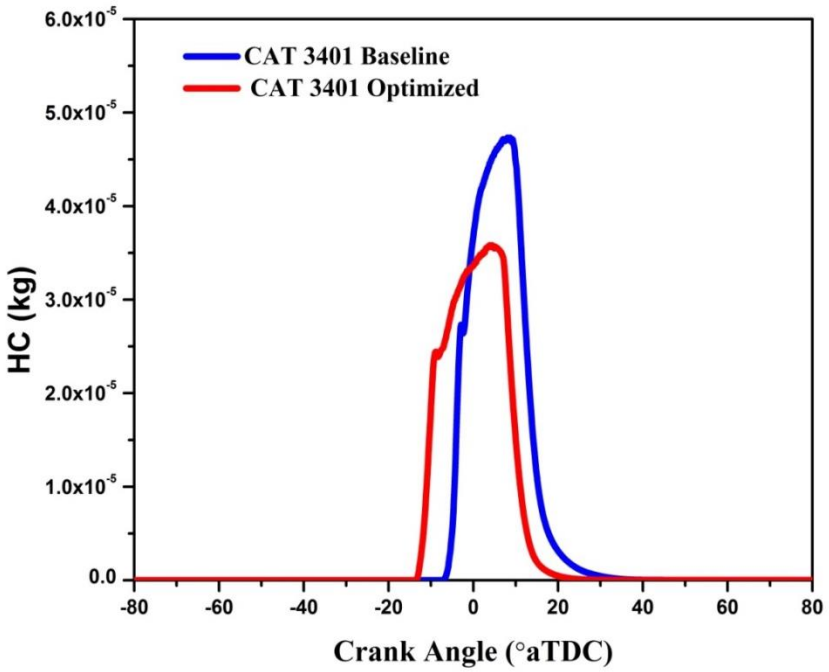

Fig.4. 29 Comparison of optimized and baseline cases for HC Vs Crank angle

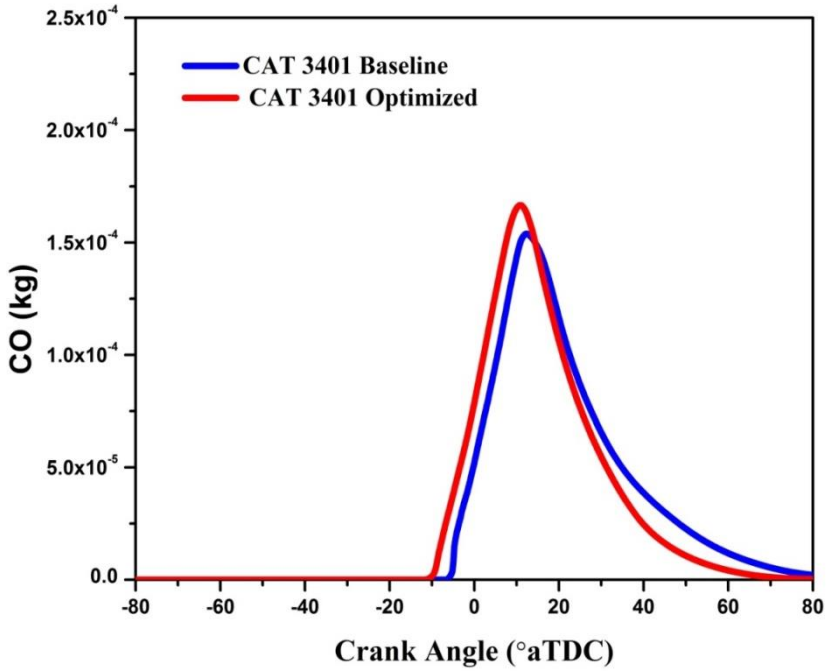

Fig.4. 30 Comparison of optimized and baseline cases for CO Vs Crank angle

4.1.4.6 Comparison of homogeneity index for baseline and optimized cases

Homogeneity of the mixture is quantified by percentage of **TFDI (Target fuel distribution index)** (Ramesh & Mallikarjuna, 2016) and it was compared for baseline and optimized cases as shown in Fig.4.31. The target range of the equivalence ratio for the practical diesel engine applications is from 0.3 to 1.2 (Akihama et al., 2001). The target equivalence ratio distribution region is depicted in the Fig.4.31 and its temperture shown in

the Fig.4.32. The corresponding formulae for TFDI, LFDI and RFDI are given in equation 4.4 to 4.6 respectively.

$$\text{TFDI (Target fuel distribution index)} = \left(\frac{mass\ of\ the\ cells\ having\ equivalence\ ratio\ from\ 0.3\ to\ 1.2}{Total\ mass}\right) \times 100 \quad (4.4)$$

$$\text{LFDI (Lean fuel distribution index)} = \left(\frac{mass\ of\ the\ cells\ having\ equivalence\ ratio\ less\ than\ 0.3}{Total\ mass}\right) \times 100 \quad (4.5)$$

$$\text{RFDI (Rich fuel distribution index)} = \left(\frac{mass\ of\ the\ cells\ having\ equivalence\ ratio\ greater\ than\ 1.2}{Total\ mass}\right) \times 100 \quad (4.6)$$

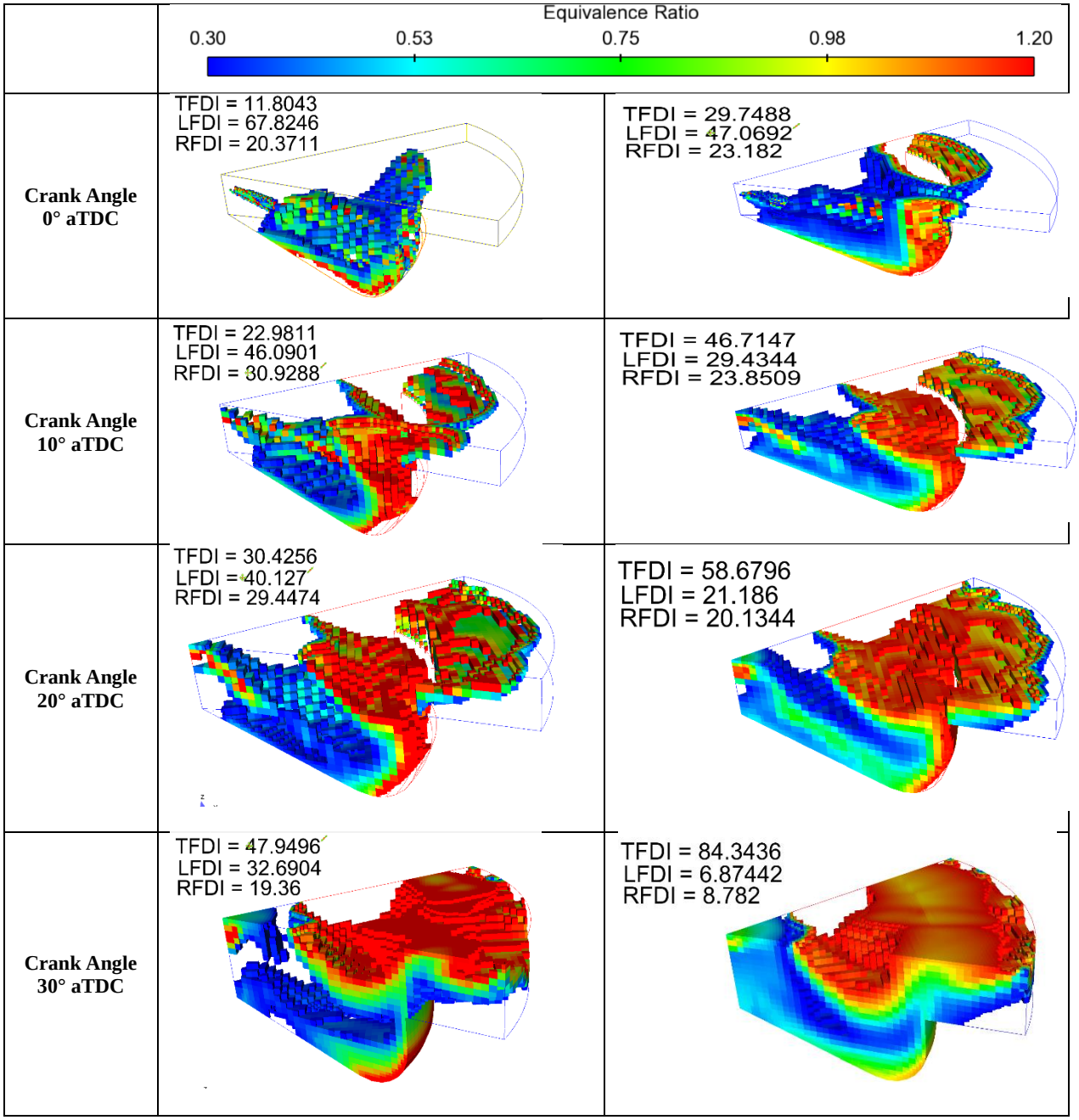

Crank Angle 40° aTDC	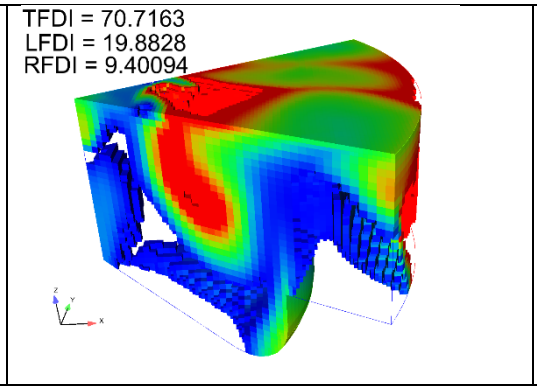	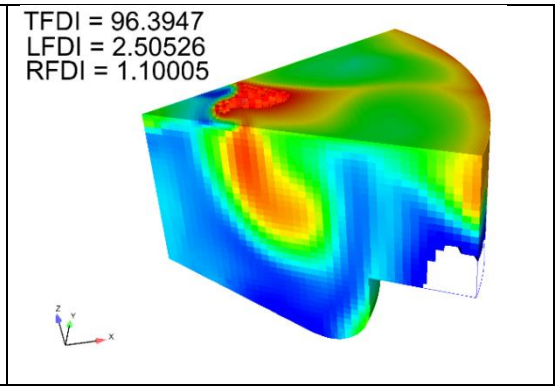
	Baseline case	Optimized case

Fig.4. 31 Homogeneity index and distribution of eqvivalence ratio baseline and optimized cases for CAT 3401 diesel engine

Figure 4.30 shows the distribution of TFDI (**Target fuel distribution index**) at different crank angle instances (from cranks angle 0 to 40°aTDC) in which dominant combustion can be realized. At 0° aTDC the TFDI of baseline and optimized were observed to be 11.8043 and 29.7488 respectively. Similarly, at all the instances the homogeneity index (TFDI) was better for the optimized case. At 40° aTDC the TFDI of baseline and optimized case have 70.7163 and 96.3947 respectively. Improved TFDI for optimized case over the baseline is an indication of the improved homogenous mixture. The temperature distribution is depicted in Fig.4.32 for the same target region. It is observed from the figure that the optimized case has lesser high temperature zones as compared to the baseline case. Because of these reasons NOx emissions were reduced as compared to baseline (Fig.4.27). It was also noted that the soot emissions were decreased when compared to the baseline case (Fig.4.28) this is due to increased homogeneity index.

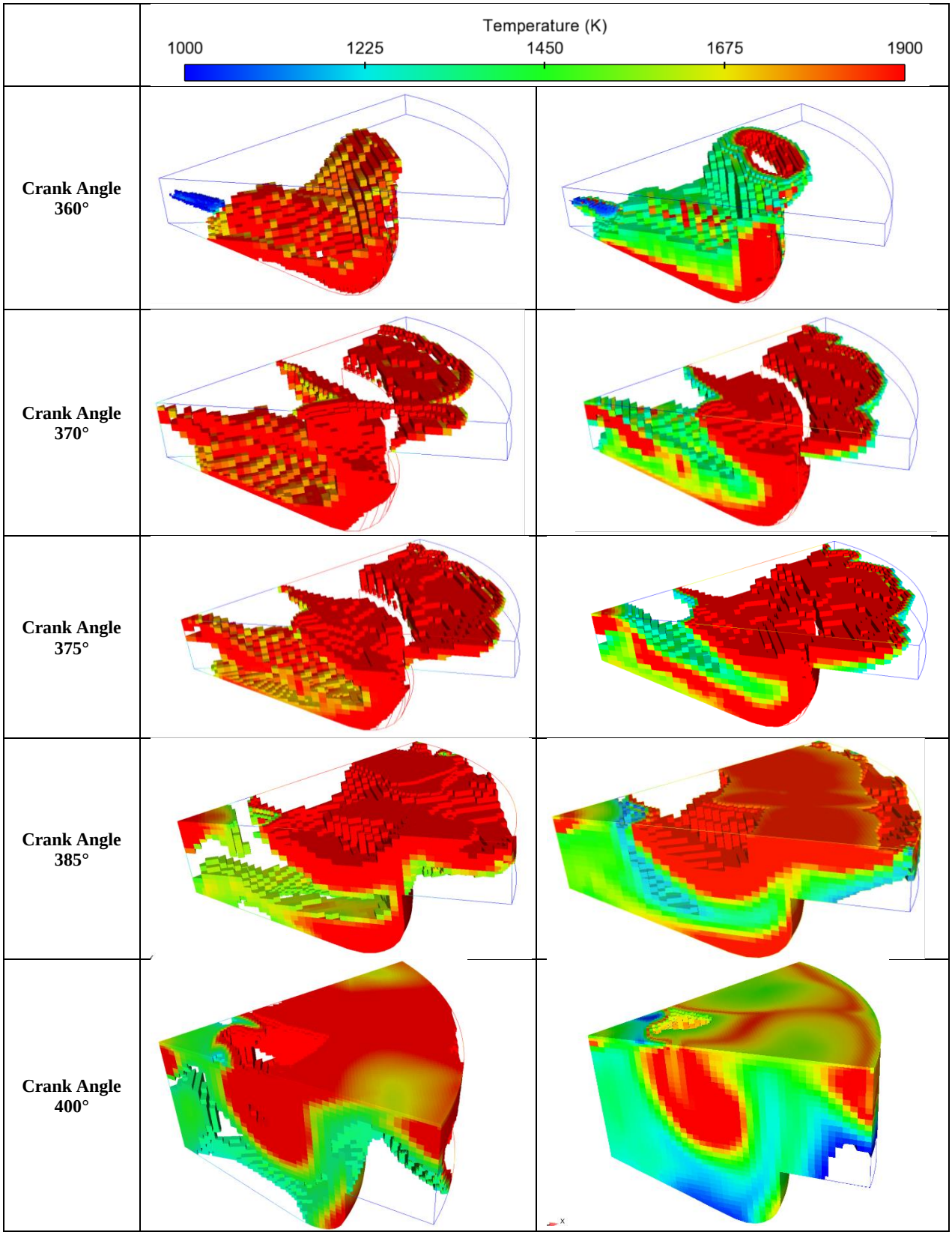

Baseline case Optimized case

Fig.4. 32 Temperature distribution of baseline and optimized cases at different crank angles

Summary

Increasing CR reduces ISFC and soot whereas it increases NOx emissions and vice versa, but this trend reverses when the SOI and FIP are at their high levels. Increasing FIP reduces soot and also slightly reduces ISFC but increases NOx significantly. But this is also not valid when the low EGR and advanced SOI co-exist. Advancing SOI reduces soot and increases NOx but the ISFC may decrease or increase and eventually will depend on the compression work. Increasing EGR alone increases the soot and ISFC whereas the NOx emissions decrease significantly, whereas this phenomenon turn round when the CR and SOI are at high levels. The single parametric study may not guarantee an optimal operating characteristics. DOE based parametric study is a systematic approach to predict the variations of performance and emission characteristics and interaction effects. Interaction effects are also playing a major role in determining the output responses. CR×FIP, CR×EGR and FIP×SOI interactions have strongly influenced the ISFC. The SOI×EGR interaction has a lesser impact compared to former but remaining two interactions (CR× SOI and FIP×EGR) are not significant enough. SOI×EGR and FIP× SOI interactions have strong influence on NOx whereas FIP×EGR and CR×FIP are relatively less significant and other two (CR× SOI and CR×EGR) are not significant. All the interaction effects of soot are significant and are equally influential.

The optimum combination of parameters was found out to be CR 14.55, FIP 855 bar, SOI 16.29° bTDC, and EGR 26.15 % of the CAT3401 diesel engine. The corresponding composite desirability was found to be 0.94. The optimal combination of the parameters simultaneously reduces NOx and soot by 40.3% and 52.38% respectively with a little improvement in ISFC. Improved TFDI along with simultaneous reduction of NOx and soot of the optimized case resembles the combustion characteristics as that of HCCI. Thus HCCI combustion characteristics seemed to be achieved by the parametric optimization of the CAT 3401 engine.

4.2 Analysis of VCR engine (Diesel)

In the previous section we have analyzed CAT 3401 which was a heavy duty engine, whereas a VCR engine is a small bore engine generally used for the Genset applications. In view of exploring the dependency of the parametric behavior on engine capacity, VCR engine is considered. The idea is to develop better performance and combustion characteristics as compared to the baseline engine configuration of the VCR engine. For this reason the same parameters (CR, SOI, EGR and FIP) were chosen to optimize the engine performance and emission characteristics.

4.2.1 Validation of VCR Engine Model (Diesel)

The simulation and experimental results are compared to validate numerical results obtained from CFD code CONVERGE^{TM} VCR diesel case. The computational domain of the VCR engine is shown in Fig 4.33. The VCR engine specifications are given in Table 4.10. Validation of the predicted numerical results was carried out by comparing the pressure variation with crank angle with that of the experimental data. Figure 4.34 shows the variation of pressure with crank angle for experimental and simulation results. The trends of simulation are similar to that of experiment. However, a slight difference of around 1.2% in peak pressure is observed. Experimental pressure shows lesser as compared to simulation. This may be due the fact that during the compression stroke the gases may escape from the crevice region and would end up with lower in-cylinder pressure. This shows that the present model is in good accordance with the experimental results of the VCR diesel engine.

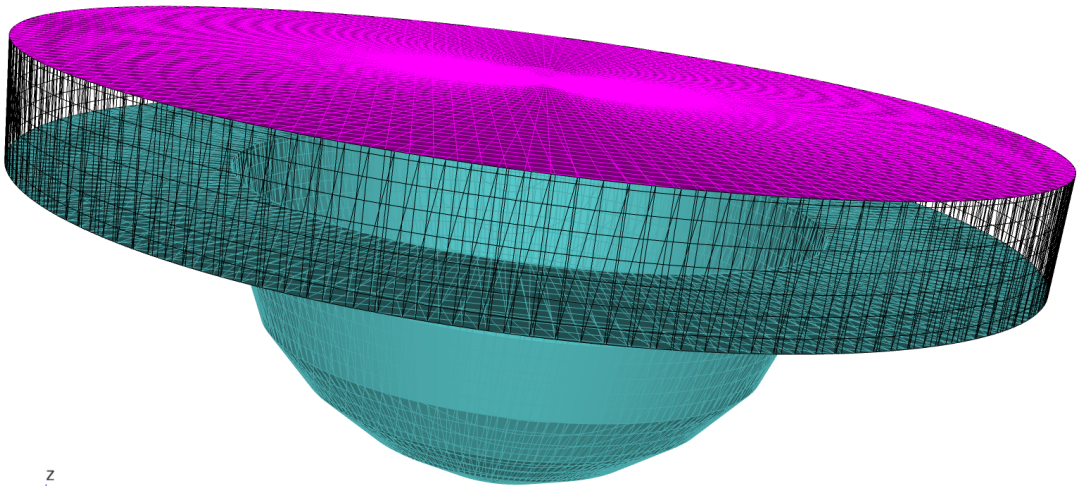

Fig.4. 33 Computational domain of variable compression ratio (VCR) engine model

Table 4. 10 Specifications of VCR engine

Cylinder bore x stroke (mm)	87.5 x 110 mm
Connecting Rod length (mm)	234 mm
Displacement Volume (L)	0.66
Compression Ratio	17.5
Number of nozzle orifice x diameter (mm)	3 x 0.255
Piston crown	Hemispherical
Intake valve closure (CA)	144.5°bTDC
Swirl ratio (nominal)	0.7
Inlet air temperature (K)	303
Inlet air pressure (kPa)	111
Engine speed (rpm)	1500 rpm
Fuel	Diesel/PB20
Type of fuel Injection	Direct Injection
Injection Pressure (MPa)	28
Fuel Injected (kg/cycle)	2.57778e-05
Overall Equivalence ratio	0.55
Injection duration	21 crank angle degrees
Start of Injection	23 °bTDC (baseline case)

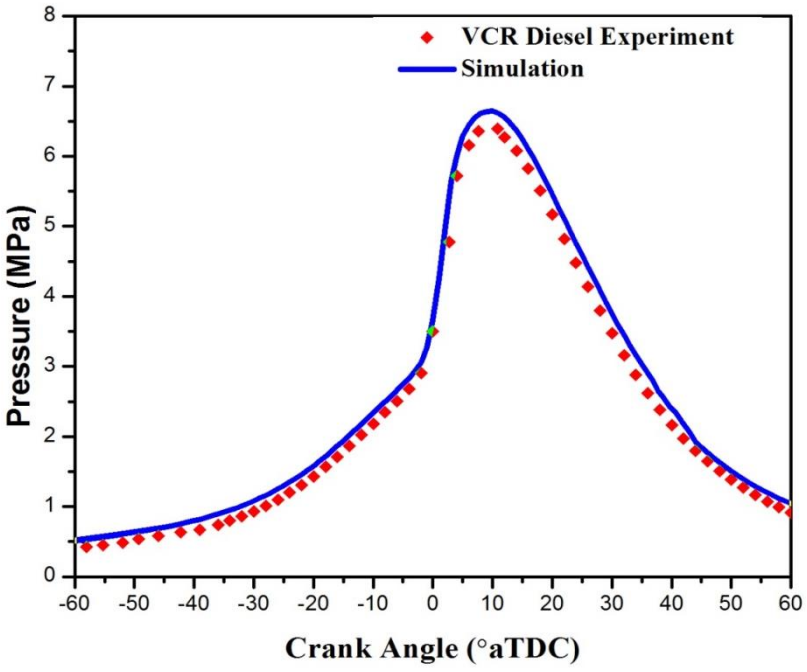

Fig.4. 34 Validation of pressure Vs Crank angle for VCR diesel engine

4.2.2 DOE Analysis of VCR diesel

Box-Behnken method was applied for designing the numerical experiments. In this method each variable is maintained at 3 equal intervals. For example, if the CR range is from 12 to 18, it is assigned as 12, 15 and 18 and considered for numerical experiment design. Since there are 4 variables and 3 center points, thus it becomes total set of 27 experiments with each block having 2 variations (means two independent variables are varied per experiment). The ranges of the each parameter have been chosen based on the similar exercise that was performed for the CAT3401.

The ranges of the selected parameters are as follows

- CR 12 to 18
- EGR 0 to 40 %
- FIP 250 to 1000 bar
- SOI 40 to 15 °bTDC

The values that are obtained from DOE (Box Behnken method) using Minitab are given below. The model took the mid value of the given range as an additional level. Total three levels have been used such as low, mid and high.

- CR 12, 15, 18
- EGR 0, 20, 40 %
- FIP 250, 625, 1000 bar
- SOI 40, 27.5, 15 bTDC

The center points of experiments were CR 15, EGR 20%, FIP 625 bar and SOI 27.5° bTDC. The experimental matrix is shown in Table 4.11.

Table 4. 11 Design matrix of the VCR diesel case based on DOE

Run	CR	SOI (bTDC)	FIP(bar)	EGR (%)
1	18	27.5	250	20
2	18	27.5	625	0
3	15	40	625	0
4	15	27.5	625	20
5	18	27.5	1000	20
6	15	27.5	1000	0
7	18	40	625	20
8	12	27.5	625	40
9	15	27.5	250	0
10	12	15	625	20
11	15	40	625	40
12	12	27.5	250	20
13	15	27.5	1000	40
14	15	15	250	20
15	12	27.5	1000	20
16	12	40	625	20
17	15	15	1000	20
18	15	27.5	625	20
19	15	15	625	0
20	15	40	1000	20
21	18	27.5	625	40
22	18	15	625	20
23	15	27.5	625	20
24	15	40	250	20
25	15	27.5	250	40
26	12	27.5	625	0
27	15	15	625	40

Table 4. 12 Experimental design and their responses for VCR diesel case

Run order	CR	SOI (°bTDC)	FIP (bar)	EGR (%)	**ISFC (g/kWh)**	**Soot (g/kWh)**	**NO_x (g/kWh)**
1	18	27.5	250	20	242.811	0.48552	4.15
2	18	27.5	625	0	195.396	0.04004	10.4732
3	15	40	625	0	182.571	0.78328	12.1134
4	15	27.5	625	20	226.281	0.61038	2.97377
5	18	27.5	1000	20	217.721	0.11951	5.03205
6	15	27.5	1000	0	208.337	0.64078	8.47935
7	18	40	625	20	195.497	0.10355	8.547
8	12	27.5	625	40	261.431	1.216	1.45875
9	15	27.5	250	0	237.53	0.74746	6.234
10	12	15	625	20	264.755	1.64901	0.5319
11	15	40	625	40	210.29	0.92654	3.897
12	12	27.5	250	20	277.856	1.22303	1.12884
13	15	27.5	1000	40	232.921	0.70414	1.48125
14	15	15	250	20	277.571	2.01875	0.9867
15	12	27.5	1000	20	256.956	0.5529	2.03835
16	12	40	625	20	218.643	0.9291	5.9634
17	15	15	1000	20	227.193	1.3965	1.5768
18	15	27.5	625	20	221.707	0.61038	2.8035
19	15	15	625	0	223.25	1.292	6.23505
20	15	40	1000	20	209.171	0.93376	7.1258
21	18	27.5	625	40	216.781	0.417	3.125
22	18	15	625	20	214.596	1.32316	3.20124
23	15	27.5	625	20	221.707	0.59442	2.73675
24	15	40	250	20	231.306	1.0526	5.3205
25	15	27.5	250	40	257.132	1.7005	0.67695
26	12	27.5	625	0	224.184	0.70167	5.125
27	15	15	625	40	237.747	2.11351	1.9125

4.2.3 Interaction effects of VCR (Diesel)

Figure 4.35 shows the interaction plots of EGR and CR at different levels of SOI and FIP (VCR diesel). It can be observed from figure that as the interaction of EGR and CR. As the EGR is increased from 0 to 40% ISFC increased from the level 195 to 265 g/kWh. It is

observed from the figure that the ISFC is favorable in the mid to high range of FIP and SOI. The operating range of CR between high and mid shows (fig (a), (b) and (d)) quite favorable in reducing ISFC. Further a detailed view can reveal that operating range was good enough in the case of high FIP and mid SOI.

Figure 4.36 represents the interaction of CR and FIP on NOx emissions at different levels of EGR and SOI. It is observed from the figure that the NOx emissions are favorable in mid to high range of EGR and low to mid-range of SOI. It can also be interpreted from the figure that the increase in the fuel injection pressure increases NOx emissions. Low EGR and the high SOI combination is not fruitful at any stage of the interaction of CR and FIP. The effect of fuel injection pressure and compression ratio on NOx emissions is mainly depends on the state of the mixture and ignition delay. As the EGR is increased the NOx decreases. This is due to the fact that EGR increases the specific heat of intake mixture, thus reduces the combustion temperature. It may also lower the amount of oxygen in the intake mixtures. This combination of reduced combustion temperatures and reduced oxygen content lowers the NOx emissions.

Figure 4.37 shows contour plots of soot for the SOI and CR at different levels of FIP and EGR. It is seen from the figure that the interaction of CR and SOI is dominant in the region of high EGR and mid to high FIP. The variation of interaction is less aggressive in the low EGR range. The interaction causes more fruitful region when the other two parameters (EGR and FIP) are set at low and high levels respectively.

4.2.4 ANOVA analysis for VCR (diesel)

The table 4.13 to 4.15 provides the **ANOVA** data of VCR engine (diesel) for the responses ISFC, NOx and soot respectively. The table reveals the linear, square and 2 way interaction effects on the responses based on its *p*-value. Especially, the *p*-value less than 0.05 indicate that the effect is significant on the response. Similarly the *p*-value greater than 0.05 indicates there is no significant effect on the response. The regression equations were developed based on the DOE analysis and are given in the equations 4.7, 4.8 and 4.9 of the responses ISFC, NOx and soot respectively. The percentage contribution of each of the terms in the equation is calculated based on the Adj SS. The formula used for this is given by "Percentage contribution" = $(\frac{Adj\ SS}{Total\ \ Adj\ SS})\times 100$.

Table 4. 13 ANOVA analysis of ISFC for VCR (diesel)

Analysis of Variance **ISFC (g/kWh)**						
Source	DF	Adj SS	Adj MS	F-Value	P-Value	Percentage contribution
Model	14	57344.5	4096.0	1268.29	0.000	99.93
Linear	4	54844.8	13711.2	4245.50	0.000	95.58
CR	1	27431.3	27431.3	8493.77	0.000	47.80
SOI	1	18997.3	18997.3	5882.29	0.000	33.11
FIP	1	5442.8	5442.8	1685.29	0.000	9.49
EGR	1	3034.2	3034.2	939.50	0.000	5.29
Square	4	311.8	78.0	24.14	0.000	0.54
CR*CR	1	93.6	93.6	28.98	0.000	0.16
SOI*SOI	1	39.9	39.9	12.35	0.004	0.07
FIP*FIP	1	49.6	49.6	15.37	0.002	0.09
EGR*EGR	1	29.0	29.0	8.97	0.011	0.05
2-Way Interaction	6	2187.8	364.6	112.91	0.000	3.81
CR*SOI	1	538.5	538.5	166.73	0.000	0.94
CR*FIP	1	561.5	561.5	173.85	0.000	0.98
CR*EGR	1	22.6	22.6	7.00	0.021	0.04
SOI*FIP	1	711.3	711.3	220.24	0.000	1.24
SOI*EGR	1	9.0	9.0	2.78	0.121	0.02
FIP*EGR	1	345.0	345.0	106.83	0.000	0.60
Error	12	38.8	3.2			0.07
Lack-of-Fit	10	38.8	3.9			
Pure Error	2	0.0	0.0			
Total	26	57383.2				
Model Summary S R-sq R-sq(adj) R-sq(pred) 1.79710 99.93% 99.85% 99.61%						

$$ISFC\left(\frac{g}{kWh}\right) = 714.7 - 34.79 \times CR - 4.964 \times SOI + 0.2263 \times FIP + 0.847 \times EGR + 0.4655 \times CR^2 - 0.01750 \times SOI^2 + 0.000022 \times FIP^2 - 0.00583 \times EGR^2 + 0.3094 \times CR \times SOI - 0.010531 \times CR \times FIP + 0.0396 \times CR \times EGR - 0.002845 \times SOI \times FIP - 0.00599 \times SOI \times EGR - 0.001238 \times FIP \times EGR \quad (4.7)$$

Table 4. 14 ANOVA analysis of NOx for VCR (diesel)

Analysis of Variance Nox (g/kWh)						
Source	DF	Adj SS	Adj MS	F-Value	P-Value	Percentage contribution
Model	14	416.095	29.721	40.13	0.000	97.91
Linear	4	371.303	92.826	125.34	0.000	87.37
CR	1	175.010	175.010	236.31	0.000	41.18
SOI	1	100.034	100.034	135.07	0.000	23.54
FIP	1	33.582	33.582	45.34	0.000	7.90
EGR	1	62.677	62.677	84.63	0.000	14.75
Square	4	12.040	3.010	4.06	0.026	2.83
CR*CR	1	11.123	11.123	15.02	0.002	2.62
SOI*SOI	1	3.494	3.494	4.72	0.051	0.82
FIP*FIP	1	0.700	0.700	0.94	0.350	0.16
EGR*EGR	1	1.238	1.238	1.67	0.220	0.29
2-Way Interaction	6	32.753	5.459	7.37	0.002	7.71
CR*SOI	1	0.399	0.399	0.54	0.477	0.09
CR*FIP	1	6.651	6.651	8.98	0.011	1.57
CR*EGR	1	8.244	8.244	11.13	0.006	1.94
SOI*FIP	1	5.371	5.371	7.25	0.020	1.26
SOI*EGR	1	8.129	8.129	10.98		1.91
FIP*EGR	1	3.960	3.960	5.35	0.039	0.93
Error	12	8.887	0.741			2.09
Lack-of-Fit	10	8.887	0.889	2736.35	0.000	2.09
Pure Error	2	0.001	0.000			
Total	26	424.983				
Model Summary S R-sq R-sq(adj) R-sq(pred) 0.860586 97.91% 95.47% 87.96%						

$$NOx\left(\frac{g}{kWh}\right) = 23.5 - 3.83 \times CR - 0.610 \times SOI + 0.00131 \times FIP + 0.436 \times EGR + 0.165 \times CR^2 + 0.000003 \times FIP^2 + 0.00518 \times SOI^2 + 0.001204 \times EGR^2 + 0.0344 \times CR \times SOI - 0.000281 \times CR \times FIP - 0.02393 \times CR \times EGR + 0.000247 \times FIP \times SOI - 0.00570 \times SOI \times EGR - 0.000133 \times FIP \times EGR \quad (4.8)$$

$$Soot\left(\frac{g}{kWh}\right) = 0.51 + 0.627 \times CR - 0.1939 \times SOI - 0.003689 \times FIP + 0.0613 \times EGR - 0.02179 \times CR^2 + 0.000001 \times FIP^2 + 0.003774 \times SOI^2 + 0.00034 \times EGR^2 - 0.00351 \times CR \times SOI + 0.000071 \times CR \times FIP - 0.001527 \times CR \times EGR + 0.000028 \times FIP \times SOI - 0.000714 \times SOI \times EGR - 0.000031 \times FIP \times EGR \quad (4.9)$$

Table 4. 15 ANOVA analysis of soot for VCR (diesel)

Analysis of Variance **Soot(g/kWh)**						
Source	DF	Adj SS	Adj MS	F-Value	P-Value	Percentage contribution
Model	14	8.60261	0.61447	98.83	0.000	99.14
Linear	4	5.20715	1.30179	209.38	0.000	60.01
CR	1	1.27662	1.27662	205.34	0.000	14.71
SOI	1	2.36798	2.36798	380.87	0.000	27.29
FIP	1	0.76602	0.76602	123.21	0.000	8.83
EGR	1	0.79653	0.79653	128.12	0.000	9.18
Square	4	2.85023	0.71256	114.61	0.000	32.85
CR*CR	1	0.20507	0.20507	32.98	0.000	2.36
SOI*SOI	1	1.85459	1.85459	298.30	0.000	21.37
FIP*FIP	1	0.21766	0.21766	35.01	0.000	2.51
EGR*EGR	1	0.09836	0.09836	15.82	0.002	1.13
2-Way Interaction	6	0.54523	0.09087	14.62	0.000	6.28
CR*SOI	1	0.06917	0.06917	11.13	0.006	0.80
CR*FIP	1	0.02562	0.02562	4.12	0.065	0.30
CR*EGR	1	0.03356	0.03356	5.40	0.039	0.39
SOI*FIP	1	0.07020	0.07020	11.29	0.006	0.81
SOI*EGR	1	0.12743	0.12743	20.50	0.001	1.47
FIP*EGR	1	0.21926	0.21926	35.27	0.000	2.53
Error	12	0.07461	0.00622			0.86
Lack-of-Fit	10	0.07442	0.00744	79.10	0.013	0.86
Pure Error	2	0.00019	0.00009			
Total	26	8.67722				
Model Summary						
S R-sq R-sq(adj) R-sq(pred)						
0.0788494 99.14% 98.14% 95.06%						

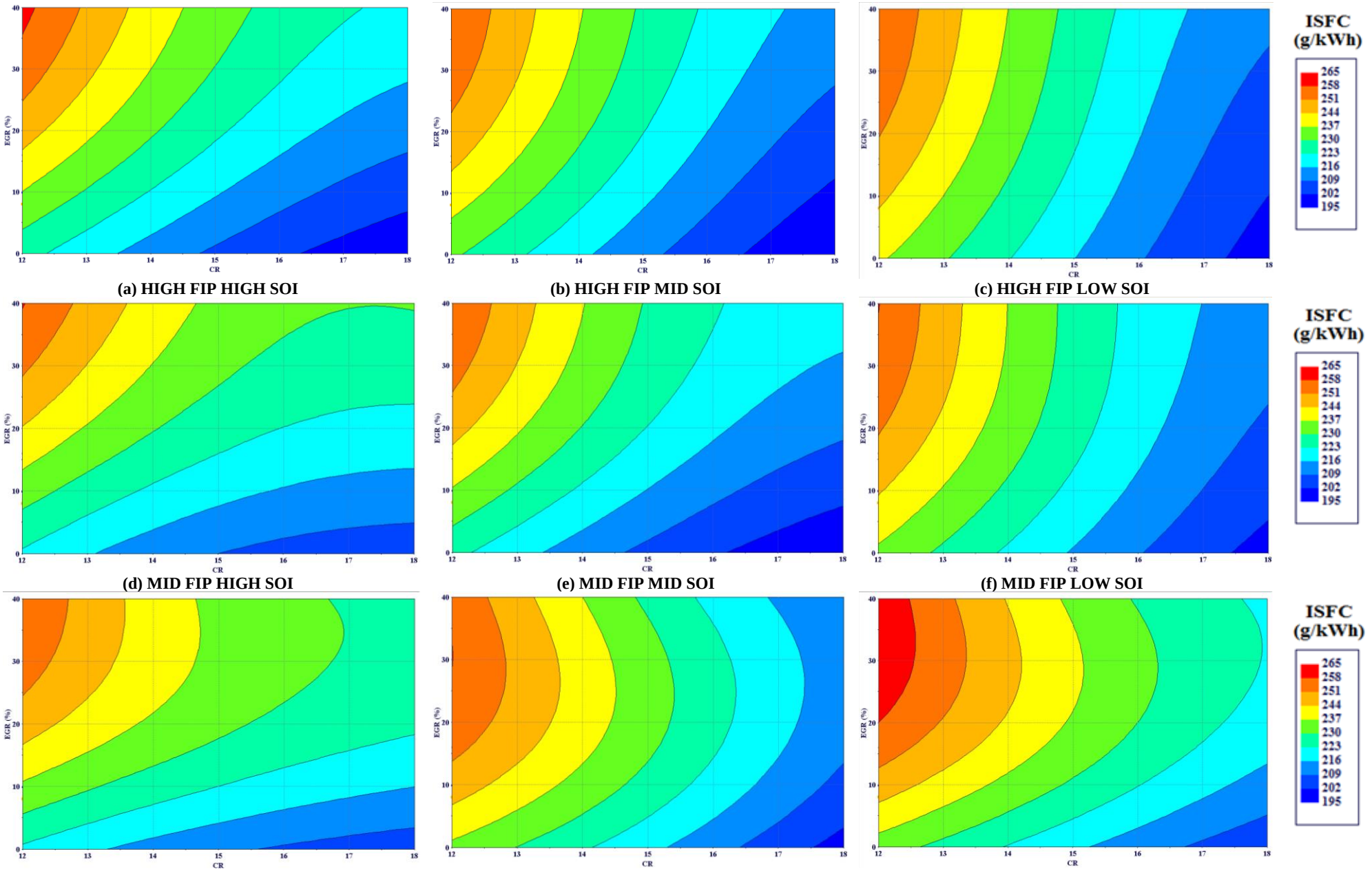

(a) HIGH FIP HIGH SOI **(b) HIGH FIP MID SOI** **(c) HIGH FIP LOW SOI**

(d) MID FIP HIGH SOI **(e) MID FIP MID SOI** **(f) MID FIP LOW SOI**

(g) LOW FIP HIGH SOI **(h) LOW FIP MID SOI** **(i) LOW FIP LOW SOI**

Fig.4. 35 Contour plots of ISFC for EGR and CR at different levels of SOI and FIP (VCR DIESEL)

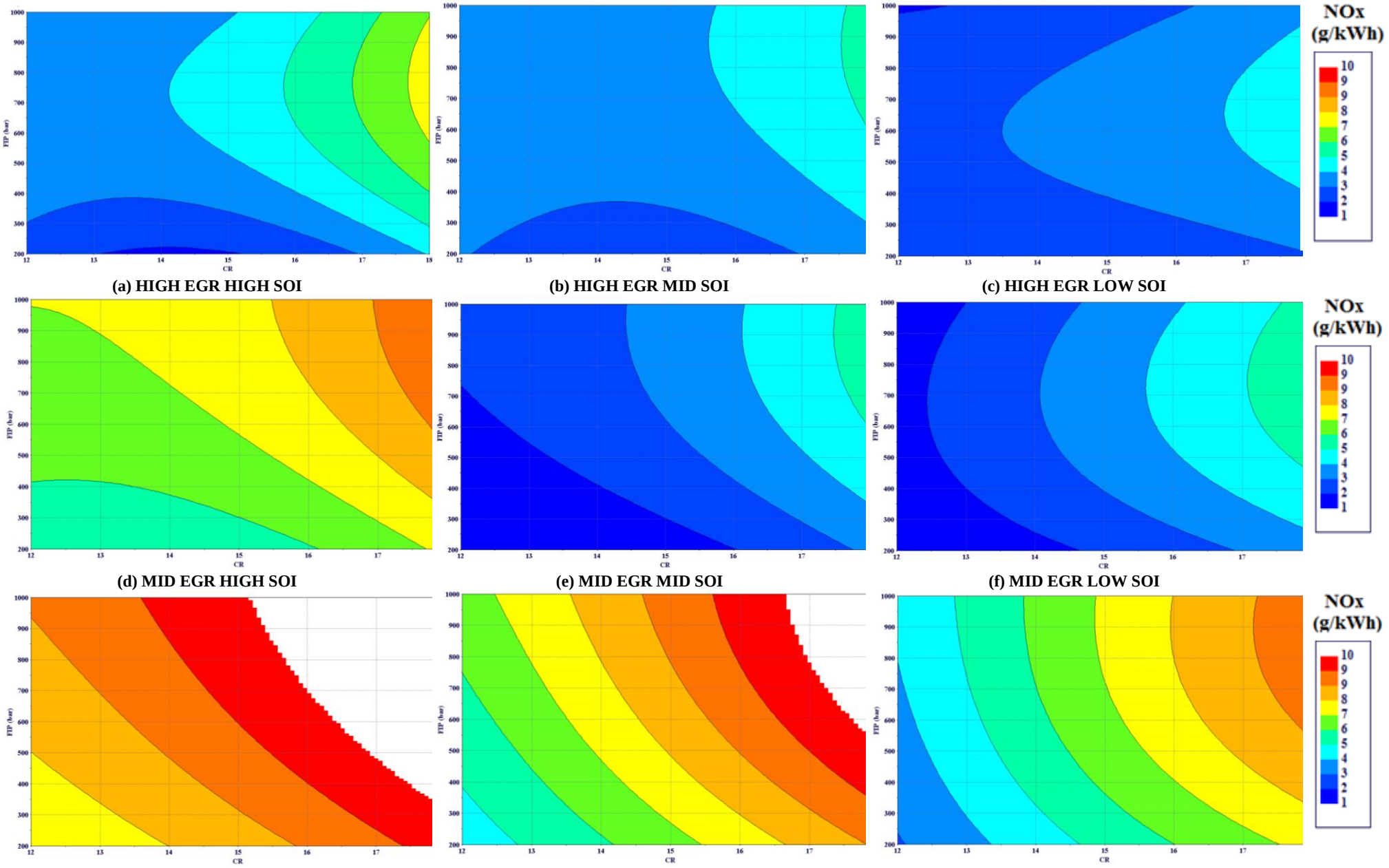

(a) HIGH EGR HIGH SOI **(b) HIGH EGR MID SOI** **(c) HIGH EGR LOW SOI**

(d) MID EGR HIGH SOI **(e) MID EGR MID SOI** **(f) MID EGR LOW SOI**

(g) LOW EGR HIGH SOI **(h) LOW EGR MID SOI** **(i) LOW EGR LOW SOI**

Fig.4. 36 Contour plots of NOx for FIP and CR at different levels of SOI and EGR (VCR DIESEL)

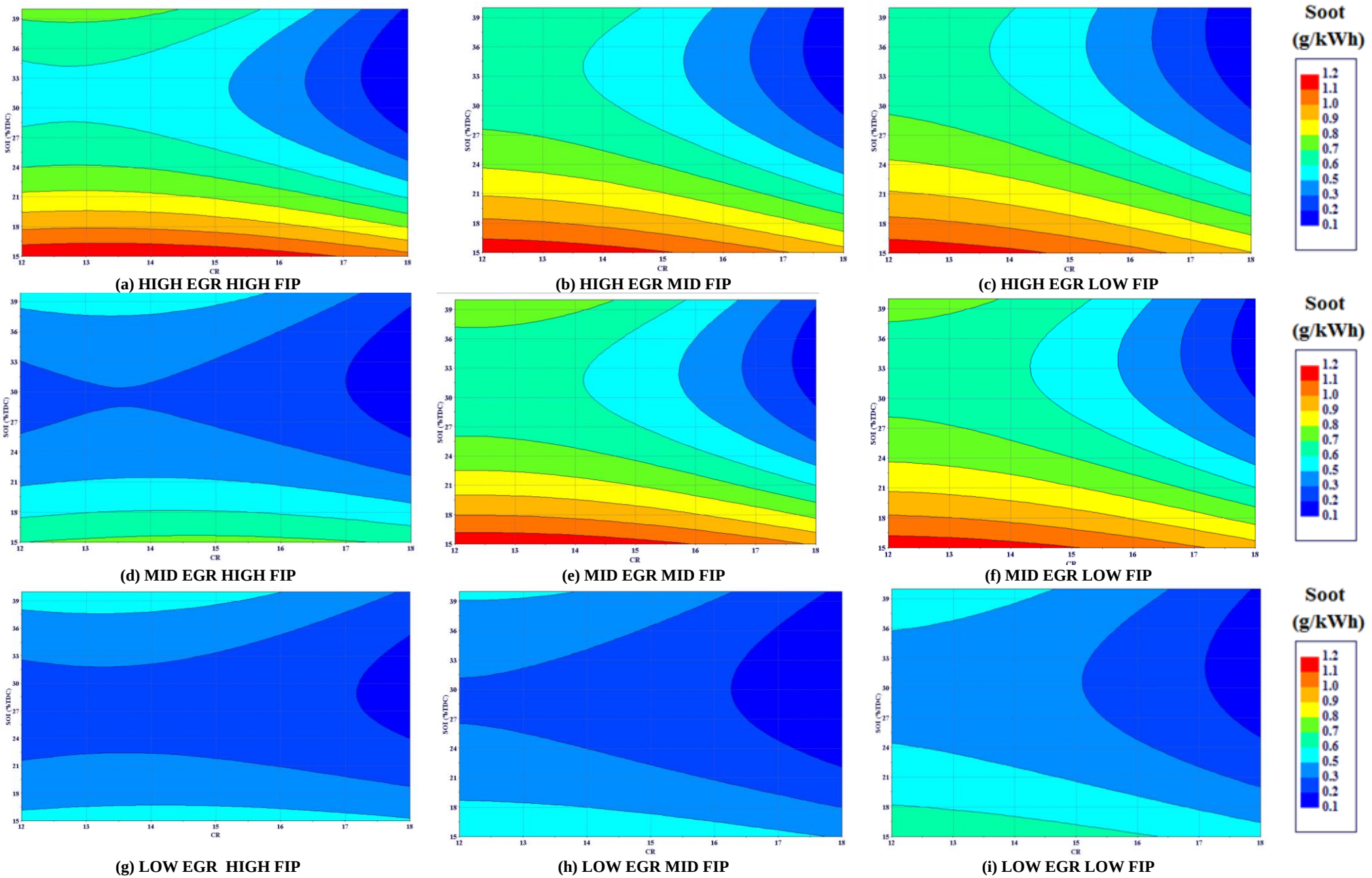

(a) HIGH EGR HIGH FIP **(b) HIGH EGR MID FIP** **(c) HIGH EGR LOW FIP**

(d) MID EGR HIGH FIP **(e) MID EGR MID FIP** **(f) MID EGR LOW FIP**

(g) LOW EGR HIGH FIP **(h) LOW EGR MID FIP** **(i) LOW EGR LOW FIP**

Fig.4. 37 Contour plots of soot for SOI and CR at different levels of FIP and EGR (VCR DIESEL)

4.2.5 Error analysis of the regression model for VCR engine

The normal probability plot for responses ISFC, NOx and soot were shown in Fig. 4.38, 4.39 and 4.40 respectively. The residuals have been spread out almost on a straight course. This is an indication that errors for the ISFC, soot and NOx are normally distributed. This implies that the regression equations are accurate.

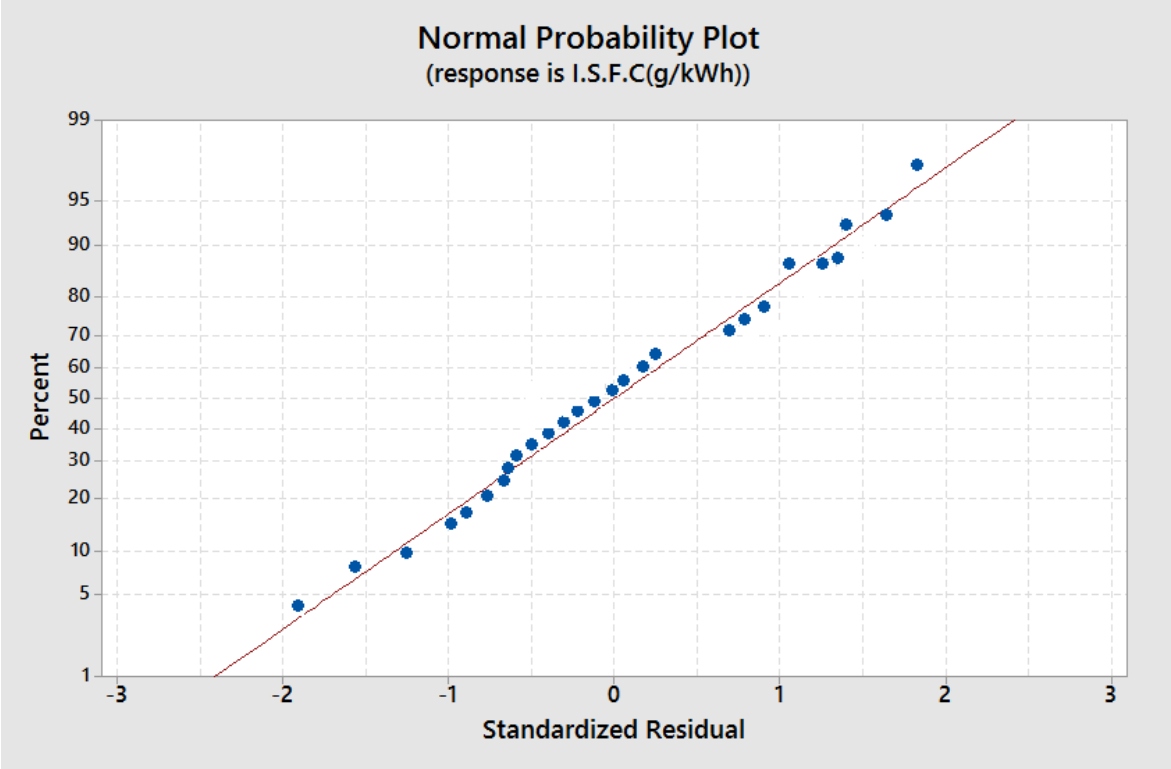

Fig.4. 38 Normal probability plot of the response ISFC for (VCR Diesel)

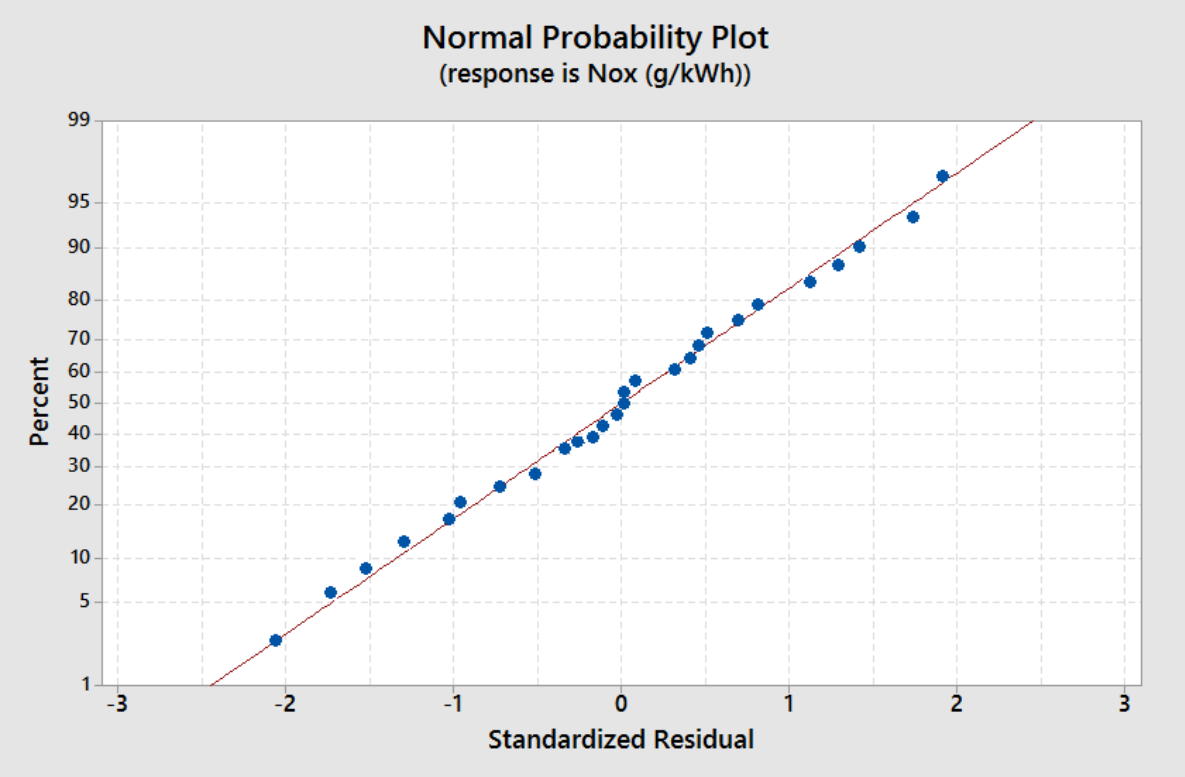

Fig.4. 39 Normal probability plot of the response NOx for (VCR Diesel)

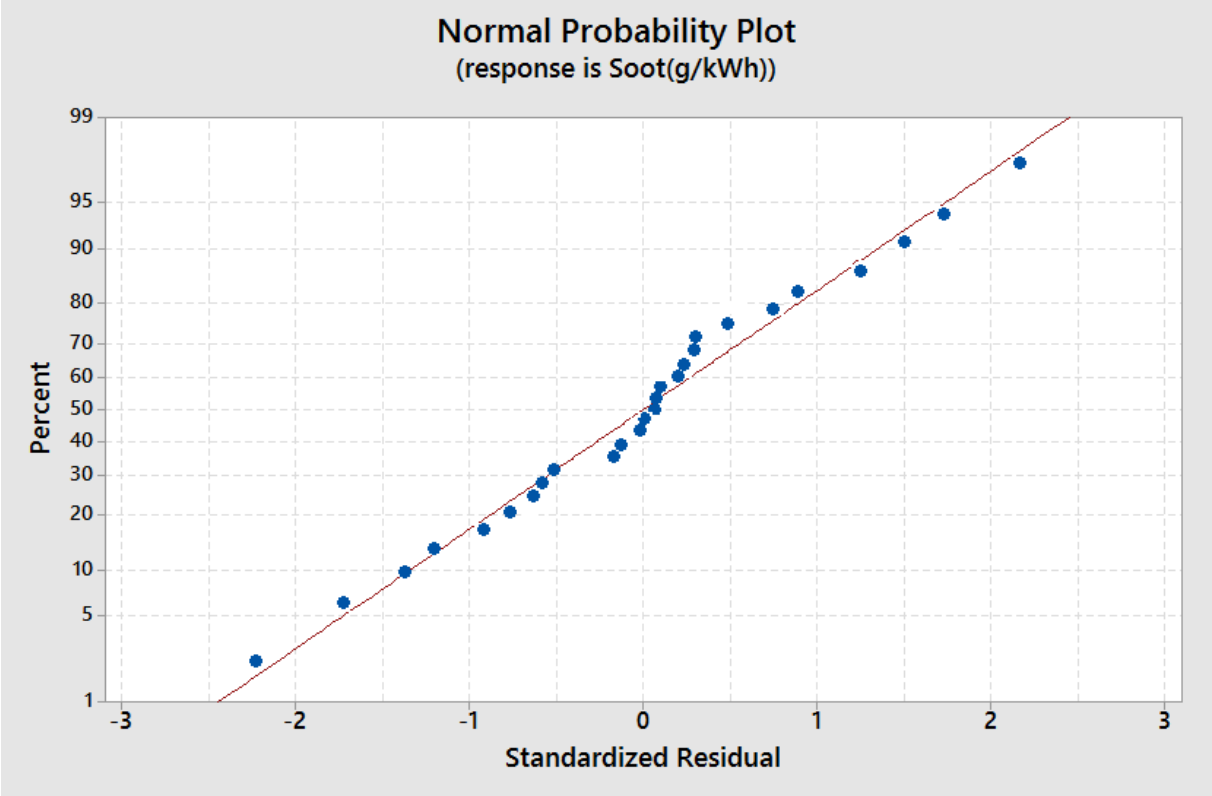

Fig.4. 40 Normal probability plot of the response soot for (VCR Diesel)

4.2.6 Optimization of VCR diesel

The objective of any engine design is to minimize emissions and maximize the performance. Here, ISFC is chosen as a performance indicator which is preferred to minimize. ISFC, soot and NOx need to be reduced simultaneously. It can be observed from the above discussions that the tradeoff is observed between the NOx and soot emissions. So there is a need for optimization of the design parameters aimed to reduce both NOx and soot without losing its performance. Optimization was performed using the desirability approach which is search based optimization technique (Derringer & Suich 1980). The whole approach is to modify all the responses (X_i) as a separate desirability function (D_i) and then will be varied in the entire range.

$$0 \leq (D_i) \leq 1 \tag{4.10}$$

If the response is at its mark value or objective, then (Di) =1 on the other hand, if the mark value is in the infeasible region then the (D_i) = 0 (H.Myers et al. 2016). Each of the desirability function is established depending upon the goal of optimization. Since the objectives are of minimization in nature.

$$D_i = \begin{cases} 1 & X_i < T_i \\ \left(\dfrac{U_i - X_i}{U_i - T_i}\right) & T_i \leq X_i \leq U_i \\ 0 & X_i > U_i \end{cases} \tag{4.11}$$

Where U_i is the upper limit of the responses (X_i), T_i is the target of the response.

Table 4. 16 Criteria of optimization used for desirability method for VCR diesel case

Parameter/ Response	**Limits**		**Criterion**	**Desirability**
	Lower	**Upper**		
Compression Ratio	12	18	In range	1
Fuel Injection Pressure (bar)	250	1000	In range	1
Start of Injection (°bTDC)	15	40	In range	1
Exhaust Gas Recirculation (%)	0	40	In range	1
ISFC (g/kWh)	182.57	277.87	Minimize	0.98
NOx (g/kWh)	0.5	12.17	Minimize	0.84
Soot (g/kWh)	0.04	2.11	Minimize	0.99
Combined				0.95

The optimum combination of the VCR diesel case was found out to be the 17.52 CR, 30.1 °bTDC SOI, FIP 736.06 bar and EGR 28.29% with a composite desirability of 0.95. The compression ratio did not alter much from the baseline case which is also beneficial in terms of the design aspect.

4.2.6.1 Comparison of optimized and baseline configuration of VCR (Diesel)

The optimized and baseline cases were compared of the VCR diesel for pressure, temperature, NOx, soot, HC and CO vs crankangle and are shown in the Fig.4.41 to 4.46 respectively. It was noticed that the optimized case is superior in performance and also could able to simultaneously reduce the NOx and soot than the baseline case. It is noticed from the Fig. 4.42 that the average temperature of the optimized case reduces during the combustion. This is because of the presence of EGR which could suppress the combustion temperature. It is also observed from Fig. 4.45 and 4.46 that the HC and CO emissions are decreased in the optimum case than the baseline. Along with the ISFC, ISEC (Indicated specific energy consumption) is also introduced to compare them with respect to the energy consumption point of view since the blends may have different calorific value. Table 4.17 gives the comparison of baseline and optimized cases of VCR diesel based on performance and emissions. It is noticed that the optimized case ISEC/ISFC decreased by 2.37% and NOx decreased by 29.11% and soot decreased by 99.1% with respect to the baseline case.

Table 4. 17 Comparison of baseline and optimized cases for VCR diesel case

	ISFC (g/kWh)	**ISEC (MJ/kWh)**	**NOx (g/kWh)**	**Soot (g/kWh)**
Baseline Case of VCR diesel	210.25	9.381	5.29	1.18
Optimized case of VCR diesel	**205.48**	**9.16**	**3.75**	**0.191**
Change w.r.t baseline	**2.37% ↓**	**2.37%↓**	**29.11% ↓**	**83.81 %↓**

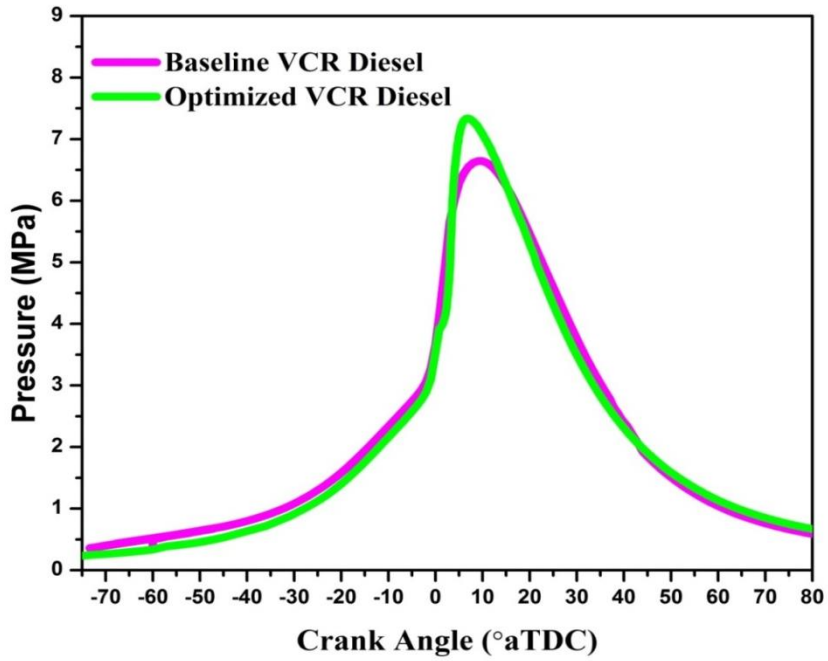

Fig.4. 41 Comparison of pressure Vs crank angle for optimized and baseline (VCR diesel)

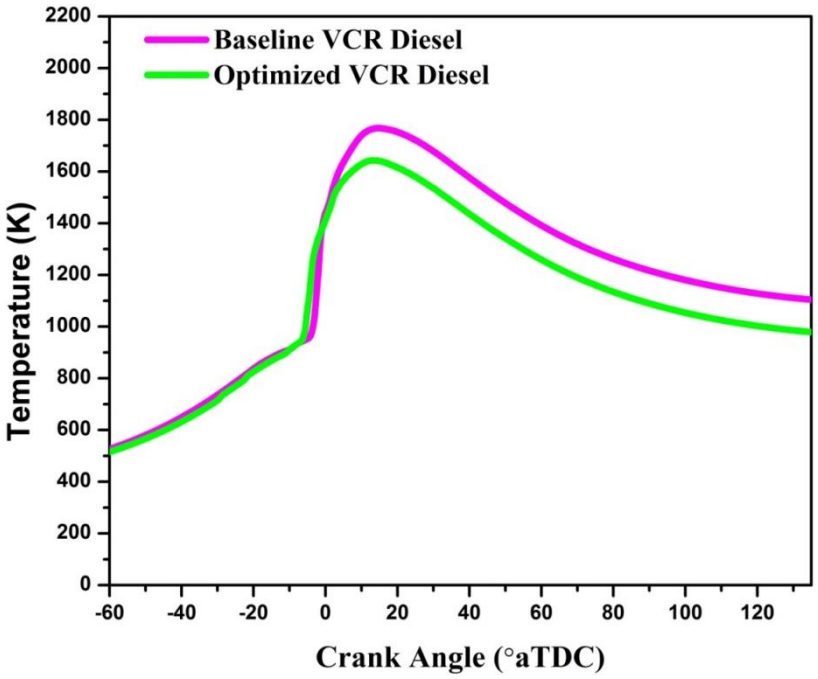

Fig.4. 42 Comparison of Temperature vs. Crank angle for baseline and optimized (VCR PB20)

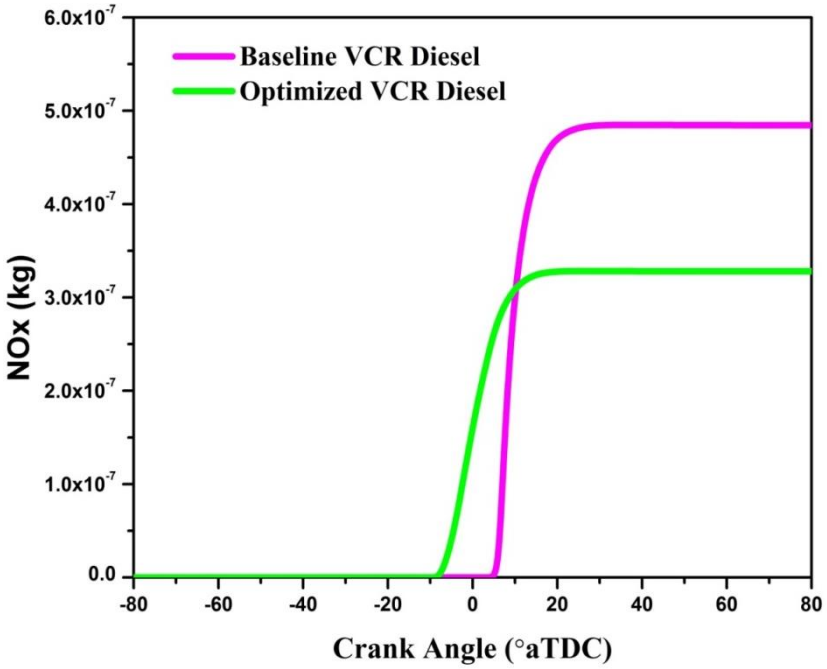

Fig.4. 43 Comparison of NOx Vs crank angle for optimized and baseline (VCR diesel)

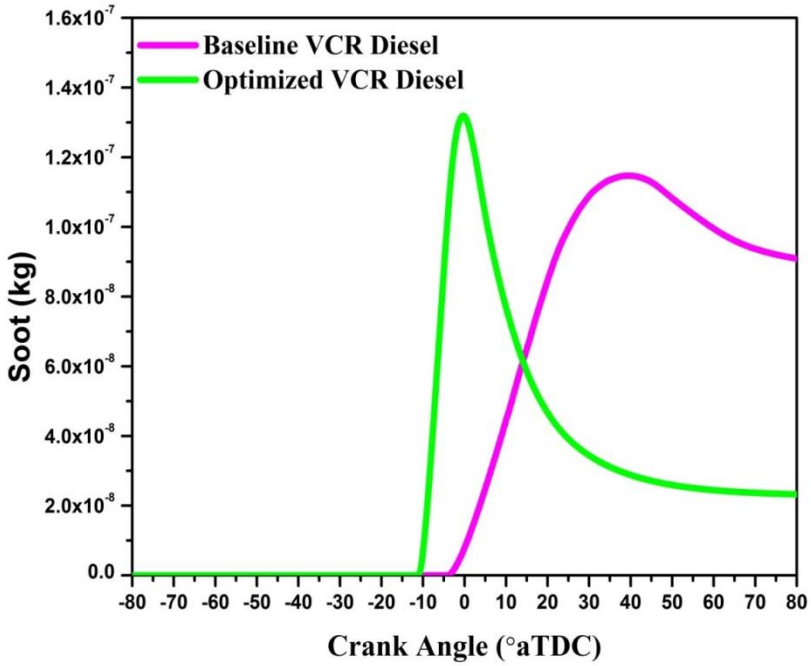

Fig.4. 44 Comparison of NOx Vs crank angle for optimized and baseline (VCR diesel)

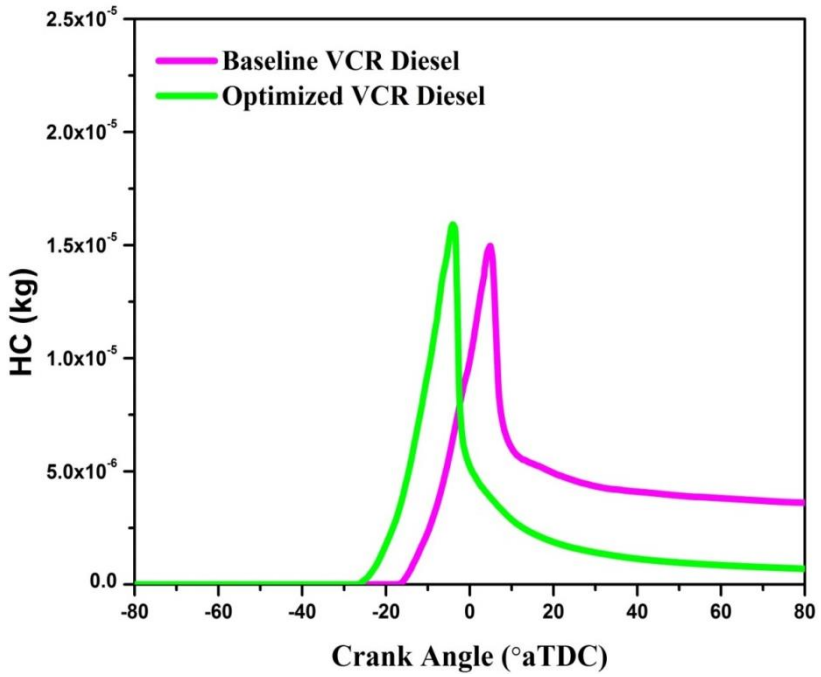

Fig.4. 45 Comparison of HC vs. Crank angle for baseline and optimized (VCR PB20)

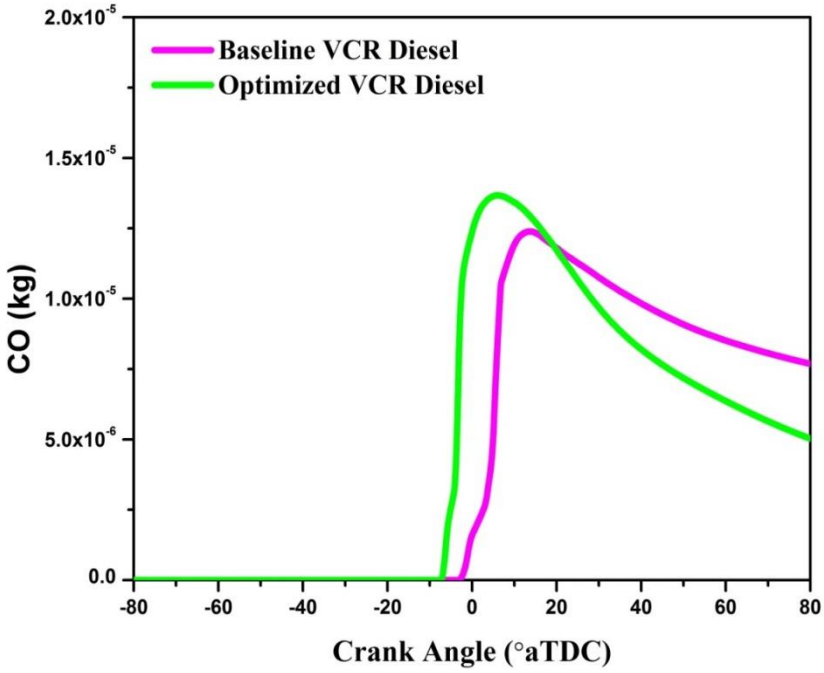

Fig.4. 46 Comparison of CO vs. Crank angle for baseline and optimized (VCR PB20)

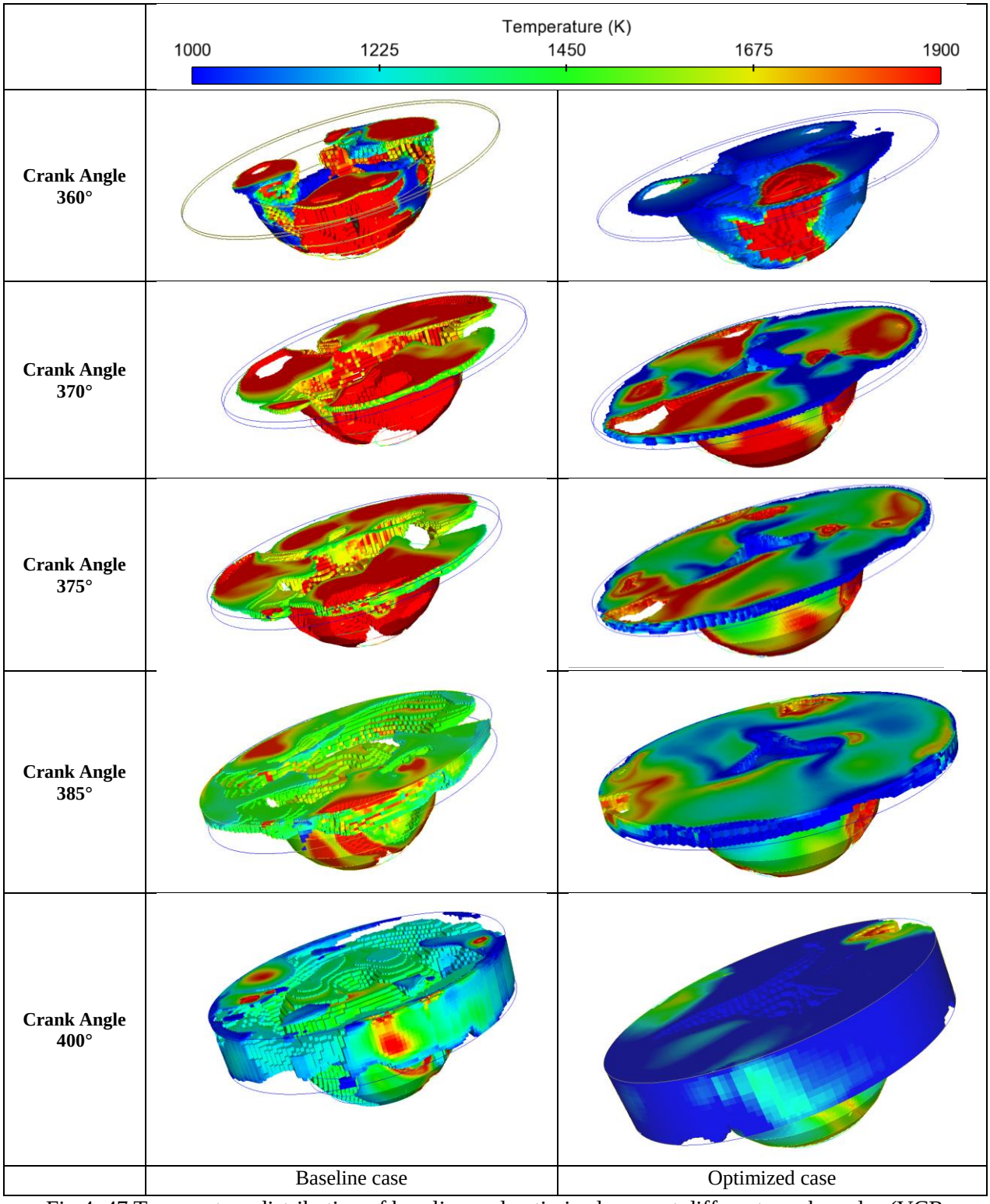

Fig.4. 47 Temperature distribution of baseline and optimized cases at different crank angles (VCR diesel)

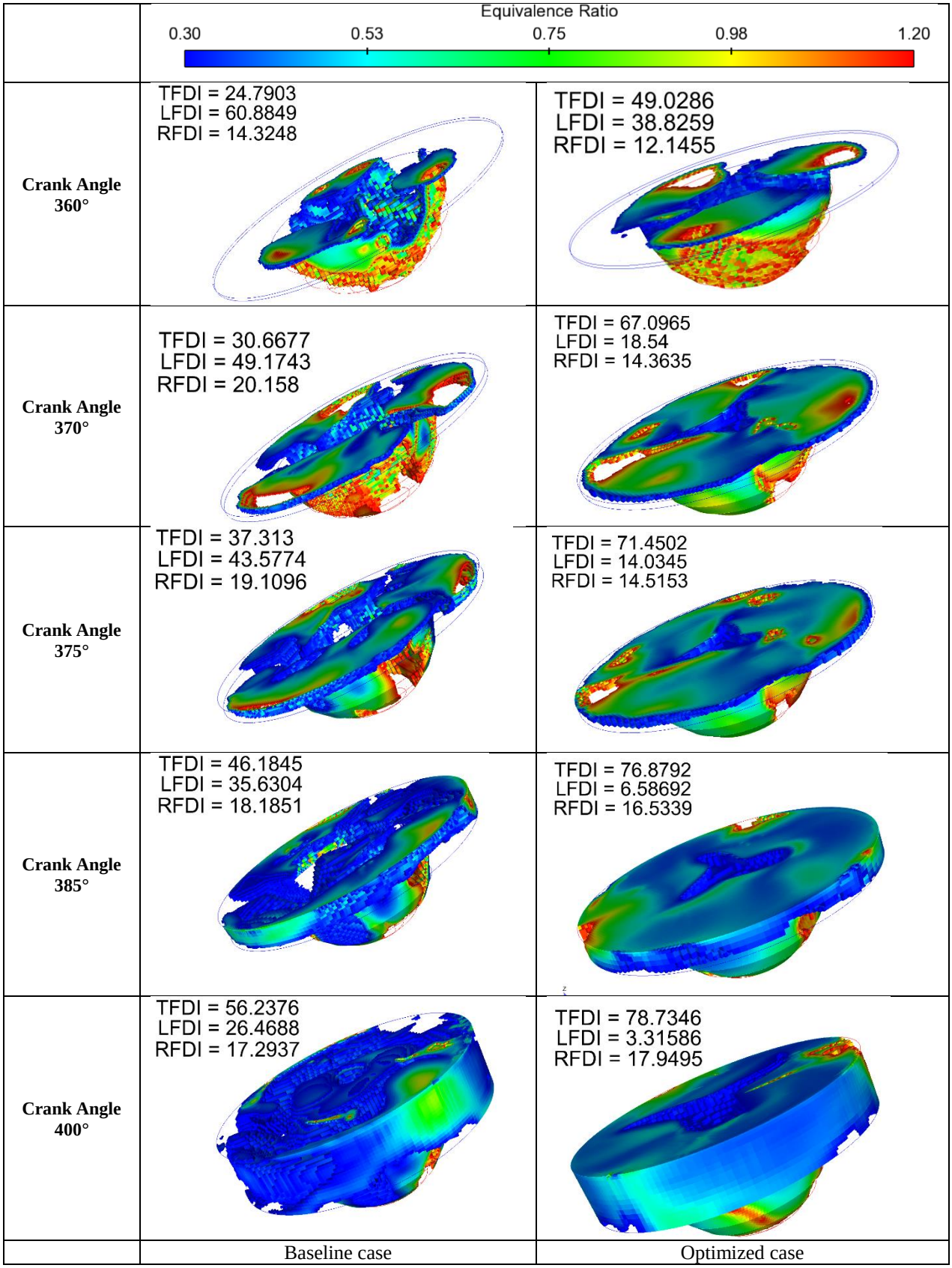

Fig.4. 48 Equivalence ratio distribution of baseline and optimized cases at different crank angles (VCR diesel)

4.2.6.2 Mixture homogeneity comparison of the baseline and optimized cases (VCR diesel)

TFDI is compared for the baseline and optimized cases at different crank angle instances (in Fig 4.48) during the combustion. It is observed that the optimized case has, the more TFDI than the baseline case in all the instances. This is a clear indication of the better homogeneous mixture formation in the optimized case than the baseline case. The better homogeneity was attained due to the advanced injection, higher fuel injection pressure and presence of EGR in the optimized case. This can be concluded that the optimized case has the combustion characteristics as that of HCCI. The Fig. 4.47 shows that the temperature distribution is also plotted in the target region. It is also observed that the target region has higher in-cylinder temperatures for baseline case and the optimized case attain lesser temperatures observed in the target distribution area.

Summary

The VCR diesel engine was analyzed using DOE based study and optimization has also been done using desirability technique. The optimal combination of CR, SOI, EGR and FIP was found, which could able to reduce the both NOx and soot. The optimum combination was also improved its ISFC (performance characteristic). The optimum combination of the VCR diesel case was found out to be the CR 17.52, SOI -30.1 °aTDC, FIP 736.06 bar and EGR 28.29% with a composite desirability of 0.95. Optimized set of combination was capable to bring down the NOx, soot, HC and CO emissions as compared to the baseline VCR diesel. ISFC, NOx and soot are reduced by 2.37%, 29.11% and 83.81 % respectively. It was likewise mentioned that the optimized case got higher target fuel distribution index (TFDI) which also proves that the better homogenous mixture was achieved.

4.3 Analysis of VCR engine (PB20)

The objective of this work is to create a validated CFD model of the Variable Compression Ratio (VCR) engine with PB20 as fuel. The study also emphasizes to analyze the effect of compression ratio, start of injection, fuel injection pressure and exhaust gas recirculation using CONVERGE^{TM} software with DOE adoption. The simulation gives different output responses to the variables deployed, such as pressure, NOx, soot, etc. In the analysis ISFC is selected as performance parameter and NOx and soot are selected as major pollutants. The whole idea is to minimize the pollutants and ISFC. In the present work we develop regression equations based on the varied responses obtained from simulation results. The equations will be optimized for multi-objective criteria using Minitab software based on desirability approach.

4.3.1 Validation of VCR engine (PB20) Model

The PB20 simulation was carried out on the VCR engine, to validate against the experimental results. Chemical reaction mechanism used in this work is adapted from the works of Brakora et al. (2012). The mechanism consists of 69 species and 192 reactions including methyl esters and NOx species. Table 3.10 gives the fuel composition of fuel that represents the physical and chemical properties of the PB20.

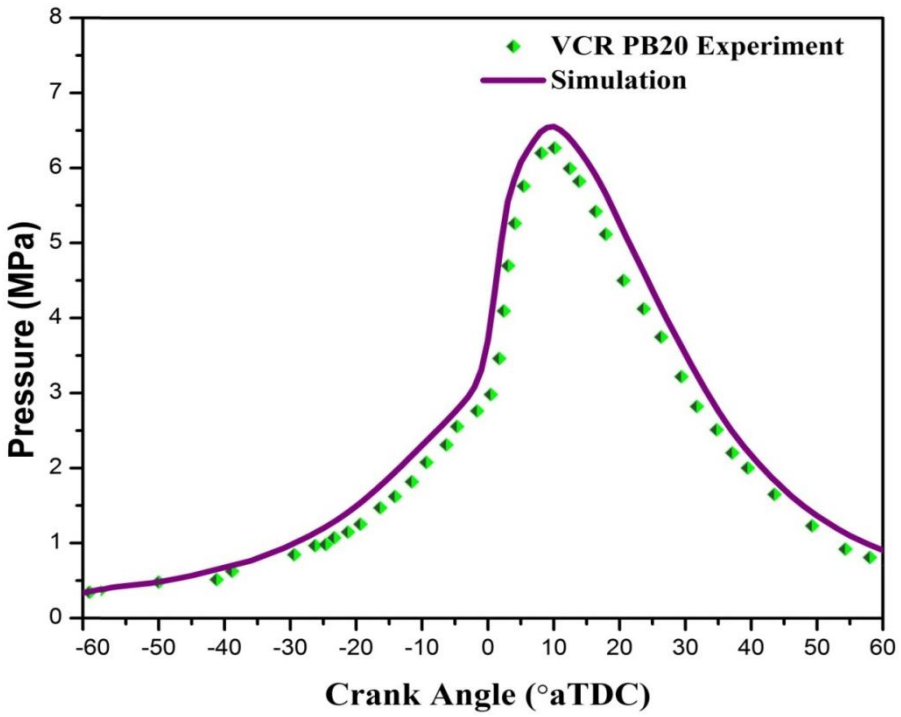

Fig.4. 49 Validation of pressure Vs Crank angle for VCR engine using PB20

The biodiesel numerical simulation model was validated against experimental data using PB 20 (20% Pongamia biodiesel+ 80% diesel) as a fuel for its operation. The experiments were performed on the VCR engine with the standard engine configuration given in the Table 4.10. Figure 4.49 shows comparsion of the experimental and simulation results for variation of pressure with respect to crank angle. Simulation results are in good agreement with experimental values.

4.3.2 DOE Analysis of VCR (PB20)

Based on the confidence attained by the validation, the present study was extended to analyze the effect of different parameters such as CR, SOI, FIP and EGR. RSM is used to study the performance and emission characteristics of the VCR engine for the parametric ranges. The parameters and their ranges were given in Table 4.19. The superiority of the DOE is to analyze the effect of the parameters in the entire range with a very minimal number of runs. A set of 27 numerical experiments was conducted based on the Box-Behnken design of the MiniTab 17 software. The responses of such designs were also tabulated in the Table.4.19.

Table 4. 18 Experimental design matrix with the three responses ISFC, soot and NOx

Run	CR	SOI (°bTDC)	FIP (bar)	EGR (%)	I.S.F.C (g/kWh)	Soot (g/kWh)	NOx (g/kWh)
1	18	27.5	250	20	253.27	0.415	4.668
2	18	27.5	625	0	225.08	0.109	11.782
3	15	40	625	0	235.51	0.106	13.627
4	15	27.5	625	20	285.35	0.518	3.345
5	18	27.5	1000	20	222.36	0.0901	5.661
6	15	27.5	1000	0	287.81	0.434	9.539
7	18	40	625	20	205.91	0.198	9.615
8	12	27.5	625	40	345.28	1.033	1.641
9	15	27.5	250	0	272.34	0.415	7.013
10	12	15	625	20	390.25	1.401	0.598
11	15	40	625	40	244.25	0.827	4.384
12	12	27.5	250	20	338.25	1.0395	1.269
13	15	27.5	1000	40	280.34	0.638	1.666
14	15	15	250	20	315.61	1.715	1.110
15	12	27.5	1000	20	355.73	0.469	2.293
16	12	40	625	20	287.25	0.789	6.708
17	15	15	1000	20	335.16	1.187	1.773

18	15	27.5	625	20	285.35	0.518	3.345
19	15	15	625	0	312.45	0.859	7.014
20	15	40	1000	20	230.31	0.793	8.016
21	18	27.5	625	40	238.26	0.435	3.515
22	18	15	625	20	261.59	1.124	3.601
23	15	27.5	625	20	285.35	0.5188	3.345
24	15	40	250	20	263.18	0.947	5.985
25	15	27.5	250	40	302.15	1.545	0.761
26	12	27.5	625	0	341.25	0.529	5.765
27	15	15	625	40	327.69	1.796	2.151

4.3.3 ANOVA analysis for VCR PB20

The table 4.20 to 4.22, shows the analysis of variance of the ISFC, NOx and soot respectively. It was noticed that the statistical analysis gives a significance of the parameters and their interactions on the responses. For ISFC all the main and square effects are significant as their *p*-value is less than 0.05. But the interaction effects such as CR×FIP, CR×EGR, SOI×EGR and FIP×EGR are not significant since their *p*-value is greater than 0.05. For the response NOx is concerned, all the main and squared effects are significant. The interaction effects of CR×FIP, CR×SOI, SOI×FIP, FIP×EGR are not significant. The other two interaction effects CR×EGR and SOI×EGR are only significant as their *p*-value is less than 0.05. From the ANOVA pertains to soot, it is noted that all the main effects, squared effects are important, whereas the only insignificant interaction was CR×EGR. Regression equations developed based on the DOE analysis is given in the equations 4.12, 4.13 and 4.14. These equations are useful in arriving optimal solutions.

Table 4. 19 Analysis of variance (ANOVA) for the response (ISFC) of VCR PB20

Analysis of Variance						
Source	DF	Adj SS	Adj MS	F-Value	*p*-value	Percentage contribution
Model	14	15173.8	1083.85	74.09	0.000	98.86
Linear	4	11541.4	2885.35	197.23	0.000	75.19
CR	1	4070.9	4070.93	278.27	0.000	26.52
SOI	1	3254.9	3254.91	222.49	0.000	21.21
FIP	1	2462.7	2462.66	168.34	0.000	16.04
EGR	1	1752.9	1752.90	119.82	0.000	11.42
Square	4	3133.4	783.35	53.55	0.000	20.41
CR*CR	1	235.4	235.41	16.09	0.002	1.53
SOI*SOI	1	139.3	139.30	9.52	0.009	0.91
FIP*FIP	1	1704.8	1704.81	116.53	0.000	11.11
EGR*EGR	1	175.6	175.60	12.00	0.005	1.14
2-Way Interaction	6	499.1	83.18	5.69	0.005	3.25
CR*SOI	1	182.4	182.43	12.47	0.004	1.19

CR*FIP	1	4.4	4.39	0.30	0.594	0.03
CR*EGR	1	62.9	62.90	4.30	0.060	0.41
SOI*FIP	1	199.4	199.42	13.63	0.003	1.30
SOI*EGR	1	43.7	43.71	2.99	0.110	0.28
FIP*EGR	1	6.2	6.21	0.42	0.527	0.04
Error	12	175.6	14.63			1.14
Lack-of-Fit	10	161.6	16.16	2.32	0.339	1.05
Pure Error	2	13.9	6.97			
Total	26	15349.4				
Model Summary S R-sq R-sq(adj) R-sq(pred) 3.82485 98.86% 97.52% 93.73%						

Table 4. 20 Analysis of variance (ANOVA) for the response (NOx) of VCR PB20

Analysis of Variance						
Source	DF	Adj SS	Adj MS	F-Value	*p*-value	Percentage contribution
Model	14	244.680	17.477	92.10	0.000	99.08
Linear	4	208.666	52.166	274.90	0.000	84.49
CR	1	27.853	27.853	146.78	0.000	11.28
SOI	1	67.796	67.796	357.27	0.000	27.45
FIP	1	4.364	4.364	23.00	0.000	1.77
EGR	1	108.652	108.652	572.57	0.000	44.00
Square	4	27.944	6.986	36.81	0.000	11.32
CR*CR	1	1.215	1.215	6.40	0.026	0.49
SOI*SOI	1	9.108	9.108	48.00	0.000	3.69
FIP*FIP	1	0.619	0.619	3.26	0.096	0.25
EGR*EGR	1	16.933	16.933	89.23	0.000	6.86
2-Way Interaction	6	8.070	1.345	7.09	0.002	3.27
CR*SOI	1	0.002	0.002	0.01	0.923	0.00
CR*FIP	1	0.000	0.000	0.00	0.975	0.00
CR*EGR	1	3.389	3.389	17.86	0.001	1.37
SOI*FIP	1	0.369	0.369	1.95	0.188	0.15
SOI*EGR	1	3.791	3.791	19.97	0.001	1.54
FIP*EGR	1	0.519	0.519	2.74	0.124	0.21
Error	12	2.277	0.190			0.92
Lack-of-Fit	10	2.247	0.225	15.05	0.064	0.91
Pure Error	2	0.030	0.015			
Total	26	246.957				
Model Summary S R-sq R-sq(adj) R-sq(pred) 0.435618 99.08% 98.00% 94.73%						

The regression equation of ISFC, NOx and soot for the VCR PB20 is as follows in the equations

$$\begin{aligned} ISFC\left(\frac{g}{kWh}\right) &= 624.6 - 31.33 \times CR - 3.43 \times SOI - 0.2279 \times FIP + 1.702 \\ &\times EGR + 0.738 \times CR^2 - 0.0327 \times SOI^2 + 0.000127 \times FIP^2 \\ &- 0.01435 \times EGR^2 + 0.1801 \times CR \times SOI - 0.00093 \times CR \\ &\times FIP - 0.0661 \times CR \times EGR + 0.001506 \times SOI \times FIP \\ &+ 0.01322 \times SOI \times EGR + 0.00166 \times FIP \times EGR \end{aligned} \quad (4.12)$$

$$NOx\left(\frac{g}{kWh}\right) = 4.70 - 0.757 \times CR - 0.224 \times SOI + 0.00391 \times FIP + 0.0386 \times EGR + 0.0530 \times CR^2 - 0.00836 \times SOI^2 + 0.000002 \times FIP^2 + 0.004455 \times EGR^2 - 0.00057 \times CR \times SOI - 0.000006 \times CR \times FIP - 0.01534 \times CR \times EGR + 0.000065 \times SOI \times FIP - 0.003894 \times SOI \times EGR - 0.000048 \times FIP \times EGR \quad (4.13)$$

Table 4. 21 Analysis of variance (ANOVA) for the response (soot) of VCR PB20

Analysis of Variance						
Source	DF	Adj SS	Adj MS	F-Value	P-Value	Percentage contribution
Model	14	7.59889	0.54278	86.41	0.000	99.02
Linear	4	4.70856	1.17714	187.41	0.000	61.36
CR	1	1.19255	1.19255	189.86	0.000	15.54
SOI	1	2.13710	2.13710	340.24	0.000	27.85
FIP	1	0.69133	0.69133	110.07	0.000	9.01
EGR	1	0.68758	0.68758	109.47	0.000	8.96
Square	4	2.42382	0.60595	96.47	0.000	31.58
CR*CR	1	0.15184	0.15184	24.17	0.000	1.98
SOI*SOI	1	1.62172	1.62172	258.19	0.000	21.13
FIP*FIP	1	0.17888	0.17888	28.48	0.000	2.33
EGR*EGR	1	0.11458	0.11458	18.24	0.001	1.49
2-Way Interaction	6	0.46650	0.07775	12.38	0.000	6.08
CR*SOI	1	0.06243	0.06243	9.94	0.008	0.81
CR*FIP	1	0.02312	0.02312	3.68	0.079	0.30
CR*EGR	1	0.00472	0.00472	0.75	0.403	0.06
SOI*FIP	1	0.06335	0.06335	10.09	0.008	0.83
SOI*EGR	1	0.11500	0.11500	18.31	0.001	1.50
FIP*EGR	1	0.19788	0.19788	31.50	0.000	2.58
Error	12	0.07537	0.00628			0.98
Lack-of-Fit	10	0.07520	0.00752	8.57	0.081	0.98
Pure Error	2	0.00017	0.00008			
Total	26	7.67426				

Model Summary

S	R-sq	R-sq(adj)	R-sq(pred)
0.0792532	99.02%	97.87%	94.35%

The regression equation of soot for the VCR PB20 is as follows in the equation

$$Soot\left(\frac{g}{kWh}\right) = 1.17 + 0.518 \times CR - 0.1811 \times SOI - 0.03427 \times FIP + 0.0431 \times EGR - 0.01875 \times CR^2 + 0.003529 \times SOI^2 + 0.000001 \times FIP^2 + 0.000366 \times EGR^2 - 0.00333 \times CR \times SOI + 0.000068 \times CR \times FIP - 0.000572 \times CR \times EGR + 0.000027 \times SOI \times FIP - 0.000678 \times SOI \times EGR - 0.00003 \times FIP \times EGR \quad (4.14)$$

4.3.4 Interaction effects of VCR PB20

The interaction effect of EGR and FIP on ISFC at different levels of CR and SOI for VCR PB20 case has been shown in the Fig 4.50. It can be observed from the figure that the interaction effect of EGR and FIP for ISFC has a relatively linear trend are observed in lower CR regions, whereas at higher levels of (advanced) SOI the interaction behaves as a nonlinear function. At mid and high levels of SOI the increase in FIP may not be fruitful in reducing the ISFC because the higher FIP reduces the ignition delay and if it combines with the advanced injection timing it further advances the start of combustion and thus reduces the indicated power.

It is observed from the Fig 4.51 that the interaction of FIP and CR on NOx is depicted at various levels of EGR and SOI for the VCR PB20 case. Increasing the compression ratio resulted in the increase in NOx emissions. This could be due to the fact that as the compression ratio is increased, it increases in cylinder temperature and pressures which in turn increase combustion temperatures. An increase in the fuel injection pressure increased in cylinder pressure and NOx emissions and decreased soot emissions. This could be due to the fact that the increase in fuel injection pressure leads to better atomization of the fuel, which results in the smallest droplet size, faster evaporation of fuel sprays. This improves reaction between fuel and air. This resulted in comparatively better combustion and contributed to higher NOx emission.

It is observed from Fig 4.52 that the interaction of the SOI and FIP on soot at different levels of CR and EGR for PB20 case. At all CR's, increasing FIP decreases soot, and as CR increases same trend follows. As FIP is increased it leads to effective atomization and proper combustion results in less soot, also the surface area of spray increases which helps in better mixing of air and fuel. Increasing CR raises the temperature of the in-cylinder charge, that will favor the vaporization of fuel, which brings good combustion characteristics and less soot. With increasing in EGR, soot also increased as diluting the charge increases unburned parts of charge. SOI and FIP are the two most important parameters that could reduce soot to a large extend, increasing FIP and advancing SOI brings down the soot, but up to a limit beyond which spray particles entering crevice region resulting in increase of soot emissions.

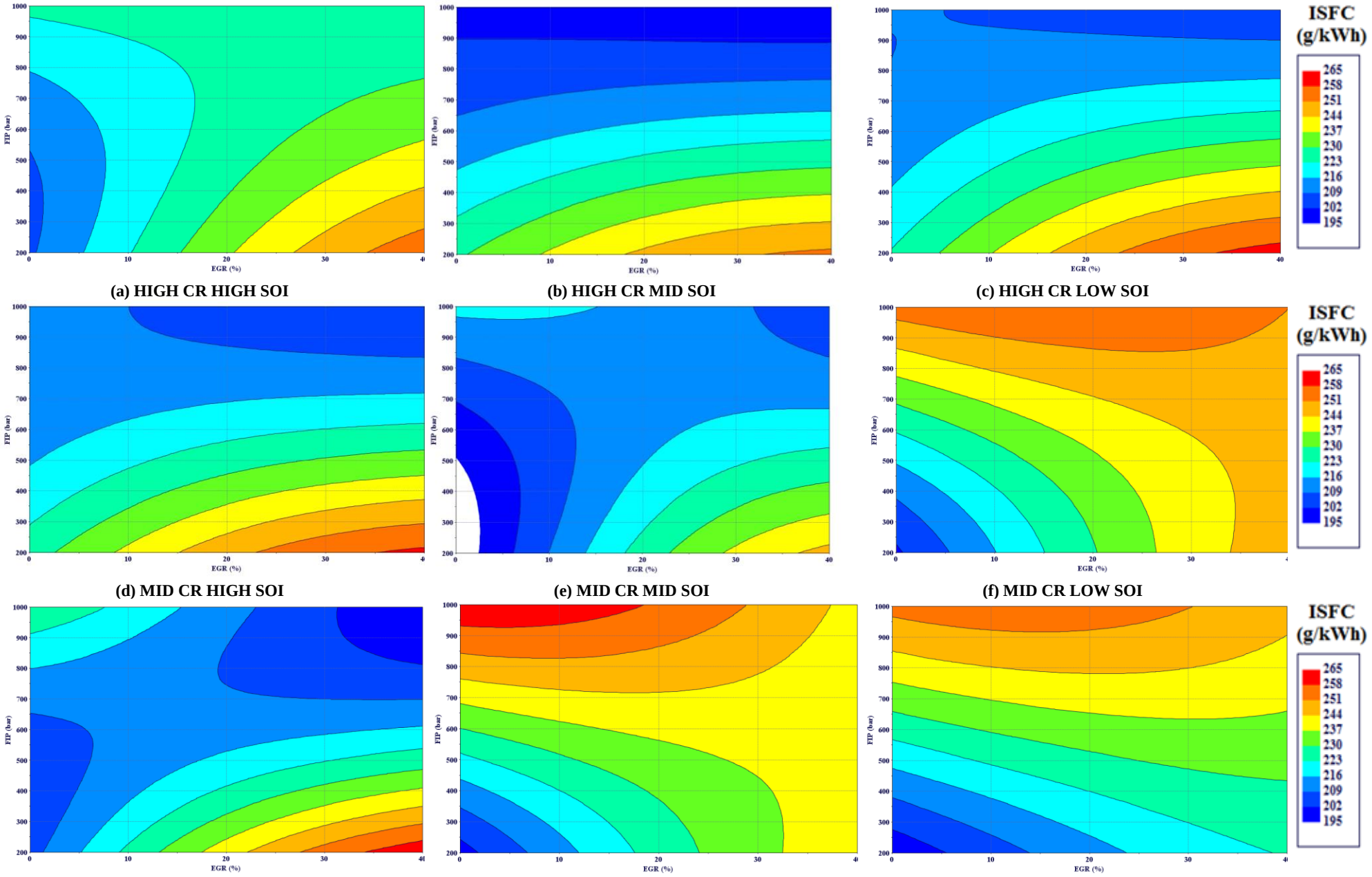

(a) HIGH CR HIGH SOI **(b) HIGH CR MID SOI** **(c) HIGH CR LOW SOI**

(d) MID CR HIGH SOI **(e) MID CR MID SOI** **(f) MID CR LOW SOI**

(g) LOW CR HIGH SOI **(h) LOW CR MID SOI** **(i) LOW CR LOW SOI**

Fig.4. 50 Contour plots of ISFC for FIP and EGR at different levels of CR and SOI (VCR PB20)

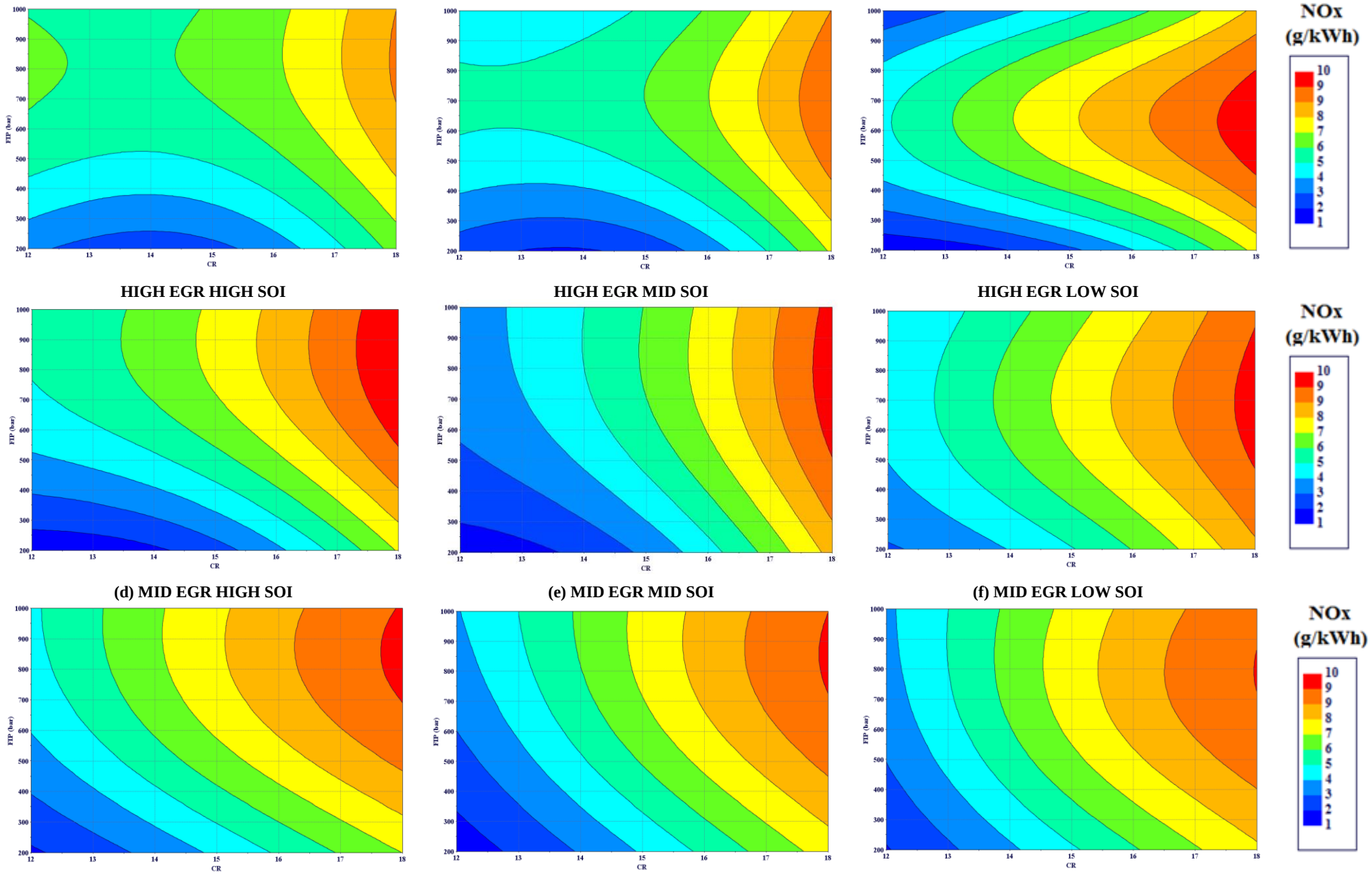

Fig.4. 51 Contour plots of NOx for FIP and CR at different levels of EGR and SOI (VCR PB20)

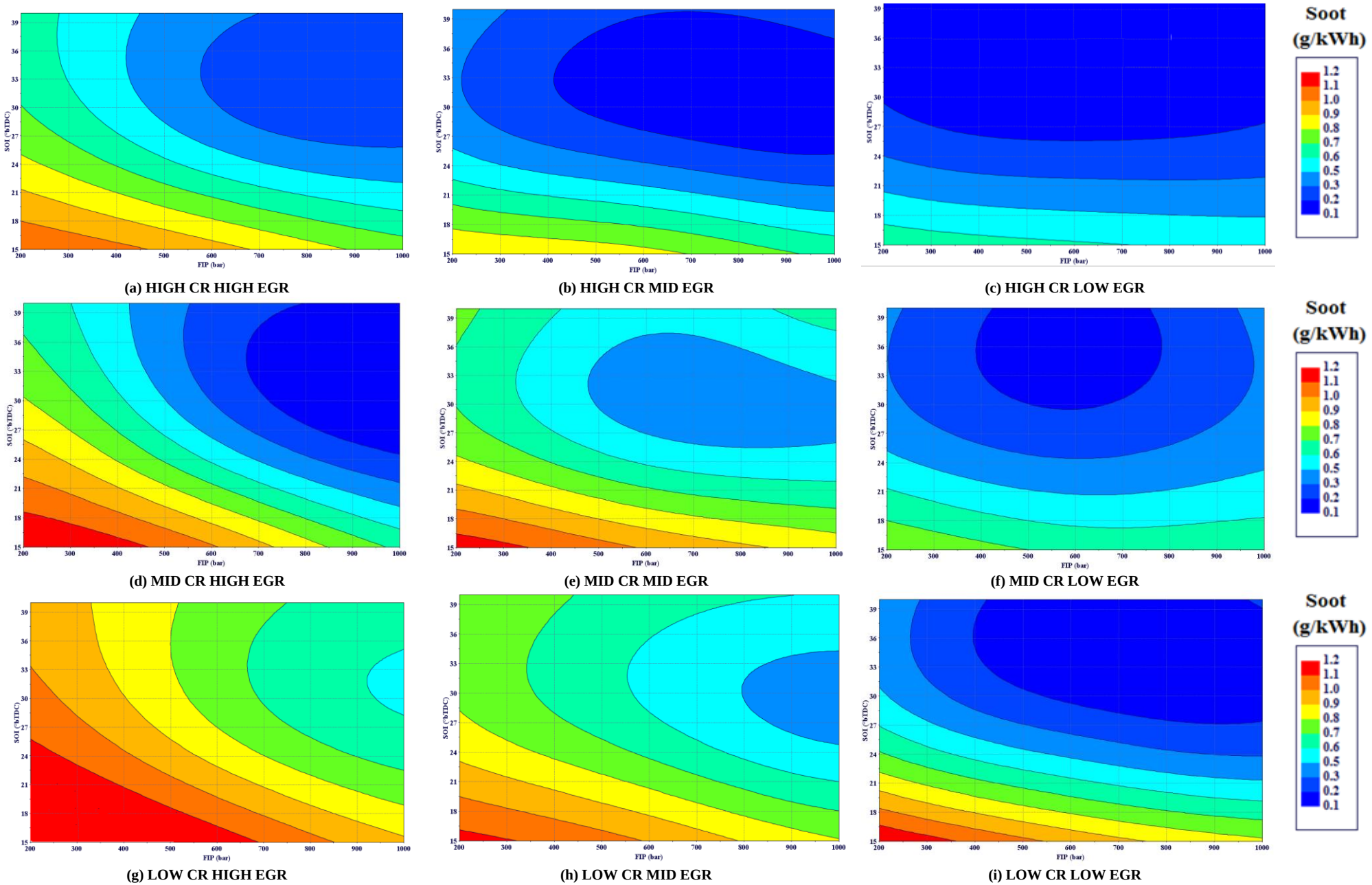

(a) HIGH CR HIGH EGR **(b) HIGH CR MID EGR** **(c) HIGH CR LOW EGR**

(d) MID CR HIGH EGR **(e) MID CR MID EGR** **(f) MID CR LOW EGR**

(g) LOW CR HIGH EGR **(h) LOW CR MID EGR** **(i) LOW CR LOW EGR**

Fig.4. 52 Contour plots of soot for SOI and FIP at different levels of CR and EGR (VCR PB20)

4.3.5 Error analysis of the regression model for VCR PB20

Figure 4.53 to 4.55 shows that the residuals have been falling in a straight line. This denotes that the errors are normally distributed. Further, it confirms the adequacy of the least-square fit. It could be observed that the predicted values are in agreement with the simulation data, this indicates that the developed regression models can yield very accurate results.

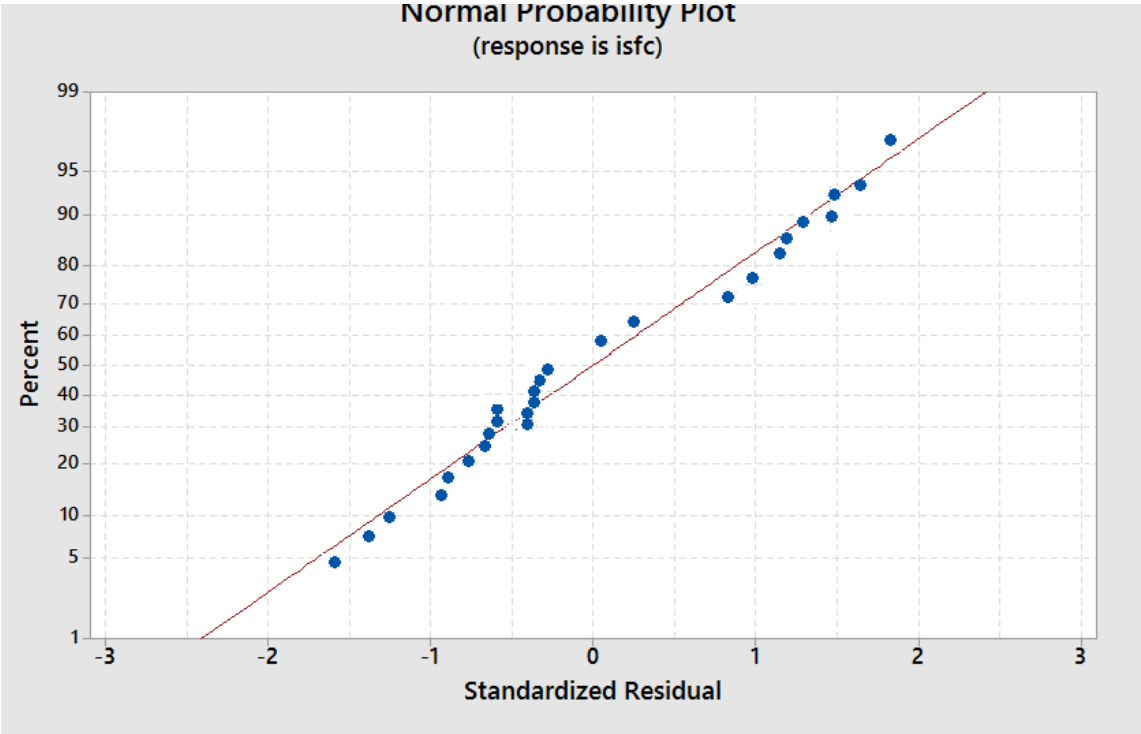

Fig.4. 53 Normal probability plot of the response ISFC for (VCR PB20)

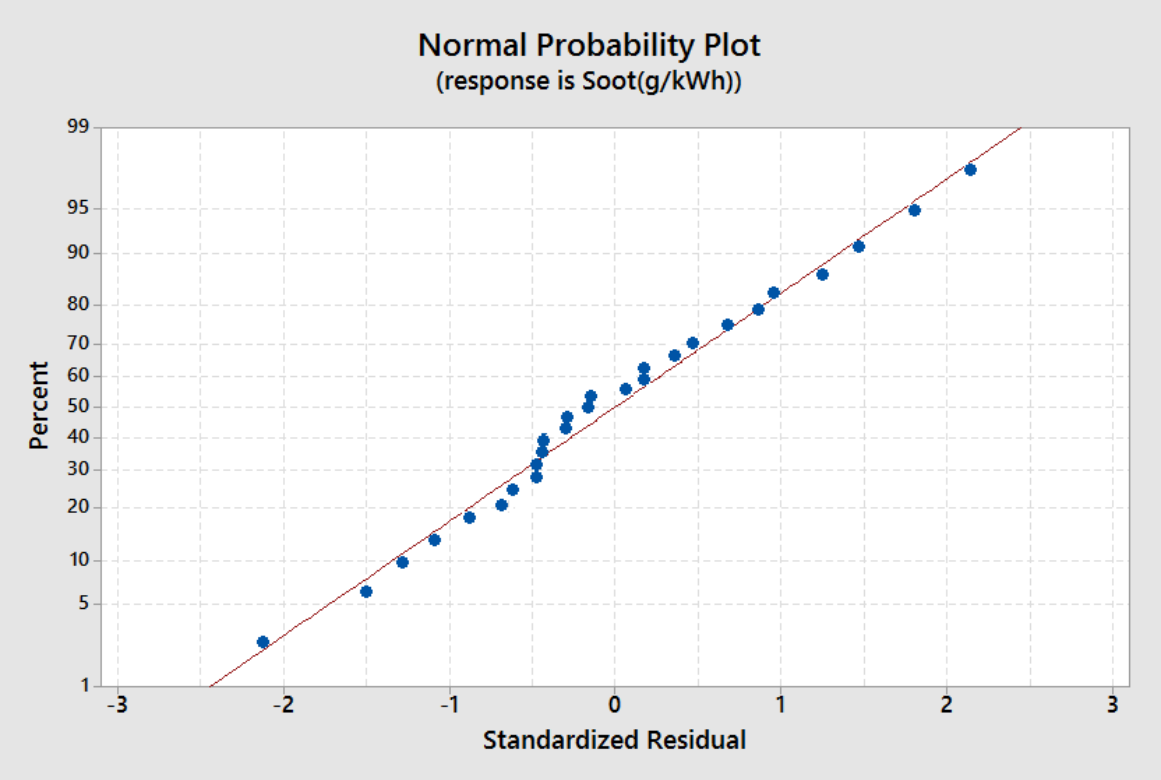

Fig.4. 54 Normal probability plot of the response soot for (VCR PB20)

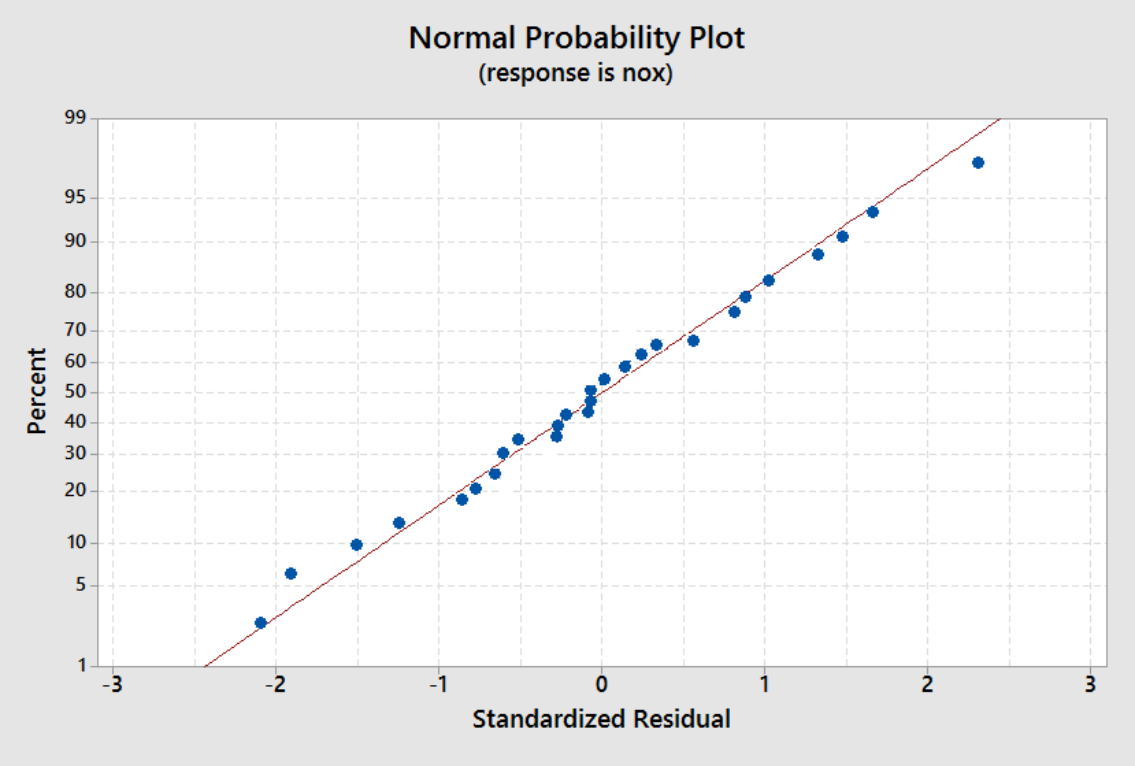

Fig.4. 55 Normal probability plot of the response NOx for (VCR PB20)

4.3.6 Optimization of VCR PB20

Composite desirability technique (Derringer & Suich, 1980) has been used to optimize the performance and emission characteristics. The optimum combination of the selected parameter set is obtained as 17.52 CR, SOI 31.2 °bTDC, FIP 820 bar and EGR 30.15%. The standards used for the desirability approach are given in the Table 4.22. Target of 205 g/kWh was set for the ISFC which is the best for the VCR diesel case. The other responses (NOx and soot) were intended to minimize.

Table 4. 22 VCR PB20 optimization standards used for the desirability of the responses

Parameter/ Response	**Limits**		**Criterion**	**Desirability**
	Lower	**Upper**		
Compression Ratio	12	18	In range	1
Fuel Injection Pressure (bar)	250	1000	In range	1
Start of Injection (°bTDC)	15	40	In range	1
Exhaust Gas Recirculation (%)	0	40	In range	1
ISFC (g/kWh)	205.91	390.25	Target	0.95
NOx (g/kWh)	0.598	13.627	Minimize	0.93
Soot (g/kWh)	0.0901	1.796	Minimize	0.96
Combined				0.95

4.3.6.1 Comparison of baseline and optimized for VCR PB20

The optimized and baseline cases are compared for the VCR PB20 in the current section. The optimum combination set was simulated and compared with the baseline configuration. Table 4.23 gives the comparison of optimized and baseline cases of VCR PB20. Results indicate that the optimum case has resulted in lower emissions and lower ISFC as compared with the baseline. This shows the superior quality of the optimum case than the baseline case in terms of both performance and emissions aspects.

Table 4. 23 Comparison of ISFC, ISEC, NOx and soot

	ISFC (g/kWh)	ISEC (MJ/kWh)	NOx (g/kWh)	Soot (g/kWh)
Baseline Case PB20	240.25	10.28	8.25	0.82
Optimized case VCR	205.48	9.16	3.75	0.191
Optimized case PB20	**210.84**	**9.02**	**3.65**	**0.144**
change w.r.t. baseline	**12.24% ↓**	**12.24 %↓**	**55.75 % ↓**	**82.43% ↓**
change w.r.t. VCR diesel optimum	**2.60% ↑**	**1.52 % ↓**	**2.66 % ↓**	**24.60 % ↓**

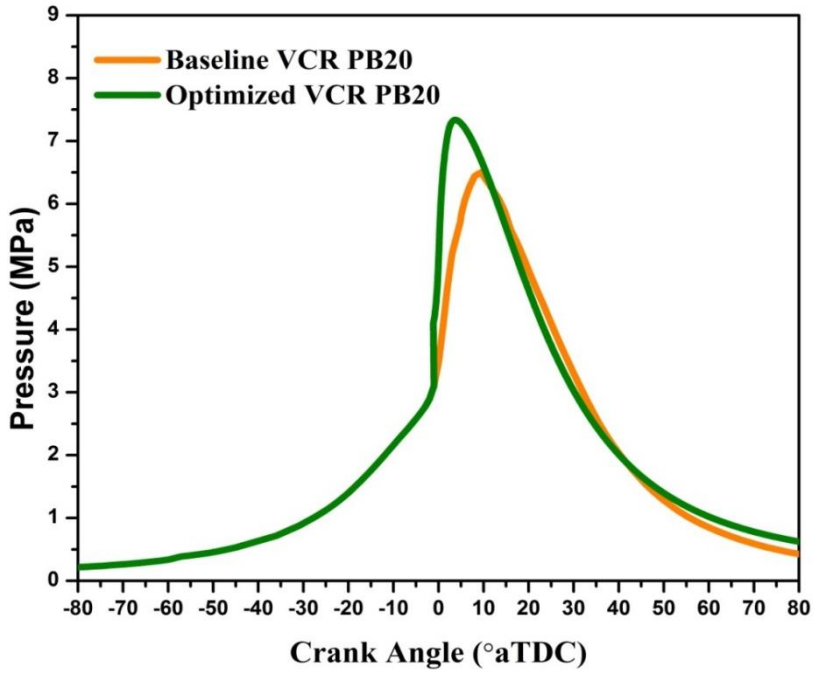

Fig.4. 56 Comparison of Pressure vs. Crank angle for baseline and optimized (VCR PB20)

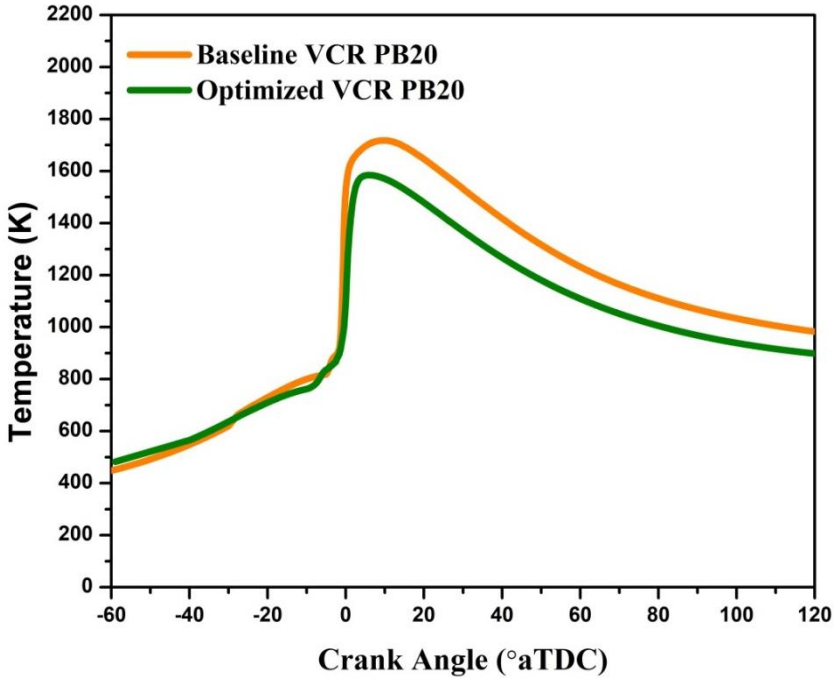

Fig.4. 57 Comparison of temperature vs. Crank angle for baseline and optimized (VCR PB20)

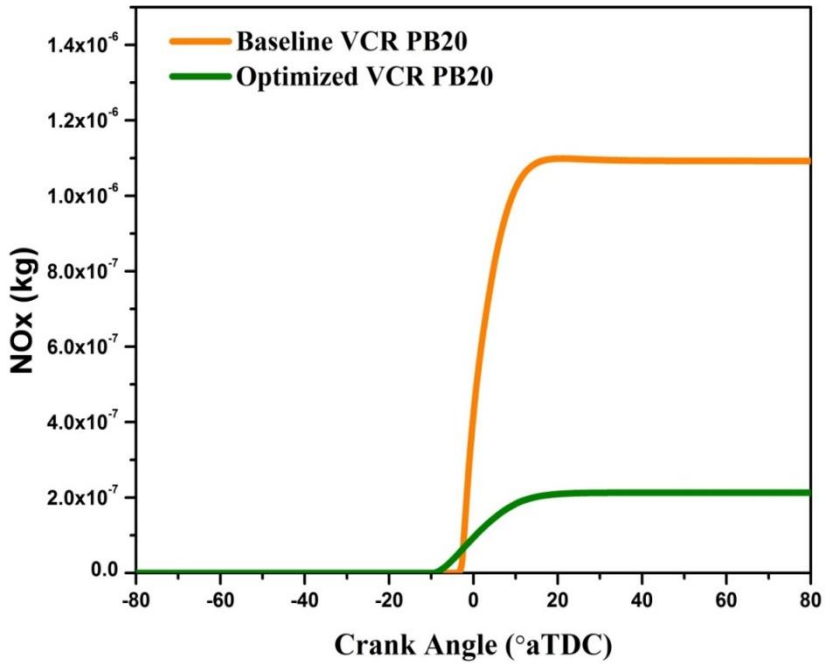

Fig.4. 58 Comparison of NOx vs. Crank angle for baseline and optimized (VCR PB20)

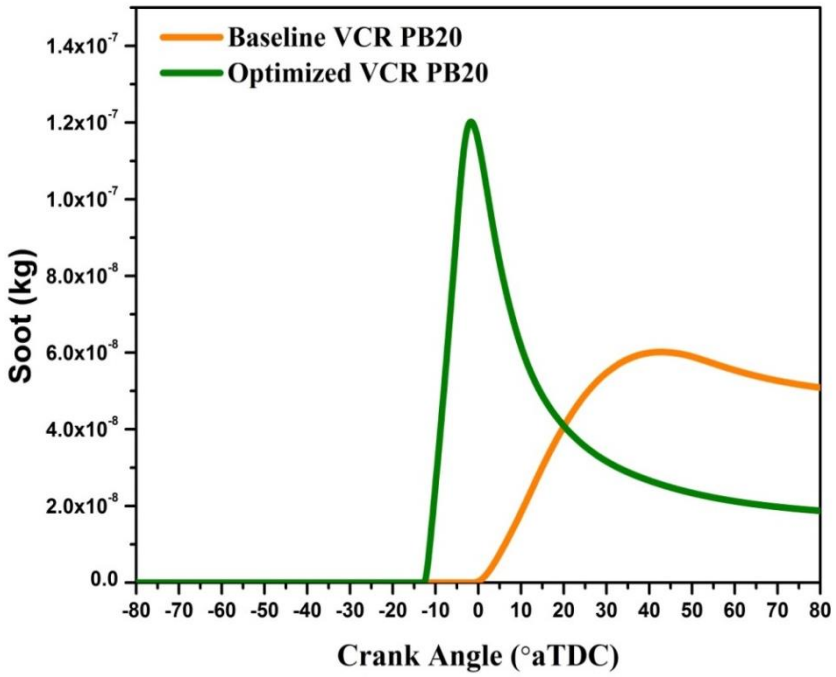

Fig.4. 59 Comparison of soot vs. Crank angle for baseline and optimized (VCR PB20)

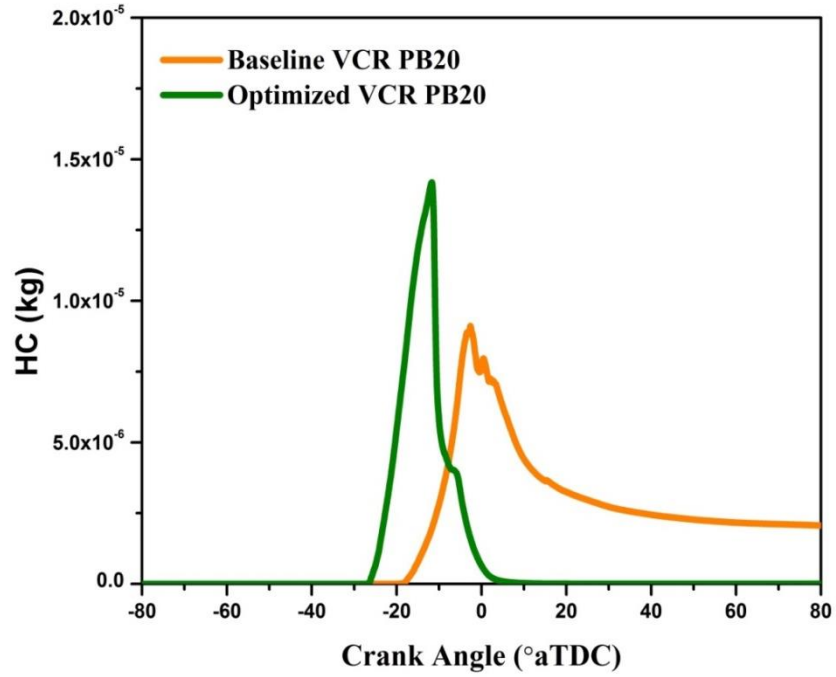

Fig.4. 60 Comparison of HC vs. Crank angle for baseline and optimized (VCR PB20)

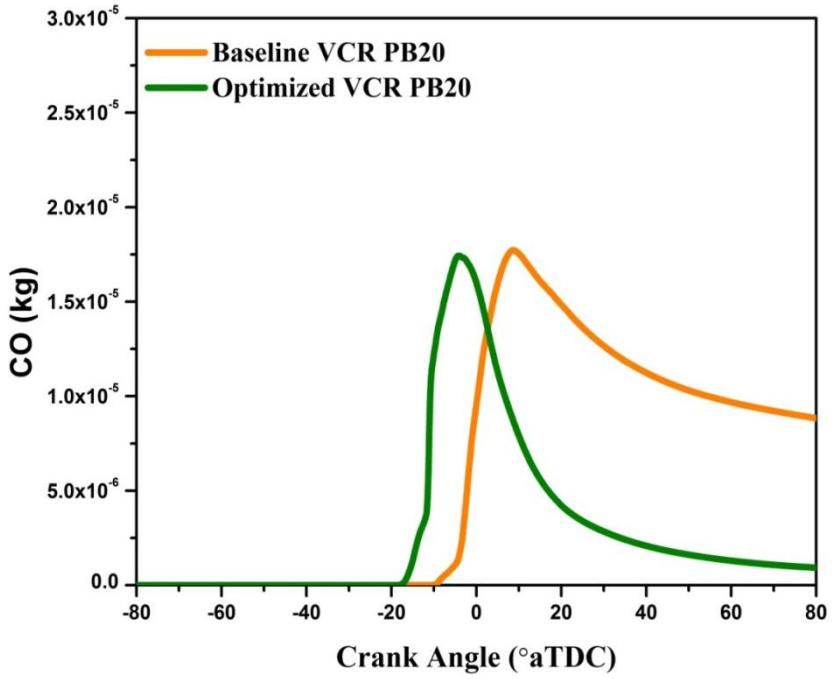

Fig.4. 61 Comparison of CO vs. Crank angle for baseline and optimized (VCR PB20)

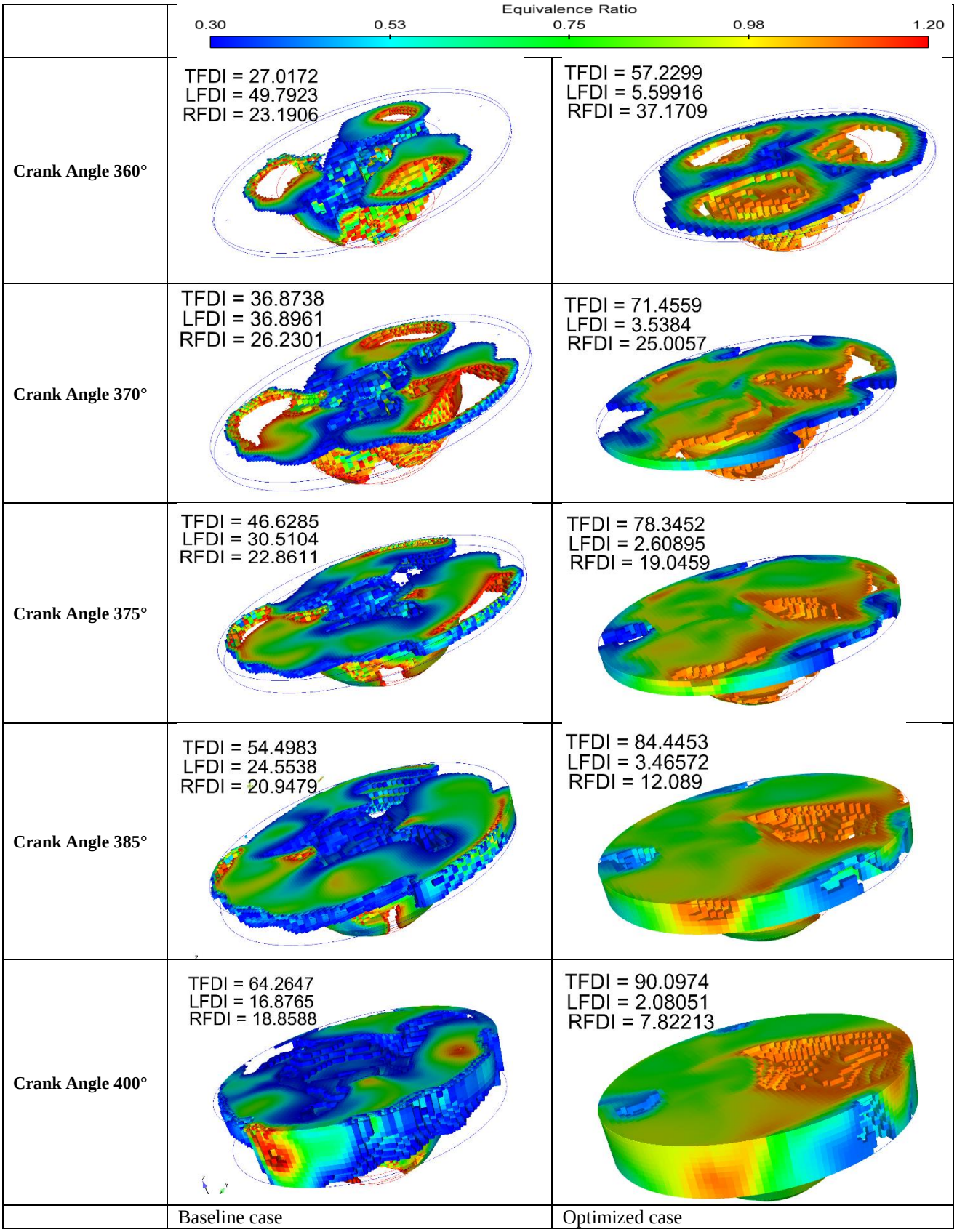

Fig.4. 62 comparisons of homogeneity of the baseline and optimized cases of the VCR PB20 at different crank angle

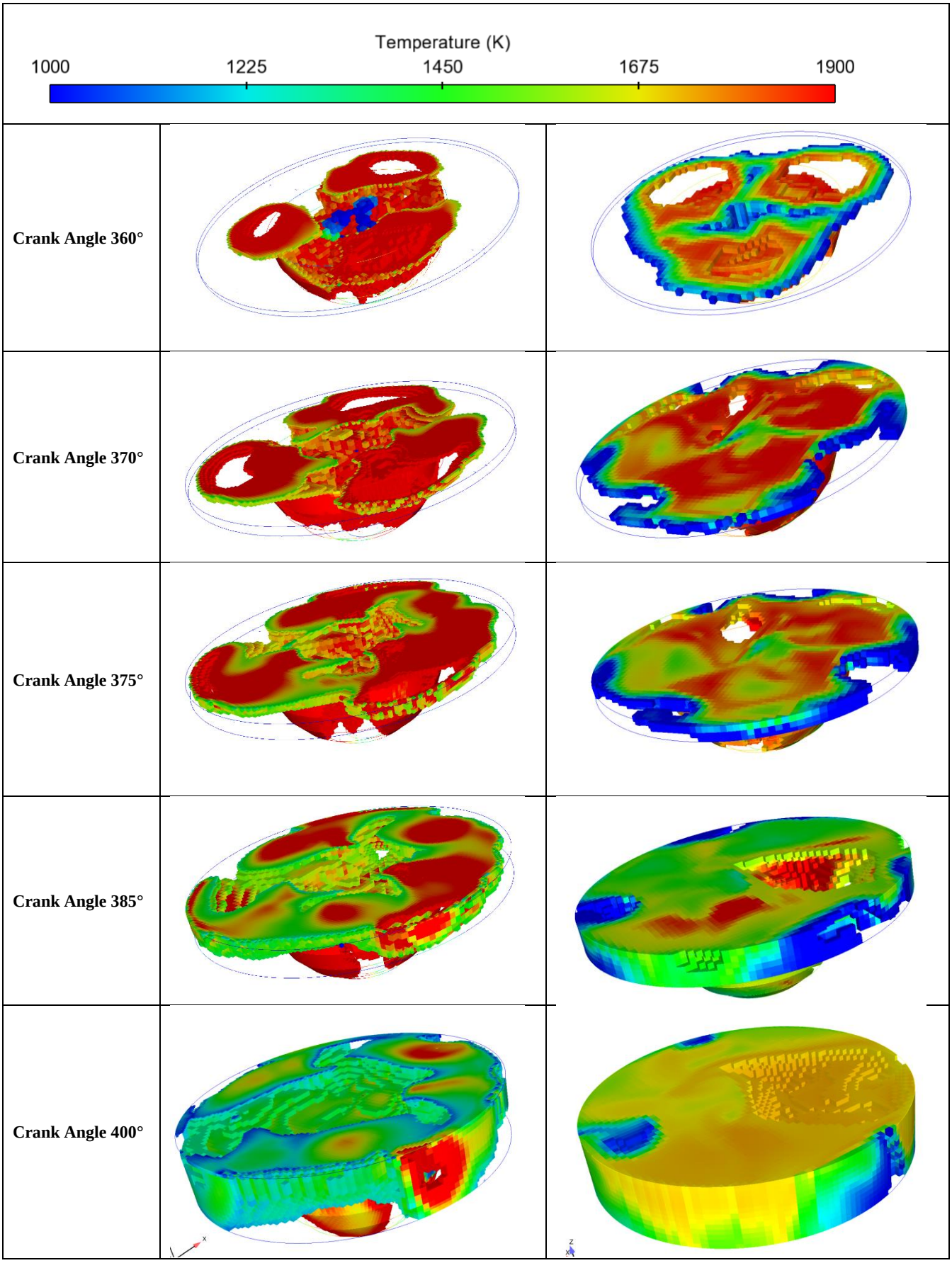

Fig.4. 63 Temperature distribution of baseline and optimized cases at differe) crank angles (VCR PB20)

4.3.6.2 Charge Homogeneity inside the cylinder for baseline and optimized of VCR PB20

In-cylinder images were captured using ENSIGHT software to show the comparison of baseline and optimized cases of the VCR PB20 case. The Fig.4.62 show that the optimized case has got the higher TFDI at all the instances compared. It was also evident from the Fig.4.63 that the temperature distribution is also uniform and moderate temperatures were observed throughout the target region for an optimized case as compared to the baseline configuration. Thus, it was concluded that the present optimized model could able to achieve HCCI combustion characteristics.

Summary

The analysis of the VCR PB20 engine model with respect to the effect of the chosen parameters was done on the performance and emission characteristics. Validation of the VCR PB20 engine model has been done with respect to the baseline configuration. Then the model was analyzed through parametric optimization in order to optimize the performance and emission characteristics. The target of the VCR PB20 was set as that of the optimized case of the VCR diesel case in terms of ISFC, NOx and soot. The optimized of PB20 case was able to reduce the NOx and soot emissions, but the ISFC was a bit higher side. This may be due the differences in the calorific value of the diesel and PB20 fuels. So for this reason ISEC (MJ/kWh) was compared for both the cases, interestingly the PB20 was found to be superior in this aspect. Hence the usage of PB20 is also justified as a replacement for conventional diesel.

4.4 Comparison of CAT3401, VCR diesel and VCR PB20

Based on the ANOVA analysis the three models (CAT3401, VCR diesel and VCR PB20) analyzed in this study are compared and given in table 4.24 – 4.26 for the three response variables (ISFC, NOx and soot) respectively with respect to the design/operating parameters.

Table 4. 24 Influential strengths of the parameters on ISFC

Influential strength of the parameters on ISFC			
ISFC	% contribution $(\frac{\text{Adj SS}}{\text{Total Adj SS}})\times 100$		
	CAT 3401	VCR Diesel	VCR PB20
CR	42.30	47.80	26.52
FIP	8.15	9.49	16.04
SOI	18.53	33.11	21.21
EGR	4.44	5.29	11.42
CR*CR	0.42	0.16	1.53
FIP*FIP	2.69	0.09	11.11
SOI* SOI	14.23	0.07	0.91
EGR*EGR	2.26	0.05	1.14
CR*FIP	1.98	0.98	0.03
CR*SOI	0.17	0.94	1.19
CR*EGR	3.92	0.04	0.41
FIP*SOI	3.68	1.24	1.30
FIP*EGR	0.06	0.60	0.04
SOI*EGR	0.65	0.02	0.28

For all the three cases (CAT3401, VCR diesel and VCR PB20) CR is the most influential parameter for ISFC is concerned. Start of Injection is the second most influential parameter in view of ISFC. This implies that the CR and SOI are the two potential parameters in deciding the engine performance. Overall the individual effects play a major role in deciding the ISFC. This means the linear relation with respect to the individual parameters are dominant over the squared and interaction effects.

In view of NOx for CAT 3401 (heavy-duty engine) is concerned SOI is the major contributor and followed by EGR. For VCR (Genset) diesel engine case CR is the most influential in deciding the NOx followed by SOI and EGR. In VCR PB20 case EGR is the most influential parameter followed by SOI and CR. This is an indication that the effects of influential parameters are also affected by the type of engine and fuel.

For soot emissions in the CAT3401 is more influenced by the SOI and followed by CR, FIP and EGR. In the other two cases, VCR diesel and PB20, soot is most influenced by SOI, and followed by its squared term, CR, EGR and FIP.

Table 4. 25 Influential strengths of the parameters on NOx

Influential strength of the parameters on NOx			
NOx	% contribution $(\frac{\text{Adj SS}}{\text{Total Adj SS}})\times 100$		
	CAT 3401	VCR Diesel	VCR PB20
CR	2.25	41.18	11.28
FIP	6.85	7.90	1.77
SOI	54.66	23.54	27.45
EGR	13.56	14.75	44.00
CR*CR	0.29	2.62	0.49
FIP*FIP	0.10	0.16	0.25
SOI* SOI	9.40	0.82	3.69
EGR*EGR	0.26	0.29	6.86
CR*FIP	0.43	1.57	0.01
CR*SOI	0.16	0.09	0.01
CR*EGR	0.15	1.94	1.37
FIP*SOI	4.33	1.26	0.15
FIP*EGR	0.72	0.93	0.21
SOI*EGR	6.15	1.91	1.54

Table 4. 26 Influential strengths of the parameters on soot

Influential strength of the parameters on soot			
Soot	% contribution $(\frac{\text{Adj SS}}{\text{Total Adj SS}})\times 100$		
	CAT 3401	VCR Diesel	VCR PB20
CR	16.21	14.71	15.54
FIP	15.92	8.83	9.01
SOI	31.15	27.29	27.85
EGR	12.33	9.18	8.96
CR*CR	2.98	2.36	1.98
FIP*FIP	2.33	2.51	2.33
SOI* SOI	5.38	21.37	21.13
EGR*EGR	1.34	1.13	1.49
CR*FIP	1.75	0.30	0.30
CR*SOI	2.10	0.80	0.81
CR*EGR	2.43	0.39	0.06
FIP*SOI	4.55	0.81	0.83

FIP*EGR	3.50	2.53	2.58
SOI*EGR	2.16	1.47	1.50

Summary

The effect of the CR, SOI, FIP, EGR and their interactions were studied on the performance and emission characteristics for all the three (CAT3401, VCR Diesel and VCR PB20) models. It was found that individual parameters are more dominant than their interaction effects on performance and emission characteristics. This is manifest from the study that the upshot of the parameters and their interaction effects are also depending on the type of engine and fuel used.

Chapter 5

Conclusions

The present CFD based study is carried out to evaluate three models, namely CAT3401, VCR diesel and VCR PB20. Four parameters such as CR, SOI, FIP and EGR were chosen to analyze the effect on the performance and emission characteristics of CAT3401 and VCR engines.

RSM is used to study the interaction effects of the parameters on the performance and emission characteristics of CAT3401 and VCR engines. The study was also extended to analyze the effect of fuel blend (PB20). All the models were analyzed and optimized in view of minimizing the emissions and improving the performance. Optimum parameters were also suggested for each of these models.

Broad conclusions

- ✓ The single parametric study approach might not attain the optimal combustion characteristics.
- ✓ An absolute tradeoff has been observed in single parametric approach between the NOx and soot emissions.
- ✓ RSM based multi-parametric study was able to predict the variations of performance and emissions characteristics and their interaction effects.
- ✓ The interaction effects also play a major role of in determining the performance and emission characteristics of the engine.
- ✓ Increasing CR reduces ISFC and soot whereas it increases NOx emissions and vice versa, but this trend reverses when the SOI and FIP are at their high levels.

- ✓ Increasing FIP reduces soot and also slightly reduces ISFC but increases NOx significantly. But this is also not valid when the low EGR and advanced SOI co-exist.
- ✓ Advancing SOI reduces soot and increases NOx but the ISFC may decrease or increase and will depend on the compression work.
- ✓ Increasing EGR alone increases the soot and ISFC whereas the NOx emissions decrease significantly, whereas this phenomenon turn round when the CR and SOI at high levels.

Specific conclusions

- ✓ It was found that the performance of the VCR is inferior to that of a CAT3401 engine with respect to the soot emissions and ISFC.

For ISFC

- ✓ In all the three CAT3401, VCR diesel and VCR PB20 cases, CR is the most influential parameter for ISFC.
- ✓ Start of Injection is the second most influential parameter in view of ISFC. This implies that the CR and SOI are two potential parameters in deciding the engine performance. However, there is a limit in advancing SOI due to the possibility of negative work.
- ✓ Overall the individual effects play a major role in deciding the ISFC. This means the linear relation with respect to the individual parameters are dominant over the squared and interaction effects.

For NOx

- ✓ As far as CAT 3401 is concerned, SOI is the major contributor followed by EGR.
- ✓ In a VCR diesel engine, CR is the most influential parameter followed by SOI and EGR.
- ✓ In VCR PB20, EGR is the most influential parameter followed by SOI and CR.

For soot emissions

- ✓ In (CAT3401) the effect is more influenced by SOI and followed by CR, FIP and EGR.
- ✓ In the other two cases, namely, VCR diesel and PB20, soot is most influenced by SOI, and followed by its squared term, CR, EGR and FIP.

Thus, it can be concluded that the effects of influential parameters also depend on the type of engine and fuel.

Interaction effects

The significance of interaction effects varies with all the three models.

In CAT3401 engine

- ✓ CR×FIP, CR×EGR, SOI×EGR and FIP×SOI interactions strongly influence ISFC.

- ✓ For NOx, SOI×EGR, FIP×SOI, FIP×EGR and CR×FIP, interactions were significant.
- ✓ All the interaction effects of soot were significant.
- ✓ The optimum combination of parameters was found to be CR 14.55, FIP 855 bar, SOI 16.29° bTDC, and EGR 26.15 % for the CAT3401 diesel engine with a composite desirability of 0.94.
- ✓ The optimal combination reduced 40.3% and 52.38% for NOx and soot respectively, with a marginal improvement in the ISFC when compared with the baseline.

VCR Diesel

- ✓ The interaction effects such as CR×SOI, CR×FIP, SOI×FIP and FIP×EGR were statistically significant on ISFC.
- ✓ The interaction effects such as CR×FIP, CR×EGR, SOI×FIP, SOI×EGR and FIP×EGR were statistically significant on NOx.
- ✓ All the interactions were significant on soot for the VCR diesel model.
- ✓ The optimum combination of VCR diesel case was found to be the CR 17.52, SOI 30.1 °bTDC, FIP 736.06 bar and EGR 28.29% with a composite desirability of 0.95.
- ✓ The corresponding ISFC, NOx and soot were reduced by 2.37%, 29.11% and 83.81 % respectively, with reference to baseline.

VCR PB20

- ✓ The interaction effects such as CR×SOI, CR×EGR and SOI×FIP are statistically significant on ISFC.
- ✓ The interaction effects of CR×EGR and SOI×EGR are statistically significant on NOx.
- ✓ The interaction effects of CR×SOI, CR×FIP, SOI×FIP, SOI×EGR, FIP×EGR are significant on soot.
- ✓ The optimum set of combination for PB20 is 17.52 CR, SOI 29.2 °bTDC, FIP 820 bar, and an EGR 30.15%.
- ✓ The optimized VCR PB20 configuration reduced the NOx and soot emissions by 2.66 %, 24.60 %, respectively, but the ISFC was a bit on the higher side when compared with optimized VCR diesel. However, ISEC (MJ/kWh) of the optimized VCR PB20 was found to be superior to the optimized VCR diesel.

Hence the use of PB20 is justified and should be recommended as a replacement for conventional diesel.

Improved TFDI (Target Fuel Distribution Index) with simultaneous reduction of NOx and soot ensures optimized combustion characteristics as that of HCCI in all the three cases.

Scope for future work

- It is crucial to mention that the optimal solutions are only for a particular load and speed other load and speed shall have different optimum conditions. Hence, in future numerical experiments can be carried out to obtain optimal conditions for various loads and speeds.
- The parametric study may be analyzed further and can be optimized using Genetic Algorithm based optimization techniques such as NSGA II, ARMOGA etc. to obtain Pareto optimal solutions.
- Preparation of homogeneous charge is the main concerned in achieving HCCI combustion characteristics. So there is a lot of scope to work on the preparation of homogeneous charge in DICI engines. Better mixture preparation by varying piston bowl shapes, swirl generation through inlet manifold, ultra high injection pressure, fuel additives etc. can be explored further.
- In the future, different injection strategies can be implemented for better charge preparation to achieve HCCI like manifold injection, extremely advanced injection, late direct injection and split injection/multiple injections combined with high EGR rates.
- HCCI combustion is also controlled by chemical kinetics and fuel properties, so volatile fuels such as alcohols can be blended with different surrogate fuels in order to attain better mixing of charge.
- The effect of turbulence on the air-fuel mixture can be studied further for better insights of the mixture preparation.
- Development and reduction of the chemical reaction mechanism for different practical fuels also have a wide scope of research for efficient and reliable combustion models.
- Optical diagnostics can be implemented for better physical understanding of the combustion phenomena.
- Extension of load range for HCCI is a challenge, so boosting the charge is also an effective way to control the HCCI combustion for different loads.
- HCCI combustion may attain sudden peaks of heat release rate, which can lead to high noise levels, so one can study to reduce the noise levels.

References

1. Agarwal, A. K., Dhar, A., Gupta, J. G., Kim, W. Il, Choi, K., Lee, C. S., & Park, S. (2015). Effect of fuel injection pressure and injection timing of Karanja biodiesel blends on fuel spray, engine performance, emissions and combustion characteristics. Energy Conversion and Management, 91, 302-314.
2. Agarwal, A. K., Srivastava, D. K., Dhar, A., Maurya, R. K., Shukla, P. C., & Singh, A. P. (2013). Effect of fuel injection timing and pressure on combustion, emissions and performance characteristics of a single cylinder diesel engine. Fuel, 111, 374-383.
3. Agarwal, D., Singh, S. K., & Agarwal, A. K. (2011). Effect of Exhaust Gas Recirculation (EGR) on performance, emissions, deposits and durability of a constant speed compression ignition engine. Applied Energy, 88(8), 2900-2907.
4. Akihama, K., Takatori, Y., Inagaki, K., Sasaki, S., & Dean, A. M. (2001). Mechanism of the Smokeless Rich Diesel Combustion by Reducing Temperature. SAE technical paper, 2001-01-06.
5. An, H., Yang, W. M., Maghbouli, a., Chou, S. K., & Chua, K. J. (2013). Detailed physical properties prediction of pure methyl esters for biodiesel combustion modeling. Applied Energy, 102, 647-656.
6. Atabani, A. E., Silitonga, A. S., Ong, H. C., Mahlia, T. M. I., Masjuki, H. H., Badruddin, I. A., & Fayaz, H. (2013). Non-edible vegetable oils: A critical evaluation of oil extraction, fatty acid compositions, biodiesel production, characteristics, engine performance and emissions production. Renewable and Sustainable Energy Reviews, 18, 211-245.
7. Bala, M., & Sandeep, T. N. N. (2011). Proximate Composition and Fatty Acid Profile of Pongamia pinnata , a Potential Biodiesel Crop, 559-562. https://doi.org/10.1007/s11746-010-1699-2
8. Beale, J. C., & Reitz, R. D. (1999). Modeling spray atomization with the Kelvin-Helmholtz / Rayleigh-Taylor hybrid model. Atomization and Sprays, (November), 623-650.

9. Béard, P., Mokaddem, K., & Baritaud, T. (1998). Measurement and Modeling of the Flow-Field in a DI Diesel Engine: Effects of Piston Bowl Shape and Engine Speed. SAE International .
10. Bendu, H., & Murugan, S. (2014). Homogeneous charge compression ignition (HCCI) combustion: Mixture preparation and control strategies in diesel engines. Renewable and Sustainable Energy Reviews, 38, 732-746.
11. Box, G. E., & Draper, N. R. (1987). Empirical model-building and response surfaces. (S.l.) : New York: Wiley.
12. Brakora, J. L., A comprehensive combustion model for biodiesel-fueled engine simulations Thesis (Ph.D.)--The University of Wisconsin - Madison, 2012
13. Brakora, J., & Reitz, R. (2013). A Comprehensive Combustion Model for Biodiesel-Fueled Engine Simulations. SAE Technical Paper, 01-1099.
14. Buchwald, R., Brauer, M., Blechstein, A., Sommer, A., & Kahrstedt, J. (2004). Adaption of Injection System Parameters to Homogeneous Diesel Combustion. SAE Technical Paper 2004-01-0936, 2004(724).
15. Dean, A. M., & Voss, D. (1999). Design and analysis of experiments (Vol. 1). New York: Springer.
16. Caton, J. A. (2014). On the importance of specific heats as regards efficiency increases for highly dilute IC engines. Energy Conversion and Management, 79, 146-160.
17. Chakravarthy, K., McFarlane, J., Daw, C., Ra, Y., & Reitz, R. (2007). Physical Properties of Soy Bio-diesel & Implications For Use of Bio-diesel In Diesel Engines. Sae 2007014030, (724).
18. Chavan, S. B., Kumbhar, R. R., Kumar, A., & Sharma, Y. C. (2015). Study of biodiesel blends on emission and performance characterization of a variable compression ratio engine. Energy and Fuels, 29(7), 4393-4398.
19. Chiang, C. H., Raju, M. S., & Sirignano, W. A. (1992). Numerical Analysis of a Convecting, Vaporizing Fuel Droplet with Variable Properties. International Journal of Heat Mass Transfer, 35.
20. Costa, R. C., & Sodré, J. R. (2011). Compression ratio effects on an ethanol/gasoline fuelled engine performance. Applied Thermal Engineering, 31(2), 278-283.
21. Curtis, E. W., Uludogan, A., & Reitz, R. D. (1995). A new high pressure droplet

vaporization model for diesel engine modeling (No. 952431). SAE Technical Paper.

22. Daubert, T. E., & Danner., R. P. (1989). Physical and thermodynamic properties of pure chemicals: data compilation. DC: Taylor & Francis;
23. Derringer, G., & Suich, R. (1980). Simultaneous optimization of several response variables. J Qual Technol, 12(4), 214–219.
24. Fang, Q., Fang, J., Zhuang, J., & Huang, Z. (2012). Influences of pilot injection and exhaust gas recirculation (EGR) on combustion and emissions in a HCCI-DI combustion engine. Applied Thermal Engineering, 48, 97-104.
25. Fang, T., Coverdill, R. E., Lee, C. F. F., & White, R. a. (2009). Air-fuel mixing and combustion in a small-bore direct injection optically accessible diesel engine using a retarded single injection strategy. Fuel, 88(11), 2074-2082.
26. Fathi, M., Saray, R. K., & Checkel, M. D. (2011). The influence of Exhaust Gas Recirculation (EGR) on combustion and emissions of n-heptane/natural gas fueled Homogeneous Charge Compression Ignition (HCCI) engines. Applied Energy, 88(12), 4719-4724.
27. Fuchs, T. R., & Rutland, C. J. (1998). Intake Flow Effects on Combustion and Emissions in a Diesel Engine. SAE International .
28. Gan, S., Ng, H. K., & Pang, K. M. (2011). Homogeneous Charge Compression Ignition (HCCI) combustion: Implementation and effects on pollutants in direct injection diesel engines. Applied Energy, 88(3), 559-567.
29. Gnana Sagaya Raj, A. R., Mallikarjuna, J. M., & Ganesan, V. (2013). Energy efficient piston configuration for effective air motion – A CFD study. Applied Energy, 102 (Supplement C), 347-354.
30. Gonzalez, M. A., Lian, Z. W., & Reitz, R. D. (1992). Modeling Diesel Engine Spray Vaporization and Combustion. SAE Paper No. 920579.
31. Grondin, O., Stobart, R., Chafouk, H., & Maquet, J. (2004). Modelling the Compression Ignition Engine for Control: Review and Future Trends., (November 2014). https://doi.org/10.4271/2004-01-0423
32. Han, Z., & Reitz, R. D. (1995). Combustion Science and Technology Turbulence Modeling of Internal Combustion Engines Using RNG κ - ε Models Turbulence Modeling of Internal Combustion Engines Using RNG k-E Models, 106, 267-295.

33. Haraldsson, G., Tunestål, P., Johansson, B., & Hyvönen, J. (2002). HCCI Combustion Phasing in a Multi Cylinder Engine Using Variable Compression Ratio. SAE International . https://doi.org/10.4271/2002-01-2858
34. Helmantel, A., Gustavsson, J., & Denbratt, I. (2005). Operation of a DI Diesel Engine With Variable Effective Compression Ratio in HCCI and Conventional Diesel Mode, 2005(724). https://doi.org/10.4271/2005-01-0177
35. Henein, N. (2006). Effect of Injection Pressure and Swirl Motion on Diesel Engine-out Emissions in Conventional and Advanced Combustion Regimes. SAE Technical …, 2006(724). https://doi.org/10.4271/2006-01-0076
36. Heywood, J. B. (1988). Internal Combustion Engine Fundementals. McGrawHill series in mechanical engineering
37. Hoekman, S. K., Broch, A., Robbins, C., Ceniceros, E., & Natarajan, M. (2012). Review of biodiesel composition, properties, and specifications. Renewable and Sustainable Energy Reviews, 16(1), 143-169.
38. Jaichandar, S., & Annamalai, K. (2012). Influences of re-entrant combustion chamber geometry on the performance of Pongamia biodiesel in a DI diesel engine. Energy, 44(1), 633-640.
39. Jayashankara, B., & Ganesan, V. (2010a). Effect of fuel injection timing and intake pressure on the performance of a di diesel engine - A parametric study using CFD. Energy Conversion and Management, 51(10), 1835-1848.
40. Jayashankara, B., & Ganesan, V. (2010b). Effect of fuel injection timing and intake pressure on the performance of a DI diesel engine – A parametric study using CFD. Energy Conversion and Management, 51(10), 1835-1848.
41. Jindal, S., Nandwana, B. P., Rathore, N. S., & Vashistha, V. (2010). Experimental investigation of the effect of compression ratio and injection pressure in a direct injection diesel engine running on Jatropha methyl ester. Applied Thermal Engineering, 30(5), 442-448.
42. Kannan, G. R., & Anand, R. (2011). Experimental evaluation of DI diesel engine operating with diestrol at varying injection pressure and injection timing. Fuel Processing Technology, 92(12), 2252-2263.
43. Kavuri, C., Singh, S., Krishnan, S. R., Srinivasan, K. K., & Ciatti, S. (2014).

Computational Analysis of Combustion of High and Low Cetane Fuels in a Compression Ignition Engine. Journal of Engineering for Gas Turbines and Power, 136(12), 121506.

44. Kim, M. Y., & Lee, C. S. (2007). Effect of a narrow fuel spray angle and a dual injection configuration on the improvement of exhaust emissions in a HCCI diesel engine. Fuel, 86(17), 2871-2880.
45. Knecht, W. (2008). Diesel engine development in view of reduced emission standards - ScienceDirect. Energy, 33, 264-271.
46. Koc, A. B., & Abdullah, M. (2013). Performance and NO x emissions of a diesel engine fueled with biodiesel-diesel-water nanoemulsions. Fuel processing technology, 109, 70-77.
47. Kumar, N. R., Sekhar, Y. M. C., & Adinarayana, S. (2013). Effects of compression ratio and EGR on performance, combustion and emissions of DI injection diesel engine. International Journal of Applied Science and Engineering, 11(1), 41-49.
48. Kwon, O.-I., Arai, M., & Hiroyasu, H. (1990). Effects of Cylinder Temperature and Pressure on Ignition Delay in Direct Injection Diesel Engine. Bulletin of the M.E.S.J., 18(1), 3-16.
49. Ladommatos, N., Abdelhalim, S. M., Zhao, H., & Hu, Z. (1996a). The Dilution, Chemical, and Thermal Effects of Exhaust Gas Recirculation on Diesel Engine Emissions - Part 1: Effect of Reducing Inlet Charge Oxygen. SAE International . https://doi.org/10.4271/961165
50. Ladommatos, N., Abdelhalim, S. M., Zhao, H., & Hu, Z. (1996b). The Dilution, Chemical, and Thermal Effects of Exhaust Gas Recirculation on Diesel Engine Emissions - Part 2: Effects of Carbon Dioxide. SAE Technical Paper. SAE Technical Paper. https://doi.org/10.4271/961167.
51. Ladommatos, N., Abdelhalim, S. M., Zhao, H., & Hu, Z. (1997a). The Dilution, Chemical, and Thermal Effects of Exhaust Gas Recirculation on Diesel Engine Emissions - Part 3: Effects of Water Vapour. SAE International . https://doi.org/10.4271/971659
52. Ladommatos, N., Abdelhalim, S. M., Zhao, H., & Hu, Z. (1997b). The Dilution, Chemical, and Thermal Effects of Exhaust Gas Recirculation on Disesel Engine Emissions - Part 4: Effects of Carbon Dioxide and Water Vapour. SAE International . https://doi.org/10.4271/971660

53. Laguitton, O., Crua, C., Cowell, T., Heikal, M. R., & Gold, M. R. (2007). The effect of compression ratio on exhaust emissions from a PCCI diesel engine. Energy Conversion and Management, 48(11), 2918-2924.
54. Lapuerta, M., Armas, O., & Rodríguez-Fernández, J. (2008). Effect of biodiesel fuels on diesel engine emissions. Progress in Energy and Combustion Science, 34(2), 198-223.
55. Li, J., Yang, W. M., An, H., Maghbouli, A., & Chou, S. K. (2014). Effects of piston bowl geometry on combustion and emission characteristics of biodiesel fueled diesel engines, 120, 66-73. https://doi.org/10.1016/j.fuel.2013.12.005
56. Lim, J., & Min, K. (2005). The effects of spray angle and piston bowl shape on diesel engine soot emissions using 3-D CFD simulation (No. 2005-01-2117). SAE Technical Paper. https://doi.org/10.4271/2005-01-2117
57. Liu, A. B., Mather, D. K., &, & Reitz, R. D. (1993). Modeling the Effects of Drop Drag and Breakup on Fuel Sprays. SAE International, No 930072.
58. Maiboom, A., Tauzia, X., & Hétet, J.-F. (2008). Experimental study of various effects of exhaust gas recirculation (EGR) on combustion and emissions of an automotive direct injection diesel engine. Energy, 33(1), 22-34.
59. Mallamo, F., Badami, M., & Millo, and F. (2005). Effect of compression ratio and injection pressure on emissions and fuel consumption of a small displacement common rail diesel engine. SAE Technical Paper, 2005(x). https://doi.org/10.4271/2005-01-0379
60. Mathur, Y. B., Poonia, M. P., Jethoo, a S., & Singh, R. (2012). Optimization of Compression Ratio of Diesel Fuelled Variable Compression Ratio Engine, 2(3), 99-101.
61. Matsumoto, A., Moore, W. R., Lai, M., Zheng, Y., Foster, M., Yen, D., … Hopkins, E. (2010). Spray Characterization of Ethanol Gasoline Blends and Comparison to a CFD Model for a Gasoline Direct Injector. SAE Int. J. Engines, 3(1), 402-425.
62. Mobasheri, R., Peng, Z., & Mirsalim, S. M. (2012). Analysis the effect of advanced injection strategies on engine performance and pollutant emissions in a heavy duty DI-diesel engine by CFD modeling. International Journal of Heat and Fluid Flow, 33(1), 59-69.
63. Mohan, B., Yang, W., & Chou, S. K. (2013). Fuel injection strategies for performance improvement and emissions reduction in compression ignition engines - A review. Renewable and Sustainable Energy Reviews, 28, 664-676.

64. Mohibbe Azam, M., Waris, A., & Nahar, N. M. (2005). Prospects and potential of fatty acid methyl esters of some non-traditional seed oils for use as biodiesel in India. Biomass and Bioenergy, 29(4), 293-302.
65. Montgomery, D. C. (2008). Design and analysis of experiments. (S.l.) : John Wiley & Sons.
66. Muralidharan, K., & Vasudevan, D. (2011). Performance, emission and combustion characteristics of a variable compression ratio engine using methyl esters of waste cooking oil and diesel blends. Applied Energy, 88(11), 3959-3968.
67. Murugesan, A., Umarani, C., Subramanian, R., & Nedunchezhian, N. (2009). Bio-diesel as an alternative fuel for diesel engines-A review. Renewable and Sustainable Energy Reviews, 13(3), 653-662.
68. Myers, R. H., Montgomery, D. C., & Anderson-Cook, C. M. (2016). Response surface methodology: process and product optimization using designed experiments. John Wiley & Sons.
69. Naik, S. N., Goud, V. V., Rout, P. K., & Dalai, A. K. (2010). Production of first and second generation biofuels: A comprehensive review. Renewable and Sustainable Energy Reviews, 14(2), 578-597.
70. O'Rourke, P. J. (1981). Collective drop effects on vaporizing liquid sprays (No. LA-9069-T). Los Alamos National Lab., NM (USA).
71. Pandey, R. K., Rehman, A., & Sarviya, R. M. (2012). Impact of alternative fuel properties on fuel spray behavior and atomization. Renewable and Sustainable Energy Reviews, 16(3), 1562-1578.
72. Pandian, M., Sivapirakasam, S. P., & Udayakumar, M. (2011). Investigation on the effect of injection system parameters on performance and emission characteristics of a twin cylinder compression ignition direct injection engine fuelled with pongamia biodiesel – diesel blend using response surface methodology. Applied Energy, 88(8), 2663-2676.
73. Park, S. (2012). Optimization of combustion chamber geometry and engine operating conditions for compression ignition engines fueled with dimethyl ether. Fuel, 97, 61-71.
74. Payri, F., Benajes, J., Margot, X., & Gil, A. (2004). CFD modeling of the in-cylinder flow in direct-injection Diesel engines. Computers & Fluids, 33(8), 995-1021.
75. Pfromm, P. H., Amanor-Boadu, V., & Nelson, R. (2011). Sustainability of algae derived

biodiesel: A mass balance approach. Bioresource Technology, 102(2), 1185-1193.

76. Pomraning, E. (2013). ICEF2013-19018, 1-11.
77. Post, S. L., & Abraham, J. (2002). Modeling the Outcome of Drop-Drop Collisions in Diesel Sprays. International Journal of Multiphase Flow, 28, 997-1019.
78. Prasad, B. V. V. S. U., Sharma, C. S., Anand, T. N. C., & Ravikrishna, R. V. (2011). High swirl-inducing piston bowls in small diesel engines for emission reduction. Applied Energy, 88(7), 2355-2367.
79. Qi, D., Leick, M., Liu, Y., & Lee, C. F. F. (2011). Effect of EGR and injection timing on combustion and emission characteristics of split injection strategy DI-diesel engine fueled with biodiesel. Fuel, 90(5), 1884-1891.
80. Raheman, H., & Ghadge, S. V. (2008). Performance of diesel engine with biodiesel at varying compression ratio and ignition timing. Fuel, 87(12), 2659-2666.
81. Raheman, H., & Phadatare, A. G. (2004). Diesel engine emissions and performance from blends of karanja methyl ester and diesel. Biomass and Bioenergy, 27(4), 393-397.
82. Ramesh, N., & Mallikarjuna, J. M. (2016). Evaluation of in-cylinder mixture homogeneity in a diesel HCCI engine – A CFD analysis. Engineering Science and Technology, an International Journal, 19(2), 917-925.
83. Reid, R. C., Prausnitz, J. M., & Poling, B. E. (1987). The Properties Of Gases And Liquids. (S.l.) : (s.n.). https://doi.org/10.1036/0070116822
84. Richards, K. J., Senecal, P. K., & Pomraning, E. (2014). CONVERGE (Version 2.3. 0) Manual. Middleton, WI. : Convergent Science, Inc.
85. Rohit Sharma. (2013). Experimental investigations of the performance and emissions of a modified CI engine operating in HCCI mode. NIT Warangal.
86. Ryan, T. A., Joiner, B. L., & Ryan, B. F. (2004). MinitabTM. (S.l.) : John Wiley & Sons, Inc.
87. Sahoo, P. K., & Das, L. M. (2009). Combustion analysis of Jatropha, Karanja and Polanga based biodiesel as fuel in a diesel engine. Fuel, 88(6), 994-999.
88. Saito, T., Daisho, Y., Uchida, N., & Ikeya, N. (1986). Effects of Combustion Chamber Geometry on Diesel Combustion. SAE International .
89. Sarangi, A. K., McTaggart-Cowan, G. P., & Garner, C. P. (2010). The Effects of Intake Pressure on High EGR Low Temperature Diesel Engine Combustion. SAE Technical

Paper. 2010-2145. https://doi.org/10.4271/2010-01-2145

90. Sayin, C., & Canakci, M. (2009). Effects of injection timing on the engine performance and exhaust emissions of a dual-fuel diesel engine. Energy Conversion and Management, 50(1), 203-213.
91. Sayin, C., & Gumus, M. (2011). Impact of compression ratio and injection parameters on the performance and emissions of a DI diesel engine fueled with biodiesel-blended diesel fuel. Applied Thermal Engineering, 31(16), 3182-3188.
92. Sayin, C., Gumus, M., & Canakci, M. (2012). Effect of fuel injection pressure on the injection, combustion and performance characteristics of a DI diesel engine fueled with canola oil methyl esters-diesel fuel blends. Biomass and Bioenergy, 46, 435-446.
93. Sayin, C., Ilhan, M., Canakci, M., & Gumus, M. (2009). Effect of injection timing on the exhaust emissions of a diesel engine using diesel-methanol blends. Renewable Energy, 34(5), 1261-1269.
94. Schmidt, D. P., & Rutland, C. J. (2000). A New Droplet Collision Algorithm. Journal of Computational Physics, 164, 62.
95. Scott, P. T., Pregelj, L., Chen, N., Hadler, J. S., Djordjevic, M. a., & Gresshoff, P. M. (2008). Pongamia pinnata: An Untapped Resource for the Biofuels Industry of the Future. BioEnergy Research, 1(1), 2-11.
96. Senecal, P. K., Pomraning, E., Richards, K. J., Briggs, T. E., C., C. Y., M., R. M., & P., & A., M. (2003). Multi-dimensional modeling of direct-injection diesel spray liquid length and flame lift-off length using CFD and parallel detailed chemistry. SAE Technical Paper, (2003-01-1043).
97. Singh, A. P., & Agarwal, A. K. (2012). Combustion characteristics of diesel HCCI engine: An experimental investigation using external mixture formation technique. Applied Energy, 99, 116-125.
98. Singh, G., Singh, A. P., & Agarwal, A. K. (2014). Experimental investigations of combustion, performance and emission characterization of biodiesel fuelled HCCI engine using external mixture formation technique. Sustainable Energy Technologies and Assessments, 6, 116-128.
99. Som, S., & Aggarwal, S. K. (2010). Effects of primary breakup modeling on spray and combustion characteristics of compression ignition engines. Combustion and Flame,

157(6), 1179-1193.

100. Song, J., Yao, C., Liu, Y., & Jiang, Z. (2008). Investigation On Flow Field In Simplified Piston Bowls for Di Diesel Engine. Engineering Applications of Computational Fluid Mechanics, 2(3), 354-365.
101. Song, R., Hu, T., Zhou, L., Liu, S., & Li, W. (2007). Effects of compression ratio on the combustion characteristics of a homogeneous charge compression ignition engine. Frontiers of Energy and Power Engineering in China, 1(4), 463-467. https://doi.org/10.1007/s11708-007-0068-0
102. Squaiella, L. L. F., Martins, C. A., & Lacava, P. T. (2013). Strategies for emission control in diesel engine to meet Euro VI. *Fuel*, 104, 183-193.
103. Yang, X., Gupta, S., Kuo, T., & Gopalakrishnan, V. (2013). ICEF2013-19043, 1-10.
104. Yao, M., Zheng, Z., & Liu, H. (2009). Progress and recent trends in homogeneous charge compression ignition (HCCI) engines. Progress in Energy and Combustion Science, 35(5), 398-437.
105. Yoon, S. H., Cha, J. P., & Lee, C. S. (2010). An investigation of the effects of spray angle and injection strategy on dimethyl ether (DME) combustion and exhaust emission characteristics in a common-rail diesel engine. Fuel Processing Technology, 91(11), 1364-1372.
106. Zeraati Rezaei, S., Zhang, F., Xu, H., Ghafourian, A., Herreros, J. M., & Shuai, S. (2013). Investigation of two-stage split-injection strategies for a Dieseline fuelled PPCI engine. Fuel, 107, 299-308.
107. Zheng, M., Reader, G. T., & Hawley, J. G. (2004). Diesel engine exhaust gas recirculation—a review on advanced and novel concepts. Energy Conversion and Management, 45(6), 883-900.

List of Publications

International Journals

S.No	Title of the paper	Name of the Journal and Publisher	Status
1	Parametric study and optimization using RSM of DI diesel engine for lower emissions	Journal of the Brazilian Society of Mechanical Sciences and Engineering **Springer, (SCI) (IF: 1.235)**	Published
2	Computational Optimization of Biodiesel Combustion Using Response Surface Methodology	Thermal Science, **(SCI) (IF: 1.093)**	Published
3	Investigating optimal operating parameters of DI diesel engine: a CFD approach using CONVERGE^{TM}	World Journal of Engineering, **Emerald Publishing** (**ESCI**)	Published
4	Effect of Fuel Injection Pressure and Spray Cone Angle in DI Diesel Engine Using CONVERGE^{TM} CFD Code	*Procedia Engineering*, **Elsevier, (Scopus)**	Published
5	Parametric Optimization Through Numerical Simulation of VCR Diesel Engine	Journal of The Institution of Engineers (India): Series C, **Springer. (Scopus)**	Published

International/ National Conferences

S.No.	Title of the paper	Name of the Conference	Status
1	Numerical Experiment of CI Engine Combustion Using CONVERGE Software.	National Conference On Fire Research and Engineering. FIRE 2014,IIT Roorkee.11-12th March 2014.	Presented
2	Numerical investigation of the effect of compression ratio on the performance of direct injection diesel engine	5th International and 41st national conference on Fluid Mechanics and Fluid Power, IIT Kanpur 12th to 14th Dec 2014.	Presented
3	Numerical investigation of split injection on Pongamia bio diesel blend	2nd International Conference on Thermal, Energy and Environment Kalasalingam University, March 25&26, 2016	Presented
4	Prediction of Physical Properties for Pongamia Biodiesel used for Combustion Modeling	International Conference on Recent Trends in Engineering, Science and Technology 2016, 1 June 2016, Hyderabad, India	Presented .
5	Numerical Investigation on the Effect of Overall Equivalence Ratio on Combustion Characteristics of DI CI Engine.	NSMERS 2016, NIT Warangal 7th Oct,2016.	Presented .